2012

Effect of surfactants and brine salinity and composition on spreading, wettability and flow behavior in gas-condensate reservoirs

Yu Zheng
Louisiana State University and Agricultural and Mechanical College, yzheng2@tigers.lsu.edu

Follow this and additional works at: https://digitalcommons.lsu.edu/gradschool_dissertations

Part of the Petroleum Engineering Commons

Recommended Citation

Zheng, Yu, "Effect of surfactants and brine salinity and composition on spreading, wettability and flow behavior in gas-condensate reservoirs" (2012). *LSU Doctoral Dissertations*. 1314.

https://digitalcommons.lsu.edu/gradschool_dissertations/1314

EFFECT OF SURFACTANTS AND BRINE SALINITY AND COMPOSITION ON SPREADING, WETTABILITY AND FLOW BEHAVIOR IN GAS-CONDENSATE RESERVOIRS

A Dissertation

Submitted to the Graduate Faculty of the
Louisiana State University and
Agricultural and Mechanical College
in partial fulfillment of the
Requirements for the degree of
Doctor of Philosophy

in

The Department of Petroleum Engineering

by
Yu Zheng
B.S., Shandong Institute of Mining Technology, 1994
M.S., Qingdao University of Science & Technology, 2004
December 2012

DEDICATION

This work is dedicated to my husband, Haibo Cao; my son, Eric; and to my parents and parents-in-law who always supported me.

ACKNOWLEDGMENTS

TABLE OF CONTENTS

LIST OF TABLES

LIST OF FIGURES

ABSTRACT

The well-known condensate blockage problem causes severe impairment of gas productivity as the flowing bottom-hole pressure falls below the dew point in gas-condensate reservoirs. Hence, this study attempts to investigate the concept of modifying the spreading coefficient and wettability using low-cost surfactants in the near wellbore region, to prevent the gas flow problems associated with condensate buildup. This study also examines the effect of brine salinity and composition on wettability, spreading and adhesion in condensate buildup regions, to evaluate the ability of brine salinity/composition for enhanced gas productivity in gas-condensate reservoirs.

In this study, experiments were performed at both ambient and reservoir conditions using reservoir fluids. Water-advancing and receding contact angles were measured using the Dual-Drop-Dual-Crystal (DDDC) technique and sessile drop method to characterize reservoir wettability and spreading behavior. Interfacial tension was measured using pendent drop shape analysis (DSA) technique and capillary rise techniques. Anionic and nonionic surfactants and nine multi-component brines varying in salinity as well as ten single-salt brines with two different salinities were tested. Oil-water relative permeabilities were generated by history matching condensate recovery and pressure drop data obtained from the coreflood experiments using Berea sandstone core.

Wettability was altered from strongly oil-wet to intermediate-wet by the anionic surfactant. The declining trend of spreading coefficient resulted from the presence of surfactants indicating the possibility of enhanced gas productivity and condensate recovery by surfactants. Coreflood results substantiated the wettability alteration to intermediate-wet induced by the anionic surfactant and 82% improvement in gas relative permeability was obtained at ambient

conditions. The variation of brine salinity and composition had little effect on wettability and interfacial tension in condensate-brine system. However, large water-receding angles were observed due to the condensate drop spreading on the quartz surface through changing brine salinity and composition. This spreading behavior was more pronounced in high salinity brine systems. This study thus demonstrates that surfactant-induced wettability alteration and spreading coefficient reduction have the benefits for improving gas and condensate production by mitigating the condensate blockage problem. This study also indicates the potential of controlling the spreading behavior of condensate using low salinity brines.

1. INTRODUCTION

1.1 Problem Statement

Gas condensate reservoirs constitute a significant portion of oil reserves in the United States, since they have been recognized as a special type different from the conventional crude oil reservoirs in the 1930's. With the development of drilling techniques, the applicable drilling depth keeps increasing and more condensate reservoirs have been found and explored. The gas condensates are composed mainly of lighter hydrocarbons thus considered more commercially valuable than crude oil as the result of added revenue from the corresponding more refined byproducts. Therefore, the importance of gas condensate reservoirs has been recognized widely, and more attention is being paid in the oil and gas industry to enhance gas and condensate recovery from gas condensate reservoirs for increased profits.

Gas condensates or retrograde gases are one of five types of reservoir fluids. The gas condensate reservoirs initially contain single gas phase at reservoir conditions. However, these reservoirs exhibit unexpected and complex thermodynamic behaviors as the reservoir pressure drops. The phase diagram of a typical retrograde gas is shown in Figure 1. It can be seen that the initial pressure of the gas condensate reservoir is above the dew point pressure (point 1), and only a single gas phase exists in the reservoir. As the pressure goes below the dew point pressure (point 2) due to isothermal depletion, liquid condensate from the gas is formed in the reservoir. More condensate accumulates around the well bore due to the steep decline in fluid pressure near the well bore region (point 3) as the operation continues. This unusual phenomenon of increasing condensation with decreasing pressure is called "retrograde condensation" which results in serious impediments to the flow of gas to the producing well. It has been eventually realized in the industry as "condensate banking" or "condensate blockage".

1
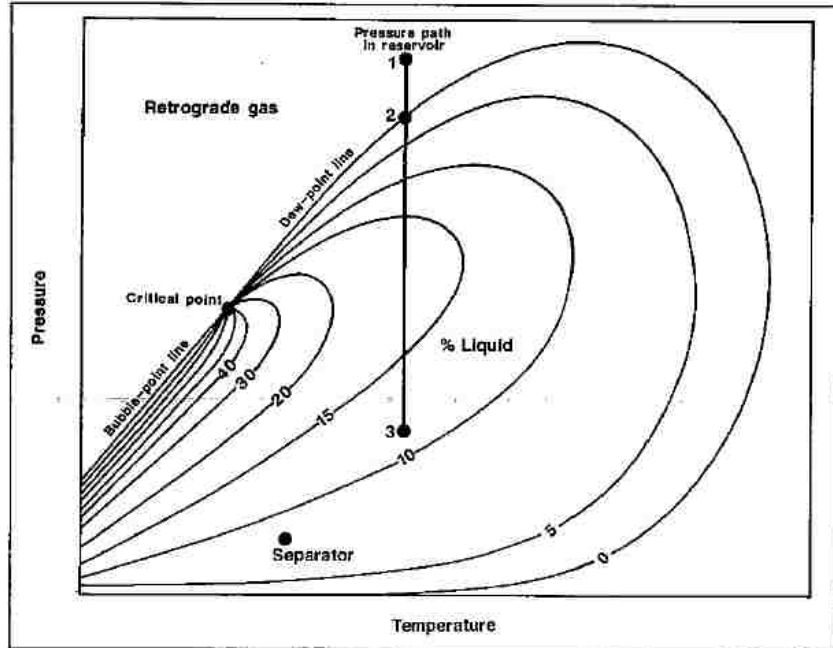
Figure 1: Phase Diagram of a Typical Retrograde Gas Reservoir (McCain, Jr. 1990)

The condensate banking has a detrimental effect on gas productivity and thus leads to a significant loss of economic revenue. The Arun condensate field in Indonesia, for example, displayed a 50% reduction in gas productivity with only about 1% of condensate buildup in the wellbore regions (Afidick et al., 1994). The conventional methods, such as gas cycling and methanol treatment, have been proposed to remedy this condensate banking problem after it occurs. However, most of them are only temporary solutions with limit success because the condensate banking forms again as production continue.

To date, waterflooding, a process of injecting water into oil reservoirs, is the most widely used method of improved oil recovery. This process is accomplished either by maintaining reservoir pressure at a high level or by sweeping the oil through the reservoir from an injection well to a producing well. In the early years of waterflooding, it is mainly applied to many mature onshore fields. With more development of offshore fields in the world, it has come to the forefront and has been utilized to the offshore fields.

Water quality has been identified as a key element to be monitored based on the fact that poor water quality can result in waterflooding failure and thus cause the economic loss. The ideal water for waterflooding should be free from suspended solid particles and bacteria, compatible with formation water and chemically interactive with compounds and elements present in the formation. Aquifer water and seawater are the two main water sources used for waterflooding.

All of above characteristics of injection water have been concerned and developed in waterflooding design for a long time in the petroleum industry. However, the composition of the salt in the injection water has not been considered as an important factor on waterflooding displacement efficiency as well as the possibility of increased oil recovery through manipulation of the injection water composition. It has been observed that the composition of the brine can have a significant effect on wettability and oil recovery. It has been also believed that brine salinity, especially low brine salinity, can improve recovery of crude oil. Although various suggestions of the mechanism behind the low salinity process have been proposed based on increasing amounts of laboratory experiment results, the exact recovery mechanisms have not been fully investigated and the mechanisms are still uncertain. In addition, there is very little known about brine salinity/composition effects in gas-condensate reservoirs.

Therefore, this study aims to experimentally investigate the concept of modifying the spreading coefficient, wettability and their influence on flow behavior using inexpensive surfactants in the near wellbore region, to mitigate the condensate banking effect. Surfactant–induced wettability alteration in condensate buildup regions can provide a permanent solution in a cost-effective manner and improve gas productivity from gas condensate reservoirs. Spreading coefficient determines the distribution of gas, water and oil in porous media and thus affects their relative flow behavior. Using surfactants to alter the three phase interfacial tensions between gas-

3

water, gas-oil and oil-water results in the spreading coefficient modification and thus improve the gas flow through the porous media. This is a new method that has not been explored to prevent condensate accumulation for enhanced gas productivity in gas condensate reservoirs. This study also focuses on the investigation of brine salinity and composition on wettability, spreading and adhesion in condensate buildup regions, and thus evaluates their effects on enhanced condensate recovery and gas productivity improvement in gas-condensate reservoirs. Unlike the conventional approach-coreflooding used in previous literature, the experimental study will be performed by using our unique advanced techniques to measure the fluid-fluid and rock-fluids interactions. This will provide a better understanding of mechanisms of condensate blockage and remediation and brine salinity effects.

1.2 Objectives

The objectives of this study are:

- To conduct the interfacial tension measurements between condensate-water, gas-water and gas-condensate to determine the fluid spreading coefficients at both ambient conditions and reservoir conditions.

- To perform the interfacial tension measurements between condensate-water, gas-water and gas-condensate in the presence of surfactants (both anionic and nonionic types) to determine the modified spreading coefficients at reservoir conditions as well as ambient conditions.

- To determine the wettability of a gas condensate reservoir by measuring dynamic contact angles in rock-water-condensate system using Dual-Drop-Dual-Crystal (DDDC) technique at both ambient and reservoir conditions.

- To experimentally investigate the wettability altering capability of anionic and nonionic surfactants by measuring dynamic contact angles at ambient as well as reservoir conditions.

- To develop the Bond Number to interpret the dynamic condensate drop behavior on rock surface.

- To conduct coreflood experiments to examine the effect of surfactants on wettability and enhanced gas productivity and condensate recovery.

- To correlate the results of surfactant–induced wettability alterations derived from contact angles with coreflood multiphase flow characteristics.

- To measure condensate-brine interfacial tensions to test the influence of brine salinity and composition on oil-water IFT.

- To study the effect of brine salinity and composition on spreading, adhesion and wettability in rock–brine–condensate system by measuring contact angles.

- To propose the mechanism for understanding the effect of surfactant and brine salinity and composition on spreading and wettability.

1.3 Methodology

In this study, the condensate from an actual sandstone gas condensate reservoir that was supplied by a major oil company, synthetic brine matching the formation brine in composition and methane were chosen to conduct interfacial tension measurements using pendent drop method by drop shape analysis (DSA) technique and capillary rise technique at both ambient and reservoir conditions. Two types of surfactants, anionic and nonionic in various concentrations, were selected to test at ambient conditions. The anionic surfactant has proved more effective in reducing IFT and altering wettability in this condensate system in ambient-condition experiments, and thus was used in both reservoir-condition (2264 psia and 210 °F) and coreflood experiments.

Nine multi-component synthetic brines varying in salinity (from de-ionized water to 125,000 ppm) and ten single salt (Na^+, Ca^{2+}, Al^{3+}, etc.) synthetic brines were studied to

investigate the effect of brine salinity and composition on spreading, wettability and adhesion in this condensate-brine system at ambient conditions. Interfacial tensions between condensate and brines, water-advancing and receding contacts, and the pH of brine were measured in all nineteen cases.

Dual-Drop-Dual-Crystal (DDDC) technique was used to measure water-advancing contact angles to infer wettability and the alterations induced by surfactants and brine salinity and composition. Sessile drop method was used to measure water-receding contact angles to characterize spreading behavior in the condensate-brine system. Bond Number and Adhesion Number were used to explain the dynamic behavior of the condensate drop on the rock surface during the surfactant injection and understand the influence of the brine salinity/composition on adhesion phenomenon in condensate-brine-rock system, respectively.

Berea sandstone core, condensate, synthetic brine and nitrogen were used to perform coreflood experiments to examine the surfactant effect on gas relative permeability and condensate recovery. A coreflood simulator was used to generate oil-water relative permeabilities by history matching condensate recovery and pressure drop data obtained from the coreflood experiments. Craig's rules of thumb (Craig, 1971) were then applied to the relative permeability curves provided by the simulator to interpret wettability and surfactant-induced wettability alterations. The correlation and comparison of wettability and surfactant-induced wettability alterations derived from contact angle measurement with coreflood results were then made.

2. LITERATURE REVIEW

2.1   Productivity Loss in Gas Condensate Reservoirs

Gas condensate reservoirs suffer a rapid decline in well productivity as the flowing bottom-hole pressure falls below the dew point in reservoirs during depletion. The formation of a condensate phase occurs near the wellbore region, and the increasing condensate develops the condensate banking or condensate blockage to impair the flow of gas to the well and thus decrease gas productivity. Many researchers including Fussell (1973), Hinchman and Barree (1985), Aziz (1985), Barnum et al. (1995) and Clark et al. (1985) have investigated the impact of condensate blocking on productivity. Based on their studies, the productivity reduction caused by this condensate buildup is pronounced. Several field examples of severe well productivity loss owning to condensate banking are also well documented in the literature (Boom et al., 1996; Afidick et al., 1994; Engineering, 1985; Duggan, 1972; Abel et al., 1970; Allen and Roe, 1950). A well-known industrial case of the condensate banking effects is the Arun field in Indonesia, one of the world's giant retrograde gas reservoirs (Afidick et al., 1994). A maximum liquid dropout of about 1.1% of this lean gas condensate reservoir caused the well productivity decline by about 50% as the pressure dropped below the dew point pressure. And the worst example at Cal Canal field in California showed that condensation even completely killed the gas well (Engineering, 1985).

The loss of well productivity for gas condensate reservoirs can be attributed to fluid properties, formation characteristics and the reduction in relative permeabilities in the vicinity of the wellbore. Relative permeability effects on the loss of well productivity have been recognized and studied over a wide range of conditions with synthetic fluids (Bang et al., 2006; Kumar, 2006; Ayyalasomayajula et al., 2003; Henderson et al. 2000) as well as with reservoir fluids

(Nagarajan et al., 2004; Mott et al., 2000). Other parameters such as fluid composition (Wheaton and Zhang, 2000; Shi and Horne, 2008), capillary number and non-Darcy flow effects (Bozorgzadeh and Gringarten, 2006; Kumar et al., 2006; Mohan et al., 2009) have also been investigated to evaluate the impact of condensate buildup on gas well productivity.

Nagarajan et al. (2004) experimentally measured gas-condensate relative permeability using three model fluids and two live reservoir fluids. The reservoir fluid results were significantly different from the model fluid results. The gas and condensate relative permeability using reservoir live fluids were found to be lower than those measured with model fluids, indicating that possibly higher condensate saturation build-up was obtained in live fluid tests. Hence, they believe that the live fluid data are more representative of the reservoir condition flow and should be used in all reservoir flow calculations.

Shi and Horne (2008) developed a methodology to enhance the productivity of gas or condensate from gas-condensate reservoirs by controlling the liquid composition which drops out close to the well. They performed coreflood experiments as well as compositional numerical simulations. Their study shows that composition and condensate saturation vary significantly as a function of producing sequence.

Mohan et al. (2009) studied the impact of non-Darcy flow and condensate accumulation on the productivity of a hydraulically fracture gas-condensate well. Two-level local-grid refinement was used to simulate very small gridblocks which must correspond to the actual fracture width to accurately model non-Darcy flow. Their simulation results show that productivity improvement is overestimated by a factor on the order of two to three if non-Darcy flow is neglected.

2.2   Remedial Methods for Gas Productivity

Several remedial methods have been proposed to remove the drop out liquid and recover gas productivity decline from condensate banking. Generally, these methods can be grouped into either decreasing the pressure drawdown and maintaining pressure above the dew point pressure or changing the phase behavior of the gas condensate fluid.

Gas cycling or the injection of dry gases (N_2, CO_2, or CH_4) to the gas condensate reservoirs is one of methods, which has been used to vaporize condensate and increase the dew point pressure and then maintain the reservoir pressure above the dew point pressure.

Luo et al. (2001) conducted coreflooding experiments to investigate the effect of revaporization on the condensate recovery using the dry gas. They found that the dry gas can vaporize both the intermediate and heavier (C20+) hydrocarbons. Also the cumulative condensate recovery was improved by the dry gas injection.

Jamaluddin et al. (2001) experimentally investigated how injection of propane affected the remediation of the liquid buildup in gas condensate reservoirs. Based on their study, both the dew point pressure and the volume of condensed liquid were reduced and propane was proved to vaporize condensate more efficiently than carbon dioxide.

Eikeland and Hansen (2007) simulated the reinjection process of dry gas into the Sleipner Ty gas condensate field. From their simulation results, high condensate recovery was obtained due to the dry gas injection. Also, the results showed that although the reservoir pressure has been below the dew point pressure through all times, the re-injected gas has reduced the condensate drop out in the reservoir and the reservoir pressure has been increased for the first two years since the start of this reinjection process.

9

Al-Abri et al. (2009) performed an experimental investigation of supercritical CO_2 injection (SCCO$_2$), methane injection and the injection of CO_2 and methane mixture on enhanced natural gas and condensate recovery. Their work demonstrates that compare to the injection of pure methane or methane-CO_2 mixtures, supercritical CO_2 injection provided favorable condensate sweep efficiency and a delayed breakthrough due to less capillary instabilities and better mobility ratios. The relative permeability curves to condensate also improved by injecting SCCO$_2$ resulting from a decrease in condensate-to-gas viscosity ratio.

Another method is hydraulic fracturing. This stimulating wells method has possibility to reduce the pressure drawdown by increasing the flowing area through inducing a fracture, resulting in less liquid condensate drop out near the well bore, thus delaying the condensate bank formation and mitigating its effect (Settari et al., 1996; Mohan, 2005; Baig et al., 2005; Othman et al., 2008).

Baig et al. (2005) studied the productivity and near wellbore behaviors of a fractured and a non-fractured well in a low permeability gas condensate reservoir by using the reservoir simulation model. The results demonstrated that the fractured well has a higher productivity than the non-fractured well and the gas productivity could also be improved as the length of the fracture increased up to a practical fracture half-length limit.

Othman et al. (2008) reported the production performance of the Angsi K-sand hydraulically fractured gas condensate reservoir which is the first tight gas reservoir development in Malaysia. The K-sand dew point is only about 100 psia below the initial pressure and hence condensate drop out near the wellbore is expected to begin almost immediately after the start of production. Also, this reservoir has low permeability (<0.01-3mD). The hydraulic fracture stimulation performed in the well resulted in a fourfold increase in gas production rate,

indicating that the hydraulic fracturing improved the well productivity and mitigate the detrimental effects of condensate dropout.

The solvent injection such as methanol has also been developed to be a remediation method to enhance the gas productivity. Du et al. (2000) conducted coreflood experiments in low permeability limestone cores to evaluate the use of methanol to restore the gas relative permeability. Their results showed that the end-point gas relative permeability was increased by a factor of 1.2 to 2.5 depending on the initial water saturation. A possible explanation for the increased gas permeability is the miscible displacement of the condensate and water phases by the methanol.

Al-Anazi et al. (2002) also experimentally examined the effect of methanol on condensate blockage in both low permeability limestone cores and high permeability sandstone cores. They found that methanol was effective in removing both condensate and water and restored the gas productivity in both low and high permeability cores. Later, they (2005) conducted a field test to investigate the effectiveness of methanol as a solvent for mitigating condensate bank on the basis of laboratory results and a single well numerical simulation. The methanol treatment was applied to a gas condensate well in the Hatter's Pond field and the results of their study proved that both gas and condensate production rates increased by a factor of two over the first 4 months and by 50% thereafter.

Although the above-cited literatures showed that their remedial methods can help mitigate the condensate bank and increase the gas productivity, all the methods have limited application and are only temporary solutions to the condensate blockage as the condensate bank forms again with time. During the dry gas injection (Luo et al., 2001), the mass transfer occurred between the dry gas injected and the original gas condensate leading to a rise in dew point

pressure and earlier retrograde condensation and thus reducing the gas condensate recovery. Hydraulically fractured wells (Othman et al., 2008) were still susceptible to the effect of condensate drop out. The wells also suffered from proppant flow back problem which has detrimental influence to the facilities and revenue loss due to increased maintenance and reduced productivity. Hence hydraulic fracturing has not always been economically feasible or cost-effective. The solvent method depends on the phase behavior of the mixture of the solvent and the condensate. The removal of the condensate bank is temporary due to the re-formation of the condensate bank. Thus, solvent treatments need to be repeated at time intervals after production is restarted.

2.3   Chemical Wettability Alteration

The newly reported method for tackling the condensate blocking problem focused on wettability alteration by using chemicals such as a polymer or surfactant. This approach provides a long term strategy for restoration of well productivity by altering the wettability of rocks in the near wellbore region of gas condensate reservoirs from strongly water-wet or oil-wet to intermediate wet.

Li and Firoozabadi (2000) were the first to experimentally examine the wettability alteration of the rock surface at room temperature by using polymers. They found that the wettability of the rock changed from strongly liquid-wet to intermediate gas-wet resulting in the increase the phase relative permeability and oil recovery. Their work was extended by Tang and Firoozabadi (2002) to test the effect of the polymer chemicals on wettability alteration at temperatures up to 90°C. The results showed that the liquid phase mobility was increased after chemical treatment. Later, Fahes and Firoozabadi (2007) performed wettability alteration at a higher temperature of 140°C and measured the effect of wettability alteration on increased liquid

mobility. Similar results obtained from their studies demonstrated that wettability alteration after chemicals treatment led to increasing liquid mobility and thus improved gas productivity. However, the drawbacks of all these studies are that they did experiment at low pressure and none of them used gas condensate fluids. They simply employed normal decane and normal tetradecane as the oil phase, distilled water or monovalent NaCl brine as the aqueous phase and air as the gas phase in their experiments, and interpreted wettability alteration by measuring receding contact angles at ambient conditions or from changes in relative permeability characteristics. The experimental findings of Ayirala and Rao (2004) revealed that n-decane is insensitive to wettability effect by using chemicals. Furthermore, the relative permeabilities are "the composite effect of pore geometry, wettability, surface tension, fluid distribution and saturation history" (Craig, 1971). Anderson (1987) suggested that since factors other than wettability can affect relative permeability curves at the same time, it better to measure wettability independently rather than to rely on Craig's rules thumb to characterize wettability. Therefore, the wettability interpretations from relative permeabilities may not be by representative of true wettability alterations reported in their studies.

Kumar et al. (2006a, 2006b) experimentally investigated the improvement in gas and condensate relative permeability by using fluorinated polymeric surfactants in methanol-water mixtures at reservoir conditions with gas-condensate fluids. From their studies, steady state relative permeability for gas and condensate was increased by a factor of 2 or 3 after surfactant solution treatment over a temperature range of 145 to 275 °F. However, they did not explain how the chemicals affect the wettability of rocks.

Noh and Firoozabadi (2008) investigated the effect of wettability alteration on high-velocity-flow coefficient in two phase gas/liquid flow in gas reservoirs. Steady-state two-phase

13

relative permeability tests were carried out in the chemical treated cores to determine the high-velocity coefficients. Their results show that the high-velocity coefficient for gas/water flow decreased significantly after the chemical treatment near the wellbore region; however, the reduction in high-velocity coefficient for gas/oil flow was less pronounced. They believed that the large reduction in high-velocity coefficient can result in significant improvement in well deliverability.

Bang et al. (2009) used synthetic fluids to do coreflood experiments and treated both Berea and reservoir sandstone cores by using a nonionic polymeric fluorinated surfactant in a mixture of organic solvents at reservoir conditions. The measured wettability index indicated that the wettability of the core was changed to neutral wet by the chemical treatment. Gas and condensate relative permeability were increased by a factor of two. They (2010) also conducted coreflood experiments to measure the effect of liquid (both water and condensate) blocking on gas relative permeability. The alteration of wettability after the chemical treatment was evaluated by measuring the USBM wettability index of treated cores. The results showed that the chemical treatment altered the wettability of water-wet sandstone to neutral-wet or mixed-wet resulting in increasing the gas relative permeability. Improvements in the gas relative permeability were a factor of approximately two. In their work, they determined wettability alteration based on imbibitions and drainage capillary curves or USBM wettability index but did not measure contact angles.

2.4   Spreading Coefficient

Spreading coefficient is usually used to describe fluid-fluid interactions. It signifies the imbalance of the fluid interfacial tensions acting along a single line which is the contact line

between fluid phases (Grattoni et al., 1997). Spreading coefficient can be either positive or negative. For the water-oil-gas system, the oil spreading coefficient S_o can be defined as below:

$$S_o = \sigma_{wg} - \sigma_{ow} - \sigma_{og} \qquad (1)$$

where σ_{wg} is the water-gas surface tension, σ_{ow} is the water-oil interfacial tension, and σ_{og} is the oil-gas interfacial tension. The defining equation of the oil spreading coefficient is also displayed in Figure 2.

Spreading coefficient determines the nature of distribution of the water, oil and gas within reservoir rock pores, thus plays a key role in gas-water-oil relative flow behaviors, recovery kinetics and the residual oil recovery. However, this role has to be considered in association with the porous medium wettability. Hence, two wettability states of reservoir rocks, water-wet and oil-wet, are presented here to elucidate how the oil spreading coefficient works in the pore space. Figure 3 shows the distribution of water, oil and gas in the reservoir rock for two wetting states. It can be seen from Figure 3 that on the water-wet rock surface if the spreading coefficient is positive, it indicates that oil tends to form a spreading film between gas and water; while the negative spreading coefficient results in the oil lenses floating on the gas-water interface. On the oil-wet rock surface, a positive spreading coefficient suggests that oil tends to isolate gas and water by spreading between them. And the negative spreading coefficient means that both gas and water phases flow as discreet globules entrained in the oil phase. Similar fluids distribution map has been presented by Vizika and Lombard (1996), and Grattoni et al (1997).

This behavior strongly affects flow properties in porous media and therefore has a strong influence on the oil recovery process. Oren and Pinczewski (1992, 1994) presented their work how the spreading coefficient affected oil-water flow dynamics in porous rocks with different wettability states. They performed immiscible tertiary gas flooding in 2D glass micromodels

under strongly oil-wet and water-wet conditions to investigate these effects and the results are summarized in Table 1. It can be seen from Table 1 that in a water-wet system oil recovery for the positive spreading coefficient was significantly higher than that for the negative spreading system; while the oil-wet system showed an opposite trend. In their study, they used air, refined oil and distilled water as the fluids instead of the real reservoir fluids to examine the effect of spreading coefficient.
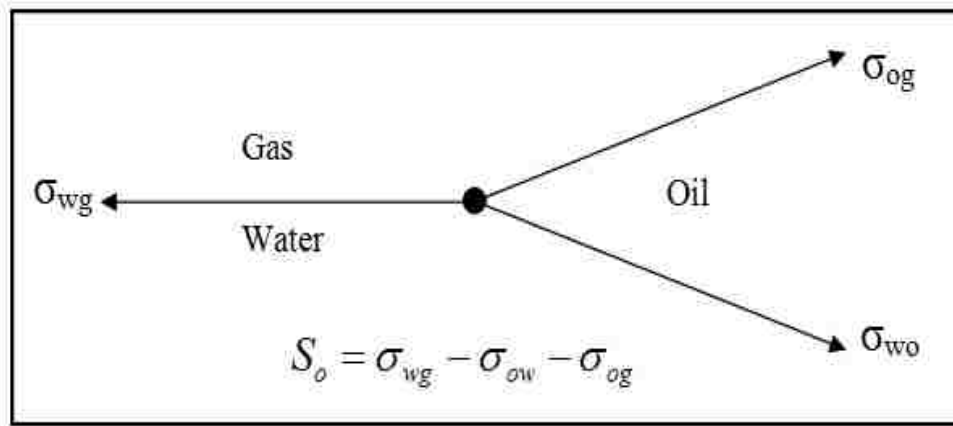
Figure 2: Schematic Depiction of the Spreading Coefficient

Figure 3: Oil-Water-Gas Distributions in O/G/W/R Systems

Table 1: Effect of Wettability and Spreading Coefficient on Gas Flood Oil Recovery in Micromodels (Oren and Pinczewski, 1994)

Parameter	Water-Wet System		Oil-Wet System	
Spreading Coefficient So	+17.7	-8.1	+17.7	-8.1
Oil Recovery, %	35.2	17.6	74.4	84.2
Water Recovery, %	81.5	93.6	60.0	61.5

Vizika and Lombard (1996) conducted gravity drainage experiments for spreading and non-spreading conditions in water-wet, oil-wet and fractionally-wet porous media. They concluded that the highest oil recoveries were obtained for $S_o > 0$ and water-wet or fractionally-wet conditions, due to oil flowing on the continuous spreading films. For $S_o < 0$, oil recoveries were deteriorated due to a loss of hydraulic continuity. Also, in oil-wet porous media, the lowest oil recoveries were obtained. Although in this condition oil could remain continuous through wetting films, it was subject to strong capillary retention.

The effect of spreading coefficient on the residual oil saturation was observed by Sharma and Filoco (2000). They conducted the drainage experiments by using air, brine (NaCl) and dodecane/dodecene on the water-wet Berea sandstone core. A small amount of iso-butanol was added to the brine aiming to alter the initial spreading coefficient from positive to negative. The results showed that the spreading system (S_o=5.5) obtained a very low remaining oil saturation compared with non-spreading system (S_o=-4.1). The good explanation is that in spreading system the oil maintains phase continuity and can flow through the oil film until the very low oil saturation approached.

Araujo et al. (2001) developed a method to calculate the spreading coefficient for solid/liquid/liquid and solid/liquid/gas systems. They evaluated the effect of the spreading

coefficient on two-phase relative permeability, and found that in water wet condition, oil recovery and relative permeability are higher for the positive spreading coefficient system than those for the negative system.

Maeda and Okatsu (2008) experimentally investigated the pore scale thin oil film drainage mechanism responsible for the mobilization of waterflood residual oil by immiscible gas floods in the strongly water-wet oil reservoir. Two methods, micro pore film flow experiment and 2 dimensional 3 phase micro flow simulation based on Lattice Boltzmann Method (LBM) were used in their study. The results showed that oil recoveries for high positive spreading coefficient systems were much higher than low positive spreading coefficient systems in high pressure and high temperature conditions. The reason for this phenomenon is that in the case of the high positive spreading coefficient value, the thin oil film was formed between gas and water resulting in oil and water spreading and flowing easily in the reservoir and thus enhancing the waterflood residual oil recovery by immiscible gas flood.

2.5   Surfactant

Surfactant is "an abbreviation for surface active agent and literally means active at surface. The surface can be between solid and liquid, between air and liquid, or between a liquid and a different immiscible liquid (Porter, 1994)." A surfactant is generally classified as anionic, nonionic, cationic or amphoteric according to the presence of formally charged hydrophilic groups in its head. In the surfactant molecule, there are two groups, a hydrophobic tail (water hating) and a hydrophilic head (water liking), resulting in the adsorption of a surfactant at a surface or interface. This surface/interface adsorption leads to pronounced physical changes, reduces the surface/interfacial tensions and alters the wettability of a surface. Hence, surfactants

have been considered for application in enhanced or improved oil recovery (EOR or IOR) process in the petroleum industry due to surfactant adsorption.

Mungan (1966) investigated the effect of interfacial tension on the displacement of a non-wetting by a wetting liquid without changing wettability and found that decreasing IFT from 40 to 0.5 dyne/cm resulted in only 8.1% additional recovery after breakthrough. Hence, the key to significant improvements in oil recovery by lowering oil-water interfacial tension for surfactant processes when ignoring surfactant aided wettability alteration is to achieve ultra-low interfacial tension e.g., $< 10^{-2}$ mN/m (Klins, 1984; Schramm, 2000; Hirasaki, et al., 2008). Klins (1984) studied the effect of capillary number on residual oil saturation and reported that four to six orders of magnitude reduction in capillary number is required for significant improvements in oil recovery. It has also been found that oil-water interfacial tension had to be reduced from 20-30mN/m to values in the range of 0.001 to 0.01mN/m to obtain low values (less than 0.05) of residual oil saturation (Hirasaki, et al., 2008).

Wettability alteration of porous reservoir rock with surfactant plays the next most important role in improved oil recovery. Hirasaki and Zhang (2004) conducted spontaneous imbibitions to evaluate anionic surfactant solutions for enhanced oil recovery in fractured oil-wet carbonate formation. They reported that the wettability of the calcite plate was altered to intermediate-wet or water-wet induced by alkaline anionic surfactant solution and thus oil recovery of spontaneous imbibition was increased.

Rao et al. (2006) conducted coreflood experiments using low-cost surfactants to investigate the impact of surfactants on wettability and relative permeability. From their study, wettability alteration to intermediate or mixed wettability in the presence of nonionic and anionic

surfactants could significantly enhance oil recovery. Especially in surfactant-induced mixed wettability cases, more than 90 percent oil recoveries were obtained.

Gupta and Mohanty (2010) experimentally studied the effect of temperature on surfactant treatment in fractured carbonate formation. They concluded that even at high temperature (90°C) surfactants could change the wettability from oil-wet to intermediate/water-wet condition and high oil recovery (approximately 60% OOIP in 30 days) from surfactant solution imbibition was obtained at very low surfactant concentrations (<0.1wt%).

A few of factors affect surfactant-induced wettability alteration. These include surfactant structure, surfactant concentration, kinetics, pore surface composition, surfactant stability, co-surfactants, electrolytes and PH, temperature, pore structure and surface roughness, and reservoir structure (Schramm, 2000).

The primary mechanism of surfactant-induced wettability alteration has been studied and well explained in the literature (Schramm, 2000; Somasundaran and Zhang, 2006). The adsorption of surfactants on solid surface and the orientation surfactant assumes determine the wettability of the mineral surface. Four characteristic regions of adsorption isotherm are illustrated in Figure 4 (a).

In region I, individual surfactant molecules adsorb on the surface due to electrostatic interaction between the surfactant head group and the charged mineral surface corresponding to the low surfactant concentration. Region II indicates the onset of the surfactant aggregates (called hemi-micelles or admicelles) at the surface through the lateral interaction of hydrophobic chains which results in a marked increase in the slope of adsorption density. In region III, the decrease in the adsorption slope demonstrates that the surface is electrically neutralized by the sufficient adsorbed surfactant ions. A plateau adsorption takes place in Region IV, indicating the

approaching to the critical micelles concentration (CMC) of the surfactant and the completion of bilayer coverage of the surface. Above the CMC, further increase in surfactant concentration does not change the adsorption density.

(a)   (b)
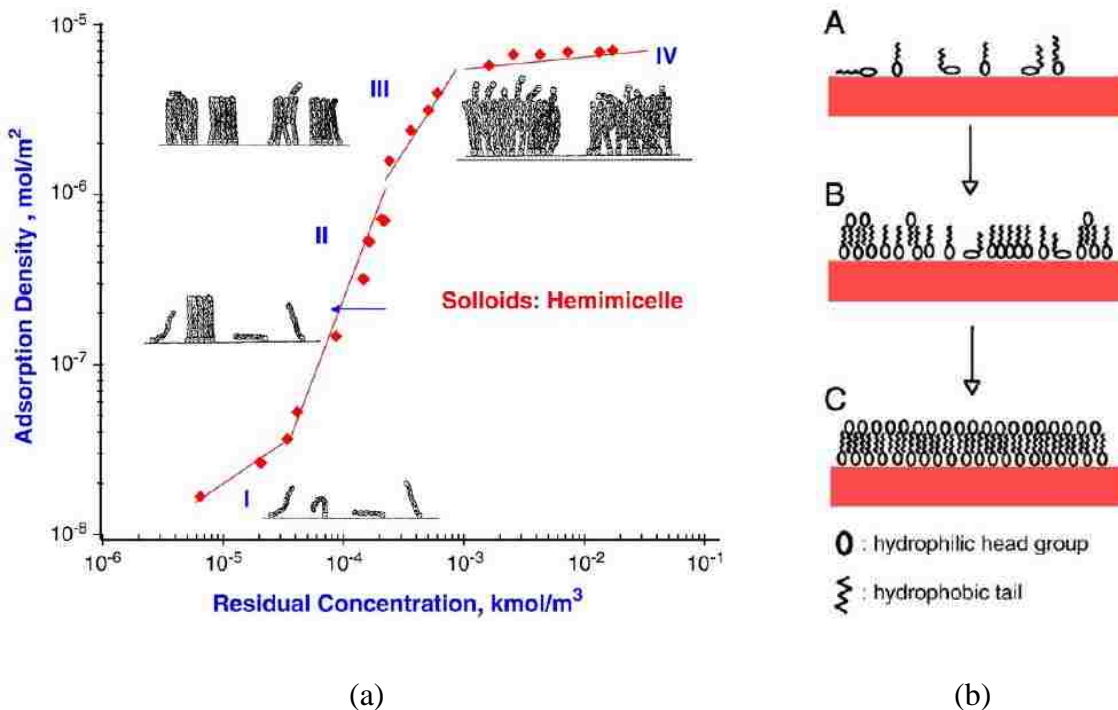
Figure 4: (a) Schematic Representation of the Growth of Aggregation for Various Regions of the Adsorption Isotherm. (b) Orientation Model for the Conformation of Surfactant at the Surfaces. A, B, C Indicate the Successive Stages of Adsorption (Somasundaran and Zhang, 2006)

The possibility of bilayered adsorption occurred above the CMC can restore wettability of the surface. Zhang et al. (1997) investigated the adsorption behavior of n-dodecyl-β-d-maltoside on the hydrophilic alumina surface and observed that the hydrophobicity of alumina surface drops further as the adsorption reaches the plateau region (IV) and the minimum hydrophobicity at this region possibly caused by the bilayer adsorption renders the surface hydrophilic. The schematic effect of surfactant orientation on the wettability is shown in Figure 4 (b). The bilayer adsorption (C) clearly shows that the hydrophilic groups of the surfactant orient towards the aqueous phase, which restores the surface to hydrophilicity. Austad and Standnes

(2003) performed spontaneous imbibitions experiments of aqueous surfactant solution into oil-wet carbonates and also found that the adsorbed anionic surfactants such as ethoxylated sulfonates onto the hydrophobic chalk surface formed a double layer creating a hydrophilic surface at the low imbibition rate.

2.6 Bond Number

Bond number is defined as the ratio of gravity forces to capillary forces. In this study, Bond number was used to quantitatively explain the condensate drop behavior on the surface. There are two types of forms of the Bond number, in which type 1 form Eq. (2) is only uses interfacial tension to represent the capillary force (Catchpole and Fulford, 1966; Hirasaki and Zhang, 2004), while type 2 Eq. (3) considers both interfacial tension and contact angles, thus uses the product of interfacial tension and the cosine of the contact angle for capillary forces (Babadagli, 2003).

$$N_B' = \frac{\Delta \rho g H D}{\sigma} \qquad (2) \qquad\qquad N_B^* = \frac{\Delta \rho g H \sqrt{\frac{k}{\phi}}}{\sigma \cos\theta} \qquad (3)$$

where N_B' and N_B^* are the Bond number, σ is the interfacial tension in mN/m, θ is the contact angle in degrees, $\Delta\rho$ is the density difference in g/cc, g is the acceleration due to gravity (cm/s^2), H is the height in cm, D is the drop diameter in cm, k is the permeability in cm^2 and ϕ is the porosity.

Ayirala et al. (2006) developed the type 2 form of the Bond number by replacing the term of $H\sqrt{\frac{k}{\phi}}$ in Eq. (3) with $(h\text{-}h_i)d$ to better discuss their experimental results of surfactant injection. From their study, they concluded that the Bond number including the contact angle term can better explain the rock-fluid interaction. The developed type 2 Bond number is expressed in Eq. (4) and the dimensions are depicted in Figure 5.

$$N_B = \frac{\Delta \rho g (h - h_i) d}{\sigma \cos\theta} \qquad (4)$$

where d and h are the diameter and the height of the drop on lower crystal at a given time t, in cm, and h_i is the initial height of equilibrium drop at time t=0 in cm.
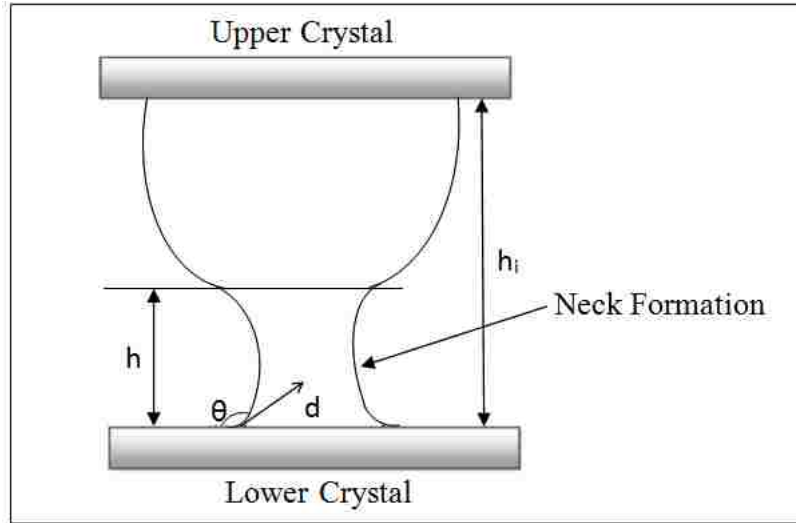
Figure 5: Schematic Description of the Equilibrium Drop between the Two Crystals

Hirasaki and Zhang (2004) concluded that an oil drop on a solid surface immersed in brine became unstable as the Bond number became unity or greater. In other words, the Bond number is less than unity or one indicating that the drop should be stable on the surface. Hence, in this study, the developed Bond number N_B defined in Eq. (4) was used to quantitatively discuss the dynamic behavior of condensate drop on the lower surface during surfactant injection at both ambient and reservoir conditions. The Bond number N_B' (in Eq. (2)) was also calculated for the purpose of comparison.

2.7   Fines Migration

Formation fines are defined as "unconfined solid particles made up of clay minerals or nonclay species deposited over geologic time or introduced during completion or drilling operation" (Sarkar and Sharma, 1990). Fines are always found in sandstone reservoirs. It is believed that the released fines migrating with flowing fluid can cause permeability reduction

23

and productivity decline during coreflood experiments. The main factors responsible for fines migration are salinity, flow rate, pH, temperature, rate of salinity change and adsorption of organic material from oil, which were investigated by several researchers.

Mungan (1965) experimentally investigated the effect of the pH and salinity change on fines permeability reduction in both consolidated and unconsolidated sandstone cores. They found that salinity and the pH change caused fines migration which blocked the pore passages and thus resulted in permeability reduction.

Clementz (1977) conducted the laboratory tests on freshly cut, consolidated Berea sandstone cores. The cores were treated by using a colloidal dispersion of heavy ends (asphaltene and resin) in solvent. The surface of the clay minerals present in the treated cores was then covered with heavy ends. Their results proved that formation clays were stabilized through adsorption of petroleum heavy ends

Gruesbeck and Collins (1982) designed laboratory testing procedures to study the effect of fines entrainment and deposition on permeability impairment. They reported that fines entrainment and redeposition were mechanism that cause abnormal productivity decline on the basis of their experimental results.

Khilar and Fogler (1983) carried out a number of experiments using Berea sandstone cores to study the water sensitivity of sandstone. Their results showed that clay particles were released only when the salt concentration falls below a critical salt concentration leading to decreasing the permeability. The rate of reduction in permeability was found to decrease with decreasing flow rate and temperature.

Valdya and Fogler (1992) performed coreflood experiments on Berea sandstone cores to examine the influence of pH and ion exchange on formation damages caused by fines migration.

They believed that ionic condition of low salinity and high pH appeared to be detrimental to formation permeability, resulting in fines migration and drastic damage. Also, salinity and pH were interrelated and therefore had to be considered simultaneously during development of injection strategies to minimize damage.

Additional factors including the presence of residual oil saturation (ROS), fractional flow of oil and water, polarity of oil and core wettability were studied by Sarkar and Sharma (1990). They conducted steady-state two-phase coreflood experiments to investigate the effect of these factors on fines migration. They concluded that both oil saturation and the wetting nature of the core significantly affected the extent and rate of permeability impairment. Wettability results determined from endpoint relative permeabilities demonstrated that oil-wet cores sustained slower and less damage than water-wet cores, because polar compounds present in the crude oil adsorbed on dry rock surfaces and thus prevented fines release.

Although fines migration can cause permeability decline, they are also considered by some researchers (Tang and Morrow, 1999; Lemon et al., 2011) as the mechanism for enhanced oil recovery or improved sweep efficiency due to the alteration of injected water salinity or composition. The details are discussed in the following section 2.8.3.

2.8   Brine Salinity and Composition

Brine salinity has been studied in the literature that it has a profound effect on the interfacial tension, reservoir wettability and oil recovery. Saline water is classified into three categories by US Geological Survey according to the salinity concentration level. The slightly saline water has around 1000 to 3000 ppm of salt. Moderately saline water is roughly about 3000 to 10,000 ppm, and highly saline water is in the range of 10,000 to 35,000 ppm. Seawater has a salinity of roughly 35,000 ppm, and it varies with location. Based on the fact that an optimal

salinity of the dissolved solids in the injection water may yield the highest oil recovery, the application of suitable brine salinity is important to improve oil recovery in existing and future water flooding projects.

2.8.1 Effect of Brine Salinity/Composition on Interfacial Tension

Among early studies on the effect of brine salinity on interfacial tension, Cai et al. (1996) conducted the experiments to measure interfacial tensions of ten normal-alkanes + water/brine and hydrocarbon mixture + water/brine systems by using a pendent drop instrument under high pressure and temperature conditions. Three types of salts, sodium chloride, calcium chloride and magnesium chloride were used in the experiments. They found that the presence of salt in the aqueous phase increased the interfacial tension, and this increase depended on the salt concentration but was insensitive to the salt species. The interfacial tension also slightly increased with an increase of the molecular weight of the n-alkane.

Abdel-Wali (1996) investigated the effect of polar compounds and salinity on the interfacial tension and wettability in rock/oil/brine systems. The polar compounds present in the crude oil were varied by adding different amounts of oleic acid and actadecylamine to the crude oil. The brine salinity was varied from 0 to 200,000ppm NaCl. Their results demonstrated that the oil-brine interfacial tension was lowered to minimum value when oleic acid concentration was 0.028gmol/l and brine salinity was 40,000ppm. Oleic acid was acting as an anionic surfactant resulting in low interfacial tension. However, the interfacial tension increased as the brine salinity increased from 40,000 to 200,000ppm NaCl because of decreasing the solubility level of oleic acid in water.

Vijapurapu and Rao (2004) studied the effect of brine dilution and surfactant addition on spreading and adhesion behavior of Yates crude oil on dolomite surface. The water-oil IFT

26

measured in their experiments initially decreased as the volume percent of brine in the mixture decreased but increased with further diluting the reservoir brine with de-ionized water. Similar behavior was found with synthetic brine. The critical spreading tension was defined as "the value of interfacial tension at which the receding contact angle reaches to 90°" based on the observation of the oil drop spreading on the solid surface when the IFT decreased below this critical value. Hence, the critical brine concentration should be determined to maximize the oil recovery based on IFT results.

Xu (2005) experimentally investigated the brine composition and salinity on interfacial tension using live crude oil at reservoir conditions. Deionized water, NaCl brine, $CaCl_2$ brine, reservoir brine and 50% dilution of reservoir brine were tested. The dilution of reservoir brine increased the value of IFT compared to the original reservoir brine IFT result. In addition, live oil-brine IFT in the pure CaCl2 brine had the highest equilibrium value compared to the other cases.

Hamouda and Karoussi (2008) presented contact angle and interfacial tension study on chalk rocks at high temperature condition. In their study, IFT measurement were conducted using a drop volume tensiometer with 0.005M stearic acid in n-decane/water containing 0.1M concentration of sodium sulfate ($NaSO_4$) or magnesium Chloride ($MgCl_2$) to test the effect of the ions in salt water. The results showed that IFT in the presence of magnesium ions was lower than that of sulfate ions or distilled water in a range of temperature from 82.4 to 158°F.

Okasha and Al-Shiwaish (2009) investigated the effect of synthetic reservoir brine salinity on interfacial tension of both dead and recombined oil in Arab-D carbonate reservoir. In their study, the synthetic brine was prepared at three different TDS levels: 241,943, 107,906 and 52,346 ppm, and the experiments were conducted at various temperatures and pressures for both

dead and live oil systems. IFT values for both dead and live oil systems showed decreasing trends as the brine salinity decreased at the same temperature and pressure conditions. IFT decreased further with dead oil system compared to live oil system due to the effect of dissolved gases in the live oil.

Alotaibi and Nasr-EL-Din (2009) measured the interfacial tension between n-dodecane and brines (NaCl solutions) with various salt contents using Pendent Drop Apparatus. Their results showed that lowering the NaCl concentration could not always reduce the interfacial tension. There existed a critical salt concentration at which a minimum interfacial tension between brine and oil could be obtained. They believed that this optimal salt concentration could improve oil recovery.

2.8.2   Effect of Brine Salinity/Composition on Wettability and Oil Recovery

Wettability is a major and important factor controlling the location, flow and distribution of fluids in a reservoir (Anderson, 1986a). More and more researchers believe that brine salinity, especially low salinity brine, had significant impact on wettability and thus oil recovery based on their laboratory studies conducted over a period of many years. One trend has appeared that the low salinity injection can obtain high oil recovery. It has also been reported that low salinity effects have been observed both in a secondary and tertiary flooding mode.

Tang and Morrow (1997) investigated the effect of brine salinity, oil composition and temperature on wettability and oil recovery by spontaneous imbibitions and waterflooding using Berea sandstone core. Salinity was varied by altering the concentration of total dissolved solids of the synthetic brine in proportion. It was reported that salinity of the connate and invading brines can have a major influence on wettability and oil recovery at reservoir temperature. Oil recovery increased with a decrease in salinity and increase in displacement temperature. Also

28

addition of alkanes (pentane, hexane and decane) to crude oil reduced the water wetness and thus increased oil recovery.

Sharma and Filoco (2000) performed centrifuge experiments to measure the drainage and imbibition relative permeability in two- and three-phase systems. Three crude oils, NaCl brines and Berea sandstone cores were used in the tests. (In drainage tests, crude oils were displaced by air at connate water, and there was no impact on oil recovery.) The oil recovery increased significantly with lowering the connate brine salinity in imbibition experiments. However, the salinity of the injection brine had no significant influence on the oil recovery. Hence, the salinity of the connate water was believed to be the primary factor controlling the oil recovery due to the wettability alternation from water-wet conditions to mixed-wet conditions.

Bagci et al. (2001) studied the effect of brine composition on oil recovery by waterflooding on limestone cores. The brines were NaCl, $CaCl_2$, KCl and binary mixture of them at two different concentrations of 2 and 5 wt%. From their study, the oil recovery increased with decrease in salinity of injected water and the highest oil recovery was 35.5% of OOIP for 2% KCl brine. Adjustment of the injected brine composition in waterflooding can provide a possible and economically feasible approach to increase oil production. Wettability alteration was mentioned as a reason for enhanced oil recovery in their study but without any further explanation or evidence of wettability alteration.

Høgnesen et al. (2005) investigated spontaneous imbibition into preferential oil-wet carbonates during a wettability alteration process. In their study, reservoir limestone, outcrop chalk cores, seawater and formation water were used at high temperature conditions. The results showed that sulfate present in the injection brine could act as a wettability modifying agent and alter it from oil-wet to water-wet. The sulfate ion concentration increasing with an increase of

temperature resulted in improved oil recovery. However, this strategy has limitations with regard to initial brine salinity and temperature.

Zhang et al. (2007) performed coreflooding experiments on consolidated reservoir cores by injecting high salinity formation brine of 29,690 ppm, low salinity brine of 1479 ppm, and two concentrations of sodium chloride (8000 and 1500 ppm). The mix-wet nature of cores was established by adsorption from crude oil in the presence of connate water. Low salinity brine injection increased oil recovery in both secondary and tertiary mode. Injection of 8000 ppm NaCl solution as a tertiary process did not show any effect on oil recovery. However, lowering NaCl salinity to 1500 ppm resulted in improved oil recovery, and thus an additional 4% OOIP recovery was obtained.

Patil et al. (2008) presented results from coreflooding experiments carried out to evaluate the potential of low salinity brine injection on EOR for Alaska North Slope as secondary recovery mode. Representative ANS cores and formation fluid samples were used in the coreflooding experiments. Injection brine salinities were varied from reservoir brine salinity of 22,000 TDS to 5500 TDS. Ultra low salinity (50-60 TDS) ANS lake water was also tested as a potential source of low salinity waterflooding. The wettability of core samples was determined using the Amott-Harvey wettability indices. Their study demonstrated that a decrease in injection brine salinity at reservoir temperature caused a reduction in residual oil saturation up to 20% and a slight increase in the Amott-Harvey wettability index and thus water-wetness of the core samples. Oil recovery also increased from 40 to 68% as changing the water salinity from 22,000 TDS to ultralow salinity ANS lake water, indicating that ANS lake water could be considered as a potential option for either waterflooding or dilution of the high salinity ANS reservoir brine.

Agbalaka et al. (2009) conducted coreflooding experiments to determine the recovery benefits of low salinity waterflood (< 2 wt % NaCl) compared to high salinity waterflood (4 wt % NaCl) and the role of wettability in any observed recovery benefit. Two sets of cores, Berea sandstone core and MPU shaly sandstone core were used at low and high temperature and pressure conditions. The results showed that low salinity waterflood had the potential for improved oil recovery either for secondary recovery or tertiary recovery process. It was also observed that heating injection brine could recover more oil than injecting brine of similar salinity at ambient temperature. In addition, an increase in water-wetness of the core samples for the decane/MPU core system by injecting low salinity brine caused a reduction in residual oil saturation and increase in the oil recovery.

Ashraf et al. (2010) reported their laboratory investigation of the relationship between rock wettability and oil recovery with low salinity water injection as secondary recovery process. Coreflooding experiments have been conducted by using synthetic brines and n-decane at room conditions on Berea sandstone cores with four different wettabilities ranging from water-wet to oil-wet. Their results showed that for all the salinity brines, oil recovery increased as wettability changed from water-wet to neutral-wet. Further alteration in wettability from neutral-wet to oil-wet led to a decrease in oil recovery. Also, oil recovery was observed higher for low salinity waterflooding than that for high salinity waterflooding when used as secondary recovery process.

Alotaibi et al. (2011) presented wettability study using low salinity water in sandstone reservoirs. Outcrop rocks (Berea and Scioto sandstone rocks) and stock-tank crude oil samples were used in all experiments. Synthetic formation brine, aquifer water, and seawater were evaluated under high pressure conditions. Contact angle as well as zeta potential of sandstone rocks and selected clay minerals was measured. On the basis of their results, they concluded that

low-salinity water altered the Berea sandstone wettability toward strongly water-wet conditions. The surface charge of Scioto sandstone was strongly affected by low-salinity water and the zeta potential of montmorillonite and chlorited clays was significantly decreased by low-salinity water. Hence, low-salinity waterflooding could improve oil recovery.

Encouraged by the observed potential of low salinity waterflooding in enhanced oil recovery at laboratory scale, several field trials have been carried out. The log-inject-log tests successfully performed near the well bore region using four different salinity brines showed that low salinity water injection significantly reduced residual oil saturation by 25 to 50% (Webb et al., 2004). Exact mechanisms for the increased production were not well understood, but the wettability alteration due to the low salinity water injection may be an important reason.

McGuire et al. (2005) used single well chemical tracer tests (SWCTT) in the Alaska field to evaluate the low salinity water injection effect on remaining oil saturation. The SWCTT results demonstrated that residual oil saturation was substantially decreased by low salinity water injection. And the low salinity EOR benefits ranged from 6 to 12% OOIP, resulting in an increase in waterflood recovery of 8 to 19%.

Robertson (2007) reported historical field evidence by using low-salinity waterflooding to improve oil recovery. The results turned out that as the salinity ratio (the ration of the salinity of the injection water to the salinity of the initial formation water) decreased, the oil recovery tended to increase. It indicated that lower salinity floods tended to obtain higher oil recovery.

Seccombe et al. (2008) presented tertiary LoSal^{TM} EOR benefits at the Endicott field located on the North Slope of Alaska. Single well chemical tracer tests (SWCTT) have also been used in this field to quantify the low salinity water injection effect as tertiary process on residual

oil saturation. There is good agreement between coreflood results and SWCT tests. The additional oil recovery is 26 percent obtained by low salinity waterflooding.

Skrettingland et al. (2011) evaluated the effect of low salinity (lowsal) waterflooding on enhanced oil recovery at the Snorre field. They conducted both coreflood experiments and a single-well chemical tracer-test (SWCTT) field pilot to measure the residual oil saturation after seawaterflood and after lowsal flooding. Regarding their study, no significant changes in the remaining oil saturation were shown in both laboratory measurements and a Snorre field test by using low salinity waterflooding. Hence the potential for IOR by lowsal flooding is low for this field case. The reason for this is believed to be that the initial wetting condition of Snorre field is close to optimal so that even for high salinity water injection like seawater injection is also efficient to improve oil recovery. Although this is a disappointed case, it provides further evidence of consistency between laboratory and field tests, which helps to screen low-salinity waterflooding candidates (Morrow and Buckley, 2011).

2.8.3 Mechanisms of Brine Salinity on Oil Recovery

As discussed above, the wettability alteration is believed to be the main mechanism for brine salinity effect on oil recovery. The characteristics of the brine solution, including the pH, types and concentrations of ions, were discussed as the main factors that can affect the wettability. Other factors, such as the clay swelling/dispersion, fines migration, and multiple-component ionic exchange (MIE), were also investigated as contributions to the oil recovery enhancement.

Enhanced oil recovery ascribing to clay swelling was discussed to be the main cause by several researchers (Smith, 1942; Martin, 1959). Based on the results of mineral oil recovery test

33

using fresh water injection, Bernerd (1967) concluded that the clay swelling and dispersion in the sandstone rock, along with increased pressure drop, improved the oil production.

Tang and Morrow (1999) summarized that fines migration played a key role in the sensitivity of oil recovery to brine salinity when they conducted coreflooding experiments on Berea sandstone cores. It was observed that oil recovery increased with the decreasing of the brine salinity. Fines, mainly kaolinite, were detached from the cores during low salinity waterflood. As a result, they believed that the detachment and stripping of mobile mix-wet fines/clays from the cores was the main mechanism for increasing the oil recovery. Lemon et al. (2011) developed a model for particle detachment to describe waterflood with fines migration and evaluate the effects of fines migration on waterflood sweep efficiency under a given injection/production rate. From their study, fines migration due to the alteration of the injected water composition were believed to increase waterflood sweep efficiency. The mechanism for this was proposed that formation damage caused by mobilized fines in the swept zone tended to make the permeability distribution across the breakthrough period more uniform. Hence, the induced formation damage resulted in the breakthrough period increase and improved sweep efficiency for a given volume of injected water. However, Lager et al. (2006) reported that no fines migration has been observed at reduced or full reservoir condition of low salinity waterflood experiments. These results question the relationship between fines migration and improved oil recovery.

According to Lager et al. (2006), multiple-component ionic exchange (MIE) between clay mineral surfaces and the injected brine was responsible for the improvement in oil recovery using low salinity waterflooding. Effluent sample analysis after coreflood showed a sharp decrease in Mg^{2+}, indicating that Mg^{2+} was strongly adsorbed at rock matrix. Thus, polar organic

compounds are believed to be desorbed and replaced with multivalent cations during the injection of low salinity brine. In theory, desorption of polar compounds form the clay surface results in an increase in oil recovery since the clay surface wettability is altered towards more water-wet surface. They designed the coreflood experiments to test this mechanism, and the results matched the predictions. This implied that the injection of low salinity water led to higher oil recovery in the presence of multivalent cations in the connate brine because the bonds holding oil in contact with the rock surface were broken which changes the wettability.

The MIE mechanism was discussed further in papers (Lager et al., 2008; Seccombe et al., 2008). The sharp drop in Mg^{2+} concentration was observed, and it confirmed the self-sharpening front inferred from the MIE mechanism (Seccombe et al., 2008). A non-sharpening front would have resulted in a highly dispersed response where concentration would have decreased gradually as observed in field tracers.

Nasralla et al. (2011) conducted the coreflood experiments to explain the mechanisms involved when recovering oil with low salinity water injection. Coreflood experiments were run in the secondary and tertiary modes to investigate the effect of water salinity (0, ~5000, ~55,000 and ~174,000mg/l) on oil recovery. They concluded that the oil recovery was improved by low salinity water injection in secondary mode but was not impacted in tertiary mode. They believed that cation exchange was responsible for higher oil recovery from low salinity water injection because cation exchange reduced electrostatic attraction forces between crude oil and the rock surface by altering the rock surface charge.

From the above review, it can be seen that the evaluations of brine salinity and composition effects on wettability and oil recovery, in almost all previous research, were based on the coreflood tests for crude oils. None of them performed an experimental investigation to

study brine salinity and composition effect near the condensate buildup region in gas-condensate reservoirs. Also, the Amott-Harvey method was mainly used in their studies to characterize wettability, but this method cannot accurately measure neutral wettability (Anderson, 1986b) nor can it be used at reservoir pressures. Wettability determination from contact angle measurement using real reservoir fluids is the best method to evaluate wettability (Anderson, 1986b).

3. EXPERIMENTAL APPARATUS AND PROCEDURES

The experiments conducted in this study include two systems, condensate-synthetic reservoir brine containing surfactants and condensate-different synthetic brines. In the first system, interfacial tension and contact angle measurements with or without surfactants were performed under both ambient and reservoir conditions using the ambient and the high-pressure high-temperature optical cells and the associated apparatus. The coreflood experiments were also conducted to test the effect of surfactants on gas relative permeability at ambient conditions. Hence, the fluids used in this first system are condensate, synthetic reservoir brine, methane and nitrogen. And two types of surfactants, anionic and nonionic, were examined. The experiments for the second system only involved interfacial tension and contact angle measurements at ambient conditions. The ambient optical cell was used in this system. The pH of brines was also measured. The fluids, therefore, used in this part are condensate and synthetic brines including multi-component and single-salt brines. The details of experimental apparatus and procedure for both systems are similar and thus are not discussed separately.

3.1 Materials

3.1.1 Fluids

The fluids used in this work were synthetic brines, condensate, methane and nitrogen. The oil phase, condensate, supplied by a major oil company is clear and the specific gravity is about 62°API. The composition of the condensate is presented in Table 2. The density and viscosity of the condensate at 22 °C were 0.7340 g/cm^3 and 1.0028 cp, respectively. The properties of heptanes plus of Buckhorn crude oil are also listed in Table 2 (Sequeira, 2006). It can be seen from Table 2 that the condensate sample contains 71.7 mole percent heptanes plus (C7+). The molecular weight of the heptanes plus (C7+) fraction in the sample is 116.5 and its

specific gravity is 0.76. In contrast, the heptanes plus (C7+) fraction of stock tank Buckhorn crude oil was about 91.3 mole percent with a molecular weight and specific gravity of 213.3 and 0.84, respectively. This condensate sample contains less heptanes plus (C7+), indicating the condensate is low in heavy ends.

Table 2: Compositional Analysis of Condensate

Component	Carbon No.	Mole %	Weight %
Methane	C1	0.002	0.000
Ethane	C2	0.045	0.013
Propane	C3	0.896	0.377
i-Butane	iC4	1.156	0.641
-Butane	nC4	3.580	1.984
i-Pentane	iC5	4.333	3.478
n-Pentane	nC5	5.590	3.846
Hexane	C6	12.722	10.455
Heptanes Plus	C7+	71.676	79.703
Total		100.000	100.000
Properties of Heptanes Plus (C7+) of Condensate		C7+ of Buckhorn stock tank oil	
Mole%	71.7	91.3	
Molecular Weight	116.5	213.3	
Specific Gravity @60/60°F	0.76	0.84	

In this study, different synthetic brines were used including multi-component brines and single-salt brines. Synthetic reservoir brine with 0.9995 g/cm^3 density and 1.2298 cp viscosity at 22 °C was prepared which had the same composition as that of reservoir brine provided by the company. The composition of reservoir brine is listed in Table 3. All brines were prepared by adding salts into the deionized water and then evacuated for one hour before use to remove dissolved gas. The salts were purchased from Fisher Scientific and had a purity of 99.9%.

Table 3: Formation Brine Compositions

Component	mol/l	g/l
$AlCl_3 \cdot 6H_2O$	0.00019	0.0459
$CaCl_2 \cdot 2H_2O$	0.00948	1.3937
$FeCl_3 \cdot 6H_2O$	0.00013	0.0351
KCl	0.00013	0.0097
$MgCl_2 \cdot 6H_2O$	0.00078	0.1586
NaCl	0.02250	1.3149
$NaHCO_3$	0.00180	0.1512
TDS	0.03501	3.1090
PH	7.47	

For multi-component brines, before evacuating they had to be filtered through Whatman No.1 filter paper under vacuum due to the precipitation observed in the system. Salinities of these brines were then determined using Hatch Conductivity Probe attached to sensIONTM5 Conductivity Meter which is supplied by Hatch Company. Multi-component brines in which the composition is same as the synthetic reservoir brine contain two sets of brines: low salinity and high salinity brines. The set of low salinity brines includes 10 times dilutes, 4 times dilutes, and twice dilutes, synthetic reservoir brine and deionized water. High salinity brines include four versions of brines which are 10 times more, 20 times more, 30 times more and 50 times more brines. Table 4 lists the types of multi-component brines and their salinities measured by Conductivity Meter. The salinity of synthetic reservoir brine shown in Table 4 is low and about 2700 ppm. The multi-component brine salinities tested in this study were varied from 0ppm to 125,500 ppm (Table 4).

Five single-salt brines with two salinities were tested in this study. The types of single-salt brines and salinities are displayed in Table 5. The salts are sodium chloride (NaCl), calcium

chloride ($CaCl_2$), magnesium chloride ($MgCl_2$), aluminum chloride ($AlCl_3$) and ferric chloride ($FeCl_3$), as shown in Table 5. Hence, ten single-salt brines were prepared to investigate the effect of ionic strength on wetting and spreading characteristics.

Table 4: Types and Salinities of Multi-Component Brines

Type of Brine	TDS, g/l	Brine Salinity, ppm
Low Salinity	0	0
	0.3109	300
	0.7773	700
	1.5545	1300
Synthetic Reservoir Brine	3.109	2700
High Salinity	31.09	26,800
	62.180	52,800
	93.271	77,910
	155.45	125,500

Table 5: Types and Salinities of Single-Salt Brines

	Type of Brine	Brine Salinity, ppm
Low Salinity	NaCl	3100
	$CaCl_2$	
	$MgCl_2$	
	$AlCl_3$	
	$FeCl_3$	
High Salinity	NaCl	93,300
	$CaCl_2$	
	$MgCl_2$	
	$AlCl_3$	
	$FeCl_3$	

Pure grade methane obtained from the Phillips Co. was used in experiments of interfacial tension (IFT) measurements without further purification. It contains 99.999% mole fraction methane. Nitrogen obtained from Capital Welders Supply Co. was used as gas phase in the coreflood experiments. The viscosity of nitrogen is 0.01761cp at 22 °C.

3.1.2   Chemicals

In this study, two surfactants with trade names ALFOTERRA 123-4S and NOVEL TDA-12 Ethoxylate supplied by Sasol North America Inc. were used. NTDA-12 is an isotridecanol fatty alcohol ethoxylate nonionic surfactant. It is water-soluble hazy liquid with the specific gravity (at 40 °C) of 1.01.

ALFO123-4S is a water-soluble anionic surfactant with an appearance of clear pale yellow liquid. It is a monoalkyl branched propoxy sulfate and has 12-13 number of hydrophobic carbons and 4 moles of propoxylation. Its mono branched alkyl hydrophobe allows for greater interaction with the oil phase while maintaining good solubility. The family of ALFOTERRA surfactants was also found to be a better anionic surfactant at wettability alteration on calcite surfaces to intermediate wet compared to cationic surfactant (Seethepalli et al., 2004).

In preparing a solution for treatment, the required weight fraction surfactant was added to the synthetic brine. Three surfactant concentrations of 500, 1500 and 3000 ppm were used in experiments of contact angle measurements at both ambient and reservoir conditions. Two concentrations (1500 ppm and 3000 ppm) were used in coreflood experiments at ambient conditions. The viscosities of 1500 and 3000 ppm surfactant solutions were 1.118 and 1.2298 cp at 22 °C, respectively.

3.1.3   Rocks

The selected gas condensate reservoir for this study is the Tahoe reservoir in the Gulf of Mexico, approximately 140 miles east/southeast of New Orleans and 105 miles south of Mobile, Alabama. The reservoir depth is about 10,000 feet subsea (White, et al, 1992). The initial reservoir pressure was about 5000 psia and has fallen now to 2264 psia. The reservoir temperature is 210 °F. The dew point pressure was reported to be about 4935 psia and the initial

producing gas-oil ratio (GOR) was 33,000 scf/STB. The reservoir is highly laminated, composed of many layers of thin shale and sandstone, but only the sandstone layers contribute to gas production. The reservoir porosity and connate water saturation are about 0.28 and 0.26, respectively.

In our experiments, quartz and Berea sandstone core were chosen to represent the sandstone reservoir rock. The quartz substrate for contact angle measurements and wettability determination was purchased from Ward's Nature Science. The glass substrates and the glass capillary tube used in the capillary rise technique were obtained from the Glass Blowing Shop of the Department of Chemistry at Louisiana State University. The types of glass used in the experiments are all of the same material, namely borosilicate. The glass capillary tube, used in IFT measurements, had an internal diameter of 0.106 cm.

Berea sandstone cores, 2 in diameter and 1ft long, were purchased from Cleveland Quarries for use in the coreflood experiments. The permeability of the fresh cores ranged from 200 to 500 mD and their porosity was around 20%.

3.2   Experimental Apparatus

3.2.1   Ambient and High-Pressure High-Temperature Optical Cells

In this work, the ambient and the high-pressure high-temperature optical cells and the associated apparatus were used for the experiments of interfacial tension (IFT) and contact angle measurements under both ambient and reservoir conditions of 2264 psia and 210 °F.

Figure 6 shows the ambient optical cell (A) and its associated apparatus including light source (B), goniometer (C) and video camera (D). The interior of the ambient optical cell was coated with Teflon against corrosion and was saliently designed for measuring interfacial tension (IFT) and contact angles. Two crystal holders, upper and lower, were positioned in the cell for

measuring contact angles. The upper crystal holder moves in the vertical direction, while the lower one moves horizontally. In addition, the lower holder can be rotated around its horizontal axis so that both of the crystal surfaces can be used for measuring contact angles. All parts of the cell which would contact with the test fluid such as brine are made of Hastalloy C-276 to prevent corrosion and consequent contamination of fluid samples during relatively long periods of time required in the experiments. A capillary tube was inserted through the bottom of the cell, and its height adjusted to meet the requirement in each experiment. The oil drop was injected by a syringe which was connected with the capillary tubing.
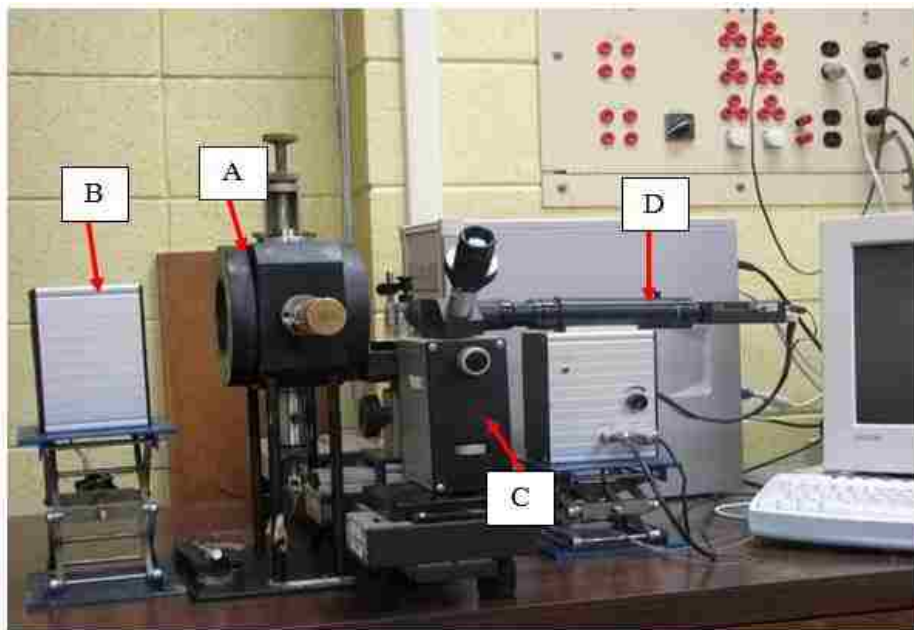
Figure 6: Ambient DDDC Optical Cell Apparatus
(A: Ambient Optical Cell; B: Light Source; C: Goniometer; D: Video Camera)

The ambient optical cell is illuminated by light source (B). The video camera (D) connected with a computer is used to record the image or video for IFT and contact angle measurements. It can also provide direct visual observations of rock-fluid-fluid interfacial behavior. The goniometer (C) is an optical instrument for measuring contact angles and distances.

DSA software from KRUSS Company is used to calculate the interfacial tension, and MB ruler software is used to measure distances and angles.

The high-pressure high-temperature optical cell as well as its associated apparatus shown in Figure 7 was used for the experiments under the reservoir conditions. This optical cell (A) has been built to measure IFT and contact angle at elevated temperatures and pressures and its design rating is 20,000 psi and 400 °F. The high-pressure high-temperature optical cell is similar to above ambient optical cell but still has its unique features as described below.

The high-pressure high-temperature optical cell has four adjustable arms. The top one and a side one are designed to hold crystals while the other side arm is used for holding the calibration ball. The bottom arm is designed for mounting the needle tip which is used to inject oil drops into the cell. All of the four arms can be rotated and moved in and out of the cell chamber during high pressure tests.
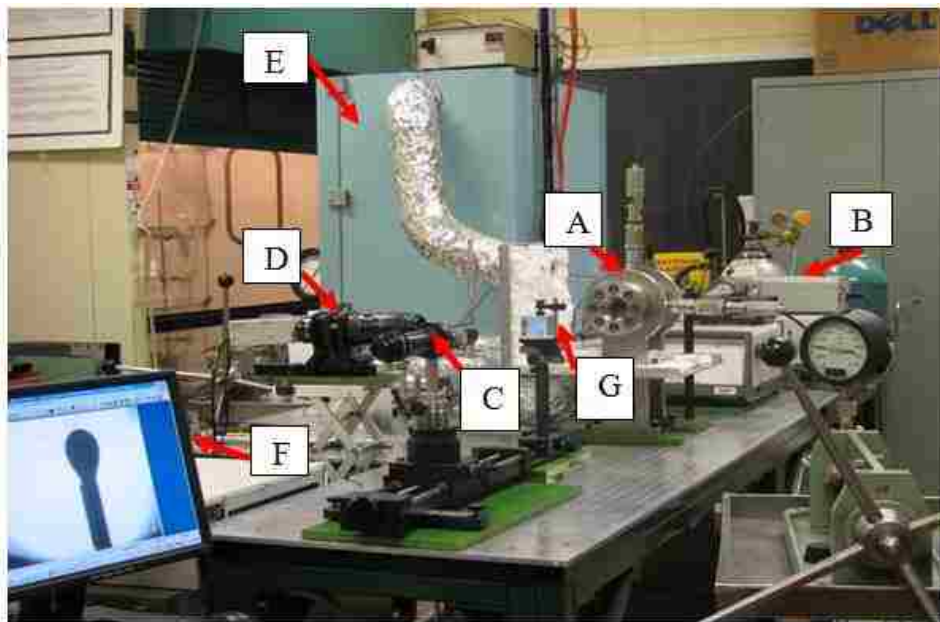
Figure 7: High-Pressure High-Temperature (HPHT) Optical Cell Apparatus
(A: HPHT Optical Cell; B: Light Source; C: Goniometer; D: Digital Video Camera; E: Oven; F: Image Analysis System; G: Beam Splitter)

The oven (E) is used to provide the high temperature required for the optical cell. The light source (B), goniometer (C) and digital video camera (D) as illustrated in Figure 7 are also used in this high-pressure high-temperature apparatus much like with the ambient apparatus. The beam splitter (G) is an optical glass used to enable the image observation for the digital camera and the goniometer at the same time. The image analysis system including a computer which is connected to the digital video camera and installed commercial software (DSA and MB Ruler) is employed to record images or videos to determine IFT and measure contact angles.

3.2.2 Coreflood Apparatus

The schematic of experimental setup for conducting unsteady state relative permeabilties measurements in this study is shown in Figure 8 and 9. A Berea sandstone core was placed in the coreholder as displayed in Figure 8 and 9, and fluids in the transfer vessel were injected with a constant rate through the pump at inlet, while the outlet pressure was maintained at atmospheric pressure. A back-pressure regulator (BPR) was used for control the upstream flowing pressure of the core only in gas flood step. The production burette and the wet test gas meter were used to measure liquid volume and gas flow rate, respectively.
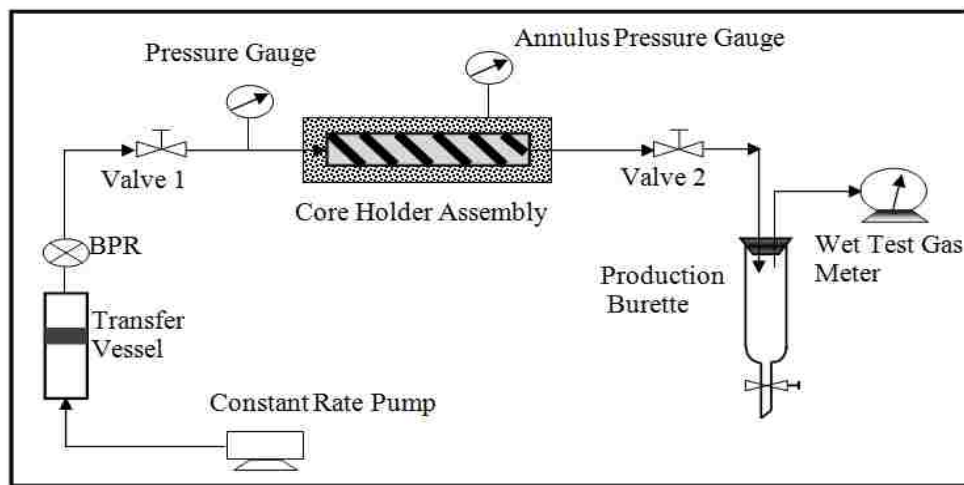
Figure 8: Schematic of Coreflood Apparatus Used for Berea Rock-Fluids System
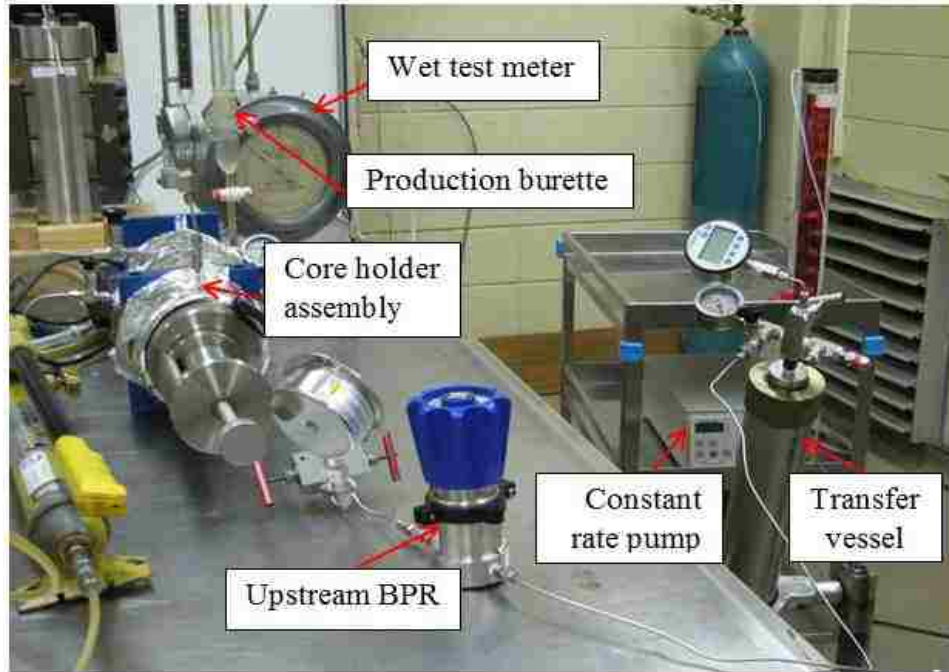
Figure 9: Coreflood Apparatus

3.3 Experimental Preparation and Cleaning

3.3.1 Optical Cells and the Associated Apparatus Cleaning

The ambient optical cell was first cleaned with de-ionized water. After each experiment, the inlet valve was opened to let some de-ionized water or brine in so that the oil floating at the top can be drained out from the outlet valve, aiming to avoid the floating oil falling down to touch and contaminate the cell's Teflon interior. Afterwards, the ambient optical cell was cleaned by toluene to dissolve all the crude oil, followed by acetone to dissolve all the toluene, and finally deionized water (DIW) was used to remove any traces of acetone. Then the cell was dried before beginning each experiment.

The high pressure in the high-pressure high-temperature optical cell after each experiment was released and lowered to ambient pressure after which the fluids were drained from the bottom of the cell. The optical cell was then disconnected from tubing and valves. The cleaning procedure for HPHT optical cell is similar to that for above ambient optical cell by

46

using the same sequence of chemicals (toluene, acetone, and DIW). After drying with nitrogen, the cell was heated by the oven to further evaporate any traces of DIW, toluene and acetone before the start of the next experiment.

The other accessories for both optical cells including all glassware such as glass window, syringe, tubing and valves were also cleaned by rinsing with toluene, followed by acetone, and then rinsed well with de-ionized water. All the solvent cleaning steps were conducted in a well-ventilated fume hood. The transfer vessels which were used to store synthetic brine and surfactant solution were cleaned with a low concentration solution of an organic acid and then flushed with de-ionized water. All of the apparatus was allowed to dry thoroughly before use.

3.3.2 Core Cleaning

The detailed core cleaning procedure has been discussed in elsewhere (Mwangi, 2010). A sequence of solvents was used to clean the core after surfactant flood. First, methylene chloride was injected into the core in both backward and forward directions about 2 pore volumes (PV). Methylene chloride acted as a buffer between the brine and the cleaning fluids to prevent salts precipitating from the brine. It was also a good organic solvent and could be used to remove part of condensate. Isopropyl alcohol (IPA) was followed to inject to the core in the forward direction about 2 PV to get rid of the connate water. Care should be taken in this step, because the pressure drop increased dramatically from several hundred psi to around 2000 psi. The pressure drop decreased as IPA broke through. The similar observation was reported during this IPA cleaning step (Mwangi, 2010). The probable explanation is to be the interaction between IPA and the rock grains.

Next, methylene chloride was re-introduced to the core in both directions about 2 PV to displace IPA, followed by toluene. Toluene removed residual condensate from the core. It was

also injected about 2 PV in the forward and backward directions. The core was then cleaned further by methylene chloride and brine. About 2 PV methylene chloride was flowed to displace toluene, followed by 2 PV brine to flush methylene chloride. Injections of methylene chloride and brine were performed in the forward and backward directions as well.

Finally, the core was evacuated for 3 to 4 hours by the vacuum pump. This last step might help decrease the pressure drop of the core and remove the traces of methylene chloride. After completion of this series of steps, the core was ready for absolute permeability test.

3.3.3   Rocks Preparation

The quartz rock sample was first cut into suitable pieces by a cutting machine, and then its surface was polished using a grinding machine with four meshes of sandpapers. The polished quartz sample was cleaned with toluene and acetone, and then soaked into a heated bath of concentrated sulfuric acid for 30 minutes. All the samples were rinsed with deionized water after cooling and dried completely in air prior to use.

The Berea sandstone cores were wrapped with a layer of Teflon tape and then placed inside a Viton rubber sleeve. The Teflon tape was used to prevent fluids from interacting with the sleeve. The Viton sleeve prevented fluids from contacting the hydraulic oil in the annulus.

3.3.4   Surfactants Thermal Stability Screening

The structural stability of the anionic and nonionic surfactants at high temperature has to be tested for specific reservoir conditions although they were used in the experiments at ambient conditions and did not show any cloudiness. Figure 10 displays the experimental equipment was set up for testing surfactants thermal stability. Surfactants were mixed with synthetic brine at a certain concentration. Surfactant solution was contained in a glass conical flask with a rubber stopper which had a hole in the center as can be seen in Figure 10. The surfactant solution in the

flask in Figure 10 was nonionic TDA-12 at 500 ppm concentration as an example. A thermometer was inserted through the hole of the stopper to measure the temperature of the surfactant solution. The flask was placed on a magnetic heating panel, and a magnetic stirring bar was also put in the flask to mix the surfactant solution to be heated evenly.
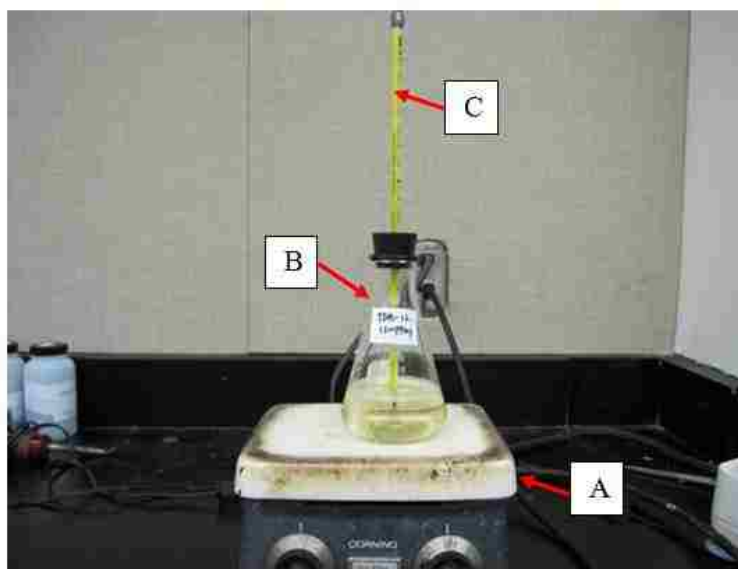
Figure 10: Experimental Set up for Thermal Stability Test
(A: Magnetic Heating Panel; B: Conical Flask; C: Thermometer)

The anionic surfactant, ALFOTERRA 123-4S, was a high performing surfactant at room temperature and showed more effectiveness. When the 500 ppm and 3000 ppm concentrations of this surfactant solution were heated up to 210 ℉ (~99 ℃), both solutions still remained clear. This demonstrates that this anionic surfactant has thermal stability and can be applied at reservoir conditions.

Figure 11 displays phase behavior pictures for 500 ppm concentrations of two nonionic surfactants TDA-12 and FC-4430 at room and reservoir temperature. It can be seen that the 500 ppm nonionic surfactant (NOVEL TDA-12 Ethoxylate) solution in brine formed a clear solution at room temperature of 72 ℉ (22 ℃). But the same solution turned cloudy at 197 ℉ (87.8 ℃)

49

and it became a fully hazy liquid at reservoir temperature of 210 ℉, indicating that this nonionic surfactant was not stable at high temperature. Therefore, this surfactant was rejected for the high temperature application for this particular condensate reservoir.

Apart from the nonionic surfactant TDA-12, several other available nonionic surfactants in our lab were also screened for high temperature condition. 500 ppm NOVEL TDA-3 and TDA-6 Ethoxylate (from Sasol North Inc.) solution in brine formed cloudy solutions at room temperature. They remained cloudy at reservoir temperature of 210 ℉. FC- 4430 and FC- 4432 nonionic surfactants from 3M Co. did not show any cloudiness at room temperature for 500ppm concentration solution in brine, but the same solutions became cloudy at 92 ℉ (33.3 ℃) as shown in Figure 11. All of these nonionic surfactants were rejected for use in the experiments at reservoir conditions as well.

Figure 11: Phase Behavior Pictures for 500 ppm Nonionic Surfactants TDA-12 and FC-4430 Solutions at 72 °F and 210 °F

3.3.5   Density Meter Calibration

The densities of fluids play a key role to obtain accurate fluid-fluid interfacial tensions (IFT) or surface tension when the pendant drop method and capillary rise technique are used. In this study, the DMA 4500 densitometer and density measuring cell DMA HP purchased from the

50

Anton Paar Company were used to measure the phase densities at ambient conditions and high temperature high pressure conditions, respectively.

The DMA 4500 density meter offers not only density measurement at ambient conditions but also the evaluation unit for DMA HP. And its maximum density deviation is 0.00010 g/cm^3. The DMA HP, the high pressure and high temperature density measuring cell which has to be connected to the DMA 4500 to display the measuring parameters, is designed to measure the density of gases and liquids at elevated pressures ranging from 0 to 10,000 psi and elevated temperatures from +14 ºF to +392 ºF.

Before each measurement, the DMA 4500 was totally cleaned with toluene and acetone and then blow dried with air. The DMA HP needs to be set at the specific temperature according to the experiment requirement and then completely cleaned with toluene, acetone and blown dry with nitrogen. The detailed procedure for using the DMA 4500 and DMA HP can be found in the manual provided by the Anton Paar Company. Both of them have similar measuring procedure, for example, activating the required method, ensuring that the measuring cell is clean and dry and then introducing the sample in the measuring cell. But the difference between them is that the temperature should first be set at often reservoir temperature for the DMA HP. In addition, a syringe is used to inject the sample for DMA 4500, while a pump is used for DMA HP to generate high pressures and inject the sample into the cell.

Two standard fluids pairs, air, degassed deionized water (DIW) and n-decane, degassed DIW, were used to calibrate DMA 4500 at 20 ºC and DMA HP at reservoir temperature of 210 °F (~99 ºC), respectively. After calibration, a value of 0.99820 g/cm^3 was obtained for DIW by DMA 4500. It showed good agreement with the published value of 0.99821 g/cm^3 from the National Institute of Standards and Technology (NIST) website.

The calibration of the DMA HP density cell was performed at pressures of 2264 and 4935 psia which correspond to the current reservoir pressure and initial reservoir pressure. After density adjustment at 210 ºF, the densities of DIW and n-decane were then measured at both pressure conditions. The density of 0.68613 g/cm^3 at 2264 psia for n-decane and 0.97432 g/cm^3 density of DIW at 4935 psia were also in good agreement with the value of 0.68610 g/cm^3 and 0.9743 g/cm^3 provided by NIST website. Both calibration results reveal that DMA 4500 densitometer and DMA HP density cell can accurately measure densities of unknown fluid samples at ambient conditions as well as reservoir conditions.

3.3.6 Conductivity Meter and pH Meter

The salinity and pH of brine are believed to be very important in determining the wettability because they strongly influence the surface charge on the rock surface and fluid interfaces, which in turn affect the adsorption of surfactants in crude oil (Anderson, 1986). In this study, the salinity and pH were determined using a Conductivity Meter and a pH meter.

The pH measurements were conducted by an Orion 9157BN pH electrode (0~14 pH) connected with a Thermo Orion pH meter (model 420A plus) purchased from Thermo Scientific. Three pH buffers (4.01, 7.00 and 10.01) were also purchased from Thermo Scientific to calibrate the pH meter before pH is measured. At least two of them were selected for calibration depending on the sample pH range. In other words, the two chosen buffers should bracket the sample pH for better accuracy.

Brine salinity was measured using Hatch Conductivity Probe attached to sensION^{TM}5 Conductivity Meter supplied by Hatch Company. The designed measurement range of Conductivity Meter for TDS/salinity is 0~50,000 mg/L (as NaCl)/0~42 ppt. The temperature can

vary from -10 to 105 ℃. The accuracy of the meter is ±0.5% of full scale for TDS and ±0.1 ppt (-2 to 35 ℃) for salinity.

Before use the Conductivity Meter, the calibration was performed using the known standards which were chosen in the expected range of the samples. In this study, two sodium chloride (NaCl) standard solutions having conductivity of 1000±10 μS/cm (500±5 mg/L TDS) and 18,000±50 μS/cm (9000±25 mg/L TDS) were used to calibrate the meter for low and median brine salinity measurement. Salinity standard solution (35.0 ppt as salinity, 0.450 molal KCl, 53.0 mS/cm Conductivity at 25 ℃) was used for high salinity calibration.

It is noteworthy here that for very high brine salinity which exceeds the maximum salinity of 42 ppt of the Conductivity Meter, the salinity measurement was performed using several times dilute of high salinity brine which would be in the range of the meter.

The calibrations for both pH meter and Conductivity meter were followed the procedure of the manual provided by the company.

3.4   Experimental Procedure

3.4.1   Interfacial Tension Measurement by Pendent Drop Method

In this study, to obtain spreading coefficients, interfacial tensions (IFT) between three systems condensate-water, methane-water and condensate-methane were needed to be determined. Pendent drop method was mainly employed for measuring interfacial tensions. Commercial DSA software was used to calculate interfacial tensions from the drop images. The procedures of interfacial tension measurement carried out in both ambient and HTHP optical cells are described as below.

Ambient-condition experiments including interfacial tension (IFT) measurements and dynamic contact angle measurements were performed at atmospheric pressure and room

temperature (23 ± 2°C or 74 ± 3°F) in the ambient optical cell. Heavy liquid such as brine or surfactant containing brine was taken in a large container, which was kept at a sufficient height above the cell to allow liquid to flow through plastic tubing by gravity. Thoroughly cleaned ambient optical cell was gradually filled up with this heavy fluid. Some fluid was allowed to drain from the outlet valve to ensure that there was no air bubbles trapped in the ambient cell. The inlet valve was then closed and the outlet was kept open during the entire time of the experiment. The light fluid such as condensate or gas was injected into the ambient optical cell using the syringe. The syringe piston was moved slowly to increase the pendent drop volume until the drop volume reached the maximum before leaving the tip of the needle.

The cleaned and sealed high-pressure-high-temperature (HPHT) optical cell was initially filled with denser fluid (synthetic brine or condensate) and then the cell pressure was increased close to reservoir pressure. The cell was left alone for several minutes to check for leaks in the system. The optical cell was then heated by the oven. Care was taken to monitor the pressure as the cell temperature was increased to reservoir temperature of 210 °F. The light fluid (condensate or gas) was then introduced through the injection tip by using a hand pump into the clean HPHT optical cell. The pump handle was moved slowly to obtain the maximum pendant drop volume.

A condensate drop in the synthetic brine at reservoir conditions serves as an example to illustrate this process of using the pendant drop technique to obtain the IFT in Figure 12. The fourth picture of Figure 12 shows the biggest condensate drop achieved. The images at this particular moment were captured and saved. This DSA software program is thus run to calculate the interfacial tension (IFT) values by fitting the experimentally measured drop contour to the theoretical curve based on Young-Laplace equation which relates the drop profile to the

interfacial tension. This procedure of IFT measurement is repeated for 10~15 pendent drop images to obtain an average value of IFT.
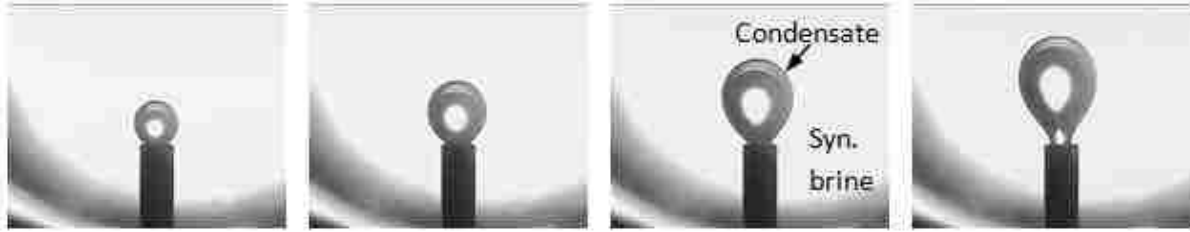
Figure 12: Schematic of Pendent Drop Method for IFT Measurement

3.4.2 Interfacial Tension Measurement by Capillary Rise Technique

In the fluid-fluid systems in the presence of surfactant, an oil or gas pendent drop was difficult to form due to low interfacial tensions. Sometimes the drop could not be stabilized at the capillary tip and quickly escaped through the surfactant solution. Therefore, at these conditions, the capillary rise technique was adopted to replace the pendent drop technique to measure the interfacial tensions. The capillary rise technique is a simple and accurate method to measure low interfacial /surface tensions. The formula for calculating interfacial tensions from this technique is given by

$$\sigma = \frac{\Delta\rho ghR}{2\cos\theta g_c} \qquad (5)$$

where: σ is interfacial tension in mN/m, $\Delta\rho$ is density difference between the two fluids in g/cm^3, R is radius of tube in cm, h is the height of capillary rise in cm, g is gravitational acceleration in 980 cm/sec^2, θ is contact angle in $^\circ$ and g_c is conversion factor ($1 \frac{g\cdot cm/sec^2}{dyne}$).

Figure 13 shows an example image of capillary rise in methane-brine system with 3000 ppm surfactant at reservoir conditions of 2264 psia and 210 °F. From Eq. (5) and Figure 13, both the capillary rise and contact angle have to be measured to calculate the IFT. It is worth to state

55

here that for the gas-water system the contact angle is very small. Hence, the contact angle was assumed to be zero for calculating IFT. The following procedure was used to measure capillary rise in this work at both ambient and reservoir conditions.
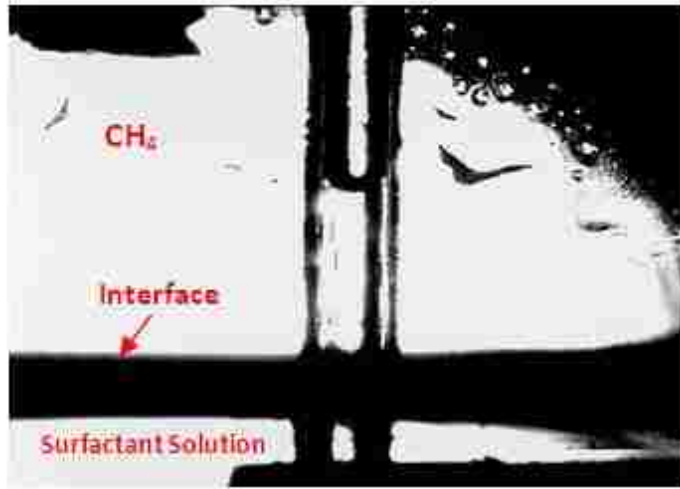
Figure 13: Image of Capillary Rise in CH_4-Brine System at 2264 psia and 210 °F Conditions (3000 ppm Surfactant Solution)

The particular quantity of surfactant solution in brine was firstly taken in the glass beaker at ambient conditions. Figure 14 depicts the process of capillary rise technique to obtain the capillary rise height used at ambient conditions. An amount of oil was added to the aqueous phase. The two liquids were thoroughly mixed with a glass stirring rod. After settling for one hour, the solution clearly separated into two immiscible phases with the denser phase (brine) at the bottom, while the lighter fluid (oil) on the top. A glass capillary tube with the diameter of 0.106 cm was then carefully inserted into the beaker below the interface of the two fluids. An adjustable stand was used to fix the position of the capillary tube so that the capillary tube is totally immersed in the two liquid fluids and the bottom end of the capillary tube did not touch the bottom of the beaker as shown in Figure 14. Subsequently, the denser fluid (surfactant solution) would rise in the capillary until the weight of the column of fluid balanced the pressure difference across the meniscus interface. The meniscus was stabilized for 20 minutes to obtain

56

the height. The beaker was placed between the light source B and the video camera D which were shown in Figure 6. The image of the capillary rise was captured by the DSA software. And the stabilized height was measured using the software MB ruler.
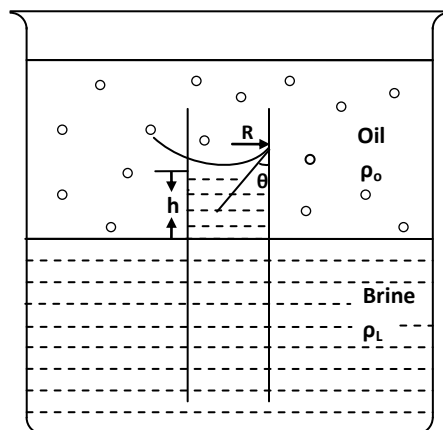
Figure 14: Schematic of Capillary Rise Technique at Ambient Conditions

The equilibrium contact angles for capillary rise technique were measured in the ambient optical cell (Figure 6). A clean and aged glass substrate was carefully placed in the lower horizontal crystal holder of the ambient optical cell. The surfactant solution was also taken in the elevated larger container and allowed to flow into the cell by gravity. After the cell was full of the solution, some solution was allowed to discharge from the top of the cell to ensure no air bubbles were trapped in the cell. Then the oil (condensate) drop was placed on the glass substrate by using the syringe from the bottom of the cell. Both valves were closed and the cell was set aside for 24 hours to age the oil drop for oil-solution-glass substrate interactions to achieve equilibrium. The equilibrium contact angle was then measured using the MB ruler software.

A glass capillary tube with a diameter of 0.106 cm was carefully placed in the HPHT optical cell and held in horizontal position by using the lower crystal holder. Once the pressure and temperature of the cell filled with surfactant solution achieved the reservoir conditions of 2264 psia and 210 °F, condensate or methane was injected into the HPHT cell to replace some

amount (about one third volume of the cell) of surfactant solution from the bypass tubing line located on top of the cell. The interface between the two immiscible phases could be observed, and the system was settled for 30 minutes to reach equilibrium at reservoir pressure and temperature. The capillary tube was then rotated to vertical position by the lower crystal holder. Subsequently, the denser fluid (surfactant solution) would rise in the capillary until the weight of the column of fluid balanced the pressure difference across the meniscus interface as shown in Figure 13. The meniscus was stabilized for 20 minutes to obtain the capillary rise. The image of the capillary rise was captured by the DSA software and its stabilized height was measured using the software MB ruler. The height of the capillary rise was then obtained by calibration against a standardized length.

The densities of condensate and surfactant solutions at ambient conditions and reservoir conditions were measured by Anton Paar DMA 4500 density meter and DMA HP density cell, respectively. The measured capillary rise height, fluid densities and contact angles (≈0 for methane) were substituted into Eq. (5) to calculate the interfacial tensions.

3.4.3   Contact Angle Measurement

In this study, Dual-Drop-Dual-Crystal (DDDC) technique, which overcomes the poor reproducibility and long test duration of other conventional contact angle techniques (Rao and Girard, 1996; Rao, 2003), was used to measure dynamic contact angles and thus determine the wetting nature in rock-oil-water systems. The sessile drop method was used to measure water-receding contact angles to determine the spreading of oil on the rock surface immersed in brine. The sequence of experimental steps is briefly described below.

Two clean crystals were mounted, one in the lower horizontal holder and the other in the upper vertical holder. After the cell was filled with brine, two separate condensate drops were

placed on the two crystals and aged for 24 hours as sessile drops to achieve the initial uniformity of oil-exposed areas on both quartz surfaces. The receding contact angles of these two sessile drops on both surfaces were measured at starting time (~0 hr) and 24 hr.

Then the lower crystal was flipped over, the two condensate drops were mingled into one big drop by lowering the upper crystal. The water-advancing and receding contact angles were created by sliding the lower crystal sideways. All of the contact angles were measured at different times until they showed negligible change. The movement of the three-phase contact line (TPCL) was also monitored at different times to further analyze the behavior of condensate drop on the lower crystal. This procedure is repeated until at least two successive shifts yield similar water-advancing contact angles.

3.4.4   Surfactant Injection Procedure

Anionic and nonionic surfactants were used to test their effects on the wettability for this condensate-brine-quartz case in the experiments at ambient conditions, and anionic surfactant was also tested at reservoir conditions. The surfactant injection experiments were carried out at three surfactant concentrations of 500, 1500 and 3000 ppm.

At the end of the aforementioned DDDC contact angle measurements to determine the reservoir wettability, the condensate drop was allowed to stay between the two substrates as it was and then brine containing the surfactant at specified concentration was injected into the cell. For ambient-condition cases, the surfactant solution was introduced to the optic cell by gravity flow. The quantity of the surfactant solution used was more than three times the volume of the cell to totally replace the normal brine previously contained in the cell. While for reservoir condition cases, the constant rate pump was employed to inject the surfactant solution to the HPHT optical cell at a rate of 11cc/min. The surfactant solution in the transfer vessel was heated

up to the reservoir temperature and then injected to the optical cell to maintain the cell's temperature at reservoir temperature of 210 ℉. More than ten times the volume of the cell of the surfactant solution was used to completely displace the normal brine previously in the cell. The total surfactant injection time was about 80 to 90 minutes. The difference of injection volume between these two conditions is due to the volume of the HPHT optical cell (about 70 cc) less than ambient-condition cell (about 400 cc).

The dynamic behavior of the condensate drop held between the two substrates was captured by the video camera during and after the surfactant injection. Also dynamic contact angles were measured during the surfactant injection period.

3.4.5 Coreflood Procedure

The coreflood experiments consisted of several series to achieve the objective. The following steps were performed in sequence in the coreflood tests.

---- Brine flood: determining pore volume and absolute permeability (K_a)

---- Decane flood: introducing initial water saturation (S_{wi})

---- Condensate flood: miscibly displacing n-decane (K_{ro})

---- Aging

---- Water/Surfactant flood (K_{rw})

---- Gas flood (K_{rg})

---- Core cleaning

A fresh or clean core was installed in the core holder and fitted with end caps. The hydraulic oil was placed in the annulus between the Viton rubber sleeve and the core holder to provide confining pressure on the core. The core was evacuated by the vacuum pump and it should maintain vacuum for several hours. Otherwise it indicated that there was a leak in the

core system. Once the core was ready, the inlet valve was open and the outlet valve was kept close, synthetic brine was then injected to the core at a very low flow rate 0.5 cc/min. When the core was completely saturated with brine, a rapid increase in the core pressure could be observed. At this point, the volume of injected brine was measured and the pore volume (PV) of the core could be calculated by subtracting the dead volume from the injected volume. Next, brine was then flowed at three different flow rates of 2, 4, 6 cc/min through the core, and the stabilized pressure drops for each flow rate were recorded to obtain the absolute permeability (K_a) to brine based on Darcy's law.

After the absolute permeability test, the core was first flooded with n-decane at 2cc/min rate to decrease the water saturation to an initial or irreducible value. When brine production could not be clearly observed in the effluent (about 5 to 6 PV n-decane injection) indicating the initial water saturation (S_{wi}) was achieved, condensate was then injected to miscibly displace n-decane for about 1.5 to 2 PV, after which the endpoint permeability to oil (condensate) was determined at the flow rates of 2, 3 and 4 cc/min. The core was then aged for 3~5 days to obtain the natural wettability. All the relative permeabilities (K_{ro}, K_{rw} and K_{rg}) reported in this study are normalized with respect to this endpoint effective oil permeability (K_o) computed in this step.

Water (brine or brine containing surfactant) displacement tests were conducted after aging the core at initial water saturation to produce oil (condensate), determine recovery and oil-water relative permeabilities. Before conducting this procedure, the inlet and outlet lines were flushed and empty to ensure the correct interpretation of the production history. The volume of condensate in these lines could not be taken into account because it was produced from the lines not from the core itself. The flood rate was 2 cc/min and total injection was about 3 to 5 PV, following which the endpoint permeability to brine (K_{rw}) at residual oil saturation (ROS) was

carried out at flow rates 3 and 4 cc/min. During the water flood period, the pressure drop across the core, the breakthrough time and oil and brine productions were recorded against time. Also, water-oil (condensate) relative permeabilities, wettability, and waterflood oil (condensate) recovery of the core were determined in this step.

The following step is gas (nitrogen) flood. As shown in Figure 7, a back-pressure regulator (BPR) was used in the upstream for gas injection to maintain the constant gas pressure at the outlet of the transfer vessel and thus provide a constant gas rate. The injected gas pressure was maintained around 250 psi by the back-pressure regulator. The wet test gas meter was used in the downstream to measure the real gas rate. Likewise, the gas endpoint permeability (K_{rg}) was determined at the pump flow rates of 8, 10 and 12 cc/min. And condensate and water productions were measured during the gas flood, as well as the pressure drop across the core and the breakthrough time.

It is worth noting here that the core was not cleaned between the base case (0 ppm surfactant flood) and the first surfactant treatment (3000 ppm) case. In other words, after completion of the base case, the core was just flooded with condensate to blow out the gas and bring back the initial water saturation and then was used to perform 3000 ppm surfactant flood. However, after the 3000 ppm surfactant flood case, the core had to be thoroughly cleaned followed by section 3.3.2 cleaning procedure and restored to its initial conditions before the start of the next test—1500 ppm case because surfactant was left in the core.

To avoid appreciable influence of capillary forces on the waterflood behavior that causes the end effects and the spreading of the displacement front, Rapoport and Leas scaling criterion for linear displacement tests, as expressed in follow, has been used to calculate the stable volumetric flow rates for use in the experiments (Rapoport and Leas, 1953).

$$L\mu u \geq 1 \qquad (6)$$

where L is the core length in cm, μ is the displacing phase viscosity in cP, and u is the flow rate per unit cross-sectional area in cm/min.

According to this criterion, the calculated minimum fluid velocity is about 0.54 cc/min (32.4 cc/hr). Hence, the waterflood investigations in above series were conducted at a flood rate of 2 cc/min which ensures the independence of oil recovery on flow rate and core length.

3.5 Coreflood Simulator

A simulation of water (brine or surfactant solution) flood process subsequently was performed using the procedure reported by Okazawa (1983) to determine relative permeabilities. In this simulation model, the analytical approach of JBN (Johnson et.al, 1959), which is based on the assumption of negligible capillary pressure effects, was used to generate relative permeabilities. The experimental production and pressure drop histories were provided in the model and relative permeabilities were thus calculated by minimizing the sum of squares of the weighted deviations of the calculated data from the experimental histories. Craig's rules of thumb (Craig, 1971) were used to interpret the relative permeability curves to infer wettability and its alterations. This is a simple approach to determine the wettability alone from the differences in oil-water relative permeability curves because fluid flow through porous media depending on several parameters such as wettability, rock pore structure, fluid-fluid interfacial tension, fluids saturations and their history, etc (Craig, 1971). Anderson (1987) also point out, "Because factors other than wettability can have a similar influence on relative permeability curves, it is preferable to make independent measurements of wettability rather than to rely solely on Craig's rule of thumb to evaluate wettability."

4. RESULTS AND DISCUSSION

The results of this study have been divided and discussed in the following six sections. The initial wettability of the representative condensate reservoir measured by DDDC technique is discussed in the first section. Interfacial tensions (IFT) and spreading coefficients in the presence and absence of surfactants are given in the following section. The third section describes the effect of surfactants on wettability. In this section, the experimental results were subdivided into two sections- during surfactant injection and after surfactant injection for better analysis. The Bond number calculations are discussed in the fourth section to quantitatively explain the condensate drop behavior on the crystal surface. For the first four sections, the experiments were conducted under both ambient and reservoir conditions. The fifth section presents the effect of surfactants on flow behavior in Berea core at ambient conditions. How brine salinity and brine composition have influenced wettability and spreading are explained in the sixth section along with some discussion of the mechanisms involved.

4.1 Wettability Determination of Condensate Reservoir at Ambient and Reservoir Conditions

Figure 15 and Figure 16 display the photographic sequence of the DDDC experiments conducted on the quartz substrate to measure contact angles in this condensate-brine system at reservoir conditions of 2264 psia and 210 °F as well as ambient conditions. From Figure 15 and 16, it can be seen that for this condensate fluids on quartz reservoir the wettabilities measured at both conditions are similar. The experiments were initiated with two separate condensate drops aging on the two smooth quartz surfaces immersed in synthetic reservoir brine under 2264 psia and 210 °F or room conditions, as shown in pictures A of Figure 15 or G of Figure 16. The lower substrate was slowly rotated after 24 hours and some of the drop was observed to float away from the lower surface while the rest of the drop was left behind on the surface with large contact

64

angles indicating an area that seemed to be oil-wet (picture B in Figure 15 and H in Figure 16). The reason for this observation is that the buoyancy force of the full condensate drop was stronger than the cohesion force in the condensate drop but weaker than the adhesion force at the condensate/substrate interface.
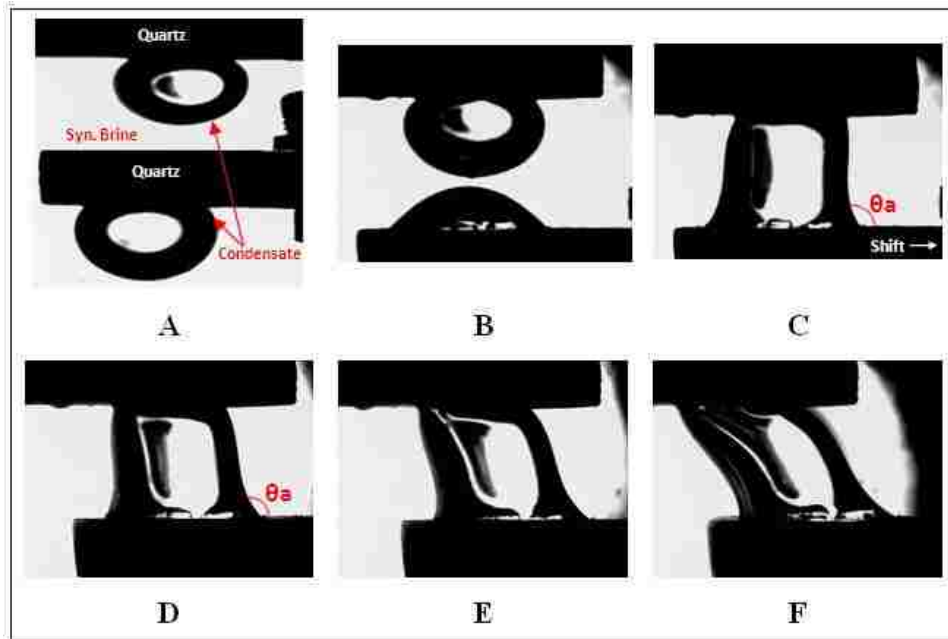
Figure 15: DDDC Procedures for Condensate-Brine-Quartz System at 2264 psia and 210 °F
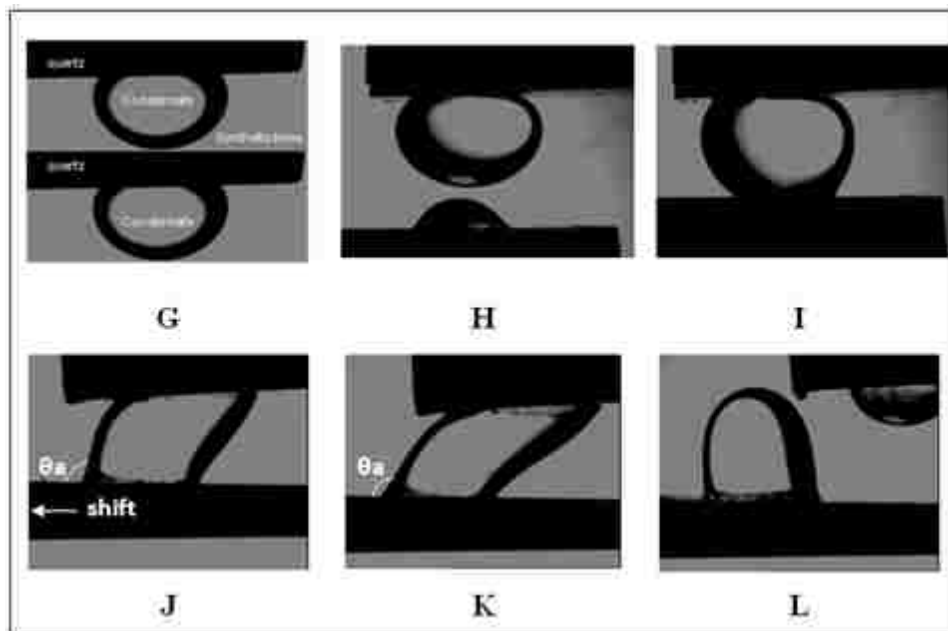
Figure 16: DDDC Procedures for Condensate-Brine-Quartz System at Ambient Conditions

The upper substrate was then brought down to contact this part of condensate drop on the lower substrate and the two drops merged into one big drop (pictures C of Figure 15 and I of Figure 16). At this point, four equilibrium receding angles and initial contact line positions, for example reservoir-condition case, L_i and R_i, between the lower left and right corners of the condensate drop from the left edge of the lower substrate were measured. Then the lower substrate was shifted horizontally toward the right side in the reservoir condition case, thereby creating the water-advancing contact angle and water-receding contact angle with this lateral substrate movement. Pictures D, E and F of Figure 15 are the depiction of the repeated shift progress of the experiment. The lower right and left contact angles represent the water-advancing angle and receding angle, respectively. And for ambient-condition case, it should be noted here that the lower substrate was moved to the left side, thus the lower left contact angle is the water-advancing angle while the right one is the receding angle as displayed in Figure 16.

The measured dynamic contact angles are plotted against contact time in Figure 16 and Figure 17 for both conditions. In reservoir-condition case, three-phase contact line (TPCL) movements were normalized by the distance between the lower right corner of the condensate drop and the left edge of the lower substrate divided by the measured initial contact line position L_i; While three phase contact line (TPCL) movements for ambient-condition case were normalized by the distance between the lower left corner of the condensate drop and the right edge of the lower substrate divided by the measured initial contact line position R_i. Normalized TPCL (R/L_i or L/R_i) distances are also plotted in Figure 16 and 17.
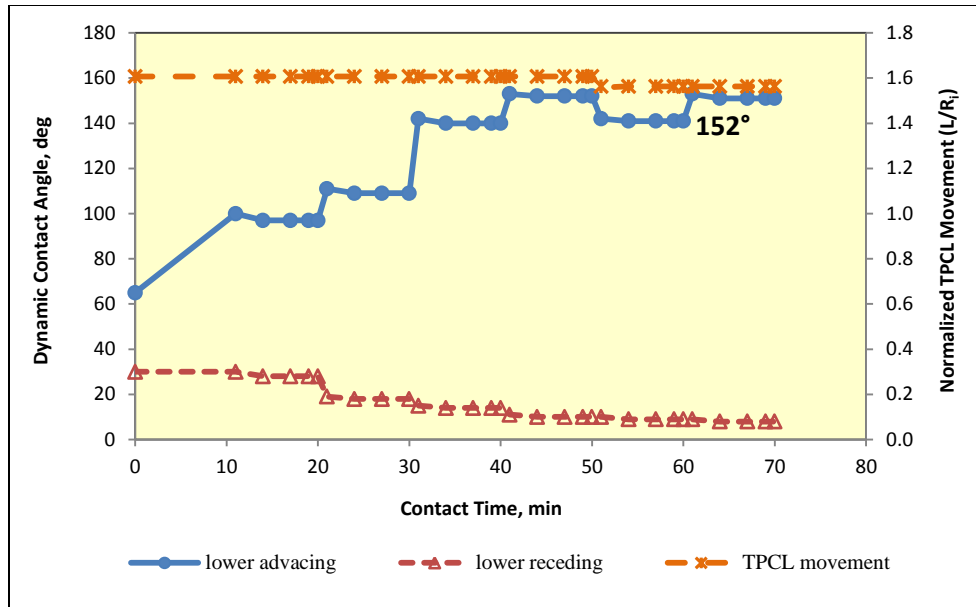
Figure 17: DDDC Contact Angles and TPCL Movements for Condensate-Brine-Quartz Surface at Ambient Conditions (Trial 1)

After mingling the two drops, the initial four angles, upper left and right angles, and lower advancing and receding angles were measured for zero contact time. At another 10 minutes, for example ambient-condition case, the first slight shift of the lower substrate created the lower advancing angle of 97º and the lower receding angle of 28º on the lower surface as can be seen in Figure 17. And the TPCL slightly moved on the lower surface. After 10 minutes the lower substrate was shifted for the second time, and the advancing angle increased to about 109º. The TPCL movement was not observed. The third and fourth sideways shifts were executed on the lower substrate, resulting in an increase of the low water-advancing contact angle up to about 152º. Until this contact time (40 min), the TPCL still retained at the same position and did not move, as indicated in Figure 17.

The following shift was made at a contact time of 50 minutes and an interesting observation was made. The TPCL slightly moved on the lower substrate surface in response to the reduction of lower advancing angle as can be seen in Figure 17. The lower advancing angle

decreased to 141º. The last shift was attempted at 60 minutes, and the lower advancing angle repeated to reach the high value of 151º along with unchanged position of the TPCL. This implies that adhesion force was very strong at condensate/substrate interface in this condensate-brine-quartz case. At the same time, a strongly adhering condensate drop as displayed in picture L of Figure 16 was left on the lower substrate surface. The measured peak lower advancing angle of 152º shown in Figure 17 demonstrates that the condensate strongly attaches to the quartz surface and therefore this system shows a strongly oil-wet nature at ambient conditions.
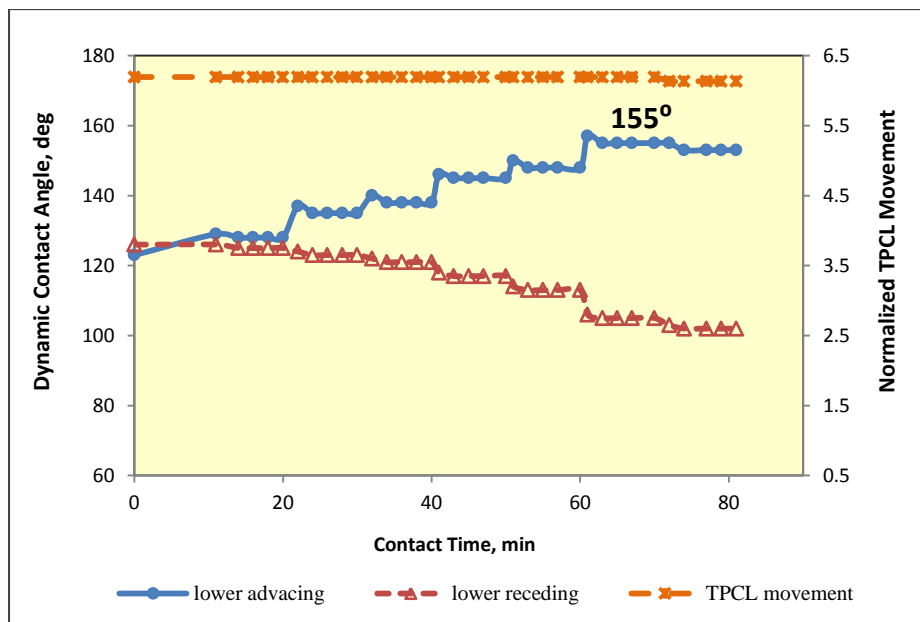
Figure 18: DDDC Contact Angles and TPCL Movements for Condensate-Brine-Quartz Surface at Reservoir Conditions (2264 psia and 210 ºF) (Trial 1)

For reservoir-condition case, the observation was similar to ambient-condition case. The measured lower water-advancing angle approached the peak value of 155º after several horizontal shifts and the TPCL slightly moved on the lower surface, as illustrated in Figure 18. This indicates that adhesion force of oil with the solid surface was stronger than cohesion and hence cohesive failure occurred in the condensate drop resulting in the drop slightly moving on

the surface. The lower advancing angle of 155° also proves that this rock-fluids system at reservoir conditions has a strongly oil-wet nature.
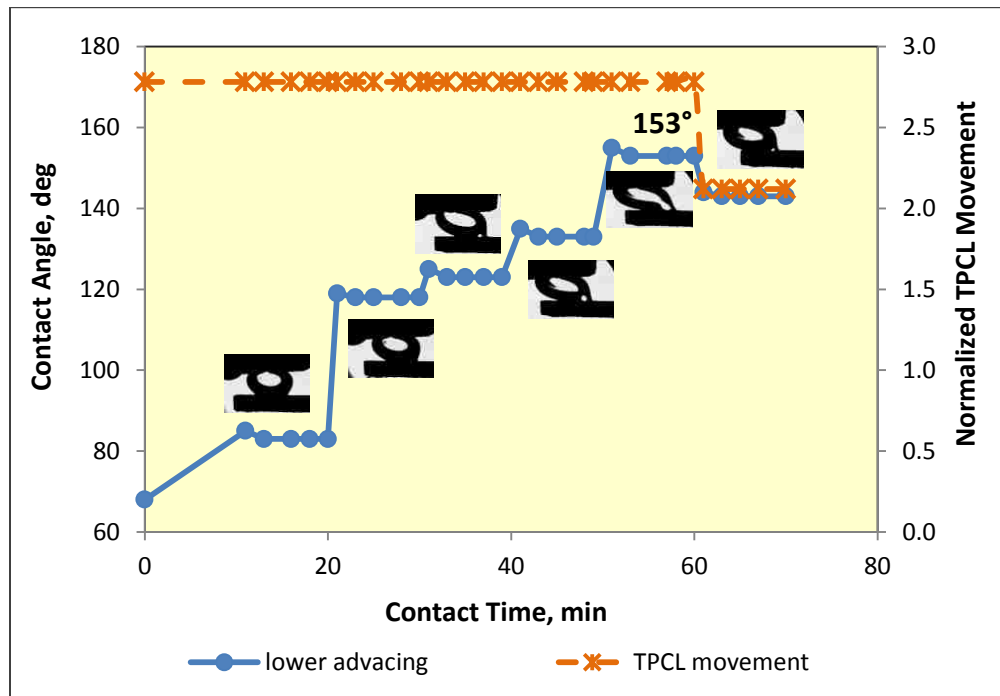
Figure 19: DDDC Contact Angles and TPCL Movements at 2264 psia and 210 °F (Trial 2)

In order to get reliable results from the DDDC technique for reservoir wettability measurement, the experiments were repeated two more times under both conditions. Figure 19 and 20 shows the contact angle measurement results of trials 2 and 3 at reservoir conditions. Figure 21 and 22 gives the results at ambient conditions. No significant TPCL movements were detected in all cases. Peak advancing angle values of 151° and 153° were obtained for 2 ambient-condition cases (Figure 21 and 22) and 153° for 2 reservoir-condition cases (Figure 19 and 20). The results of the repeatable experiments indicate that this sandstone condensate reservoir has a strongly oil-wet nature at both reservoir conditions of 2264 psia and 210 °F and ambient conditions. All cases also prove that DDDC technique has the capability of reproducibly measuring contact angles (within 2°) to characterize reservoir wettability.
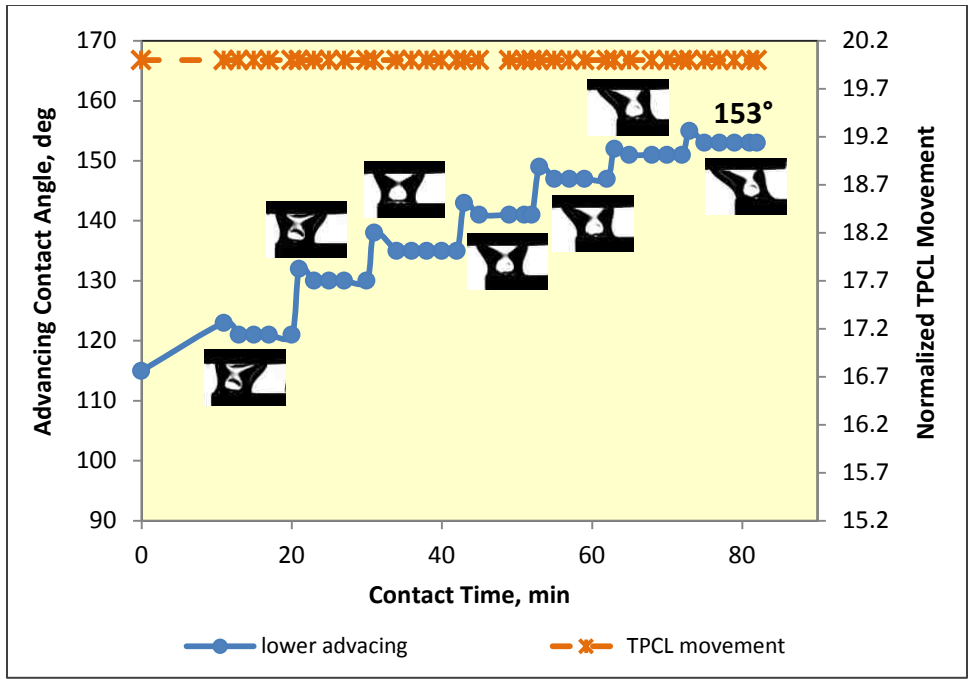
Figure 20: DDDC Contact Angles and TPCL Movements at 2264 psia and 210 °F (Trial 3)
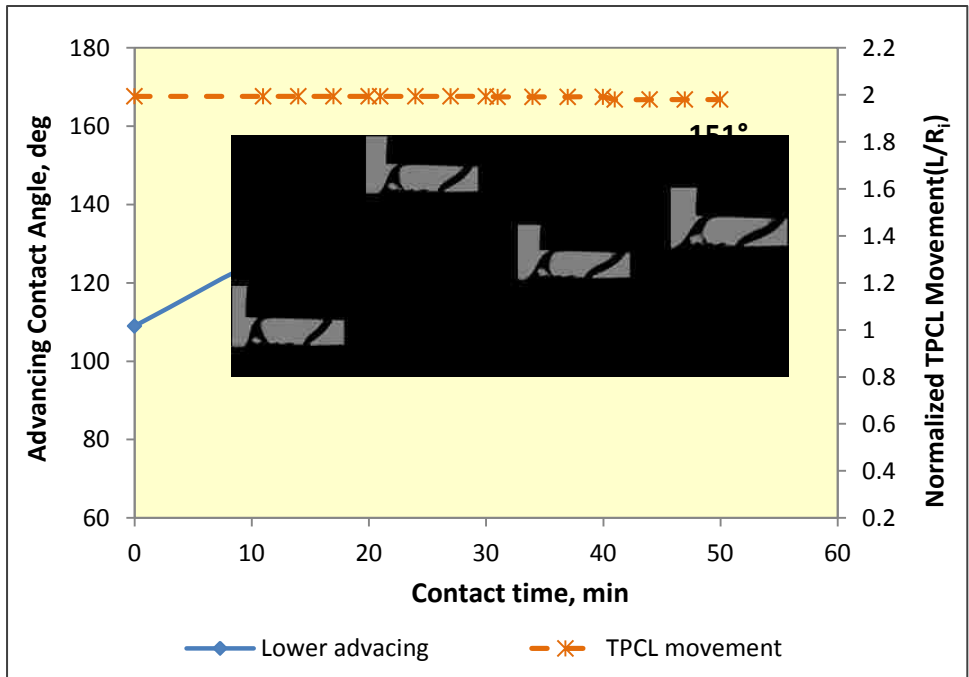
Figure 21: DDDC Contact Angles and TPCL Movements at Ambient Conditions (Trial 2)
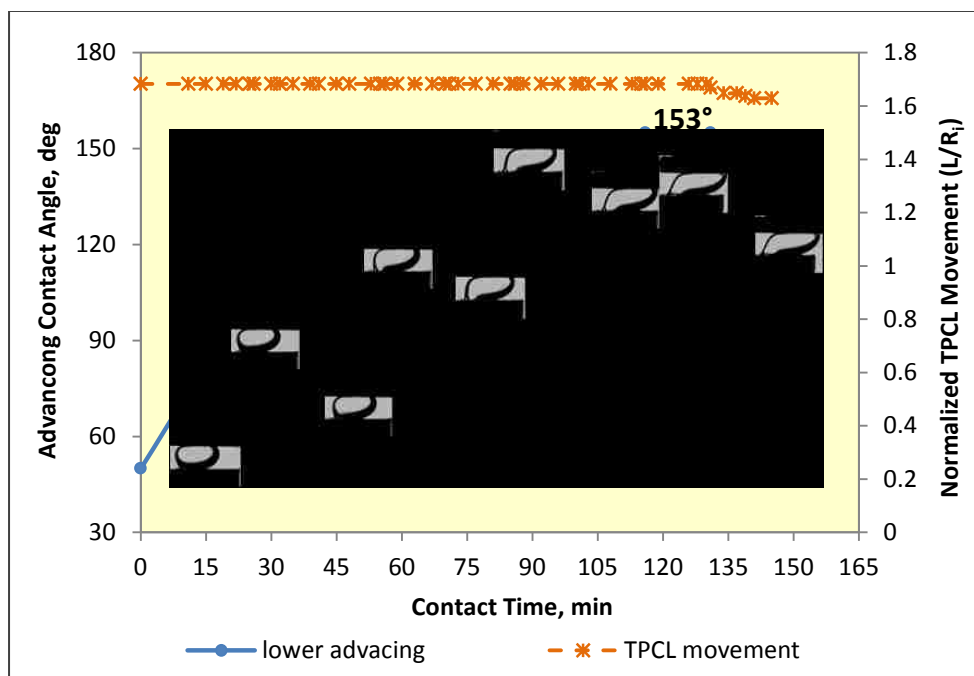
Figure 22: DDDC Contact Angles and TPCL Movements at Ambient Conditions (Trial 3)

4.2   Interfacial Tension and Spreading Coefficient

Interfacial tensions (IFT) with and without surfactants were measured at both ambient conditions and reservoir conditions. At ambient conditions, two kinds of surfactants, anionic and nonionic, at the concentration levels of 500, 1500, and 3000 ppm were used to test their capabilities of modification in interfacial tensions and spreading coefficient. The results demonstrated that the reduction in interfacial tension induced by the nonionic surfactant was higher than that by the anionic surfactant. In other words, the anionic surfactant exhibits high effectiveness in reducing interfacial tension.

Furthermore, these two surfactants were screened for their thermal stability at reservoir temperature 210 ºF (~99 ºC) (described in Section 3.3.5). The result also showed that the nonionic surfactant was unstable and formed a cloudy liquid at reservoir temperature hindering the visual observation of the drop. However, the anionic surfactant was stable and could be

applied at reservoir conditions. Hence, only the anionic surfactant was used at reservoir conditions. The following sections give the results of interfacial tension (IFT) and spreading coefficient obtained under both conditions.

4.2.1 Interfacial Tension Calibration

To ensure the accuracy of IFT measurements, calibration experiments were performed by using the pendant drop method by DSA technique before starting any IFT measurements in condensate-brine-methane systems. Known standard fluid pairs were used to examine the optical cell, DSA software, and the various experimental procedures.

In this study, because water-oil, gas-water and gas-oil interfacial tensions were needed to determine spreading coefficients, several known standard fluid pairs had to be selected to conduct calibration experiments corresponding to water-oil, gas-water and gas-oil systems. For a water-oil system, the standard fluid pair of n-decane and de-ionized water was chosen to carry out the calibration. Methane with de-ionized water (DIW) and n-decane with air were used to calibrate gas-water and gas-condensate system. The images of ten to fifteen drops or bubbles were captured during the experiments to obtain the average interfacial tension. The IFT calibration results are listed in Table 6. It can be seen from Table 6 that the results of interfacial tensions in the calibration experiments are in good agreement with the published values reported by other workers (Hough et al., 1951; Jennings and Newman, 1971, DSA software database by Kruss Company). Also, the low standard deviations strongly implied low variation in the measurements and this provided a strong evidence of the reliability, precision and accuracy of the equipment in our laboratory.

Capillary Rise technique was calibrated with a known low-IFT standard fluid pair of de-ionized water (DIW) and n-butanol. In this calibration experiment, the inner diameter of glass

capillary tube was 0.106 cm and an IFT value of 1.794 mN/m was calculated using the measured height in Eq. (5). Compared with the value of 1.80 mN/m reported by Mannhardt (1987), there is good agreement between them for this standard fluid system.

Table 6: Interfacial/Surface Tensions for Calibration Experiments

Fluid Pair	Interfacial Tension, mN/m	Standard Deviation	Interfacial Tension from the references, mN/m	Relative Error, %
DIW- n-Decane	51.23	±0.20	51.2 (Hough et al., 1951), 52 (DSA software database, Kruss Company)	±0.39
DIW -Methane	71.43	±0.12	71.2 (Jennings and Newman, 1971)	±0.17
n-Decane- Air	23.50	±0.18	23.9 (DSA software database, Kruss company)	±0.77

4.2.2 Interfacial Tension and Spreading coefficient at Ambient Conditions

Interfacial tensions for condensate-brine and brine containing surfactant systems obtained from ambient-condition experiments are summarized in Table 7. The calculated oil spreading coefficients based on Eq. (1) (in Section 2.4) are also presented in Table 7.

Table 7: Interfacial Tensions and Spreading Coefficients at Ambient Conditions

Parameter (mN/m)	Brine-Condensate System	Anionic Surfactant System			Nonionic Surfactant System		
		500ppm	1500ppm	3000ppm	500ppm	1500ppm	3000ppm
σ_{wg}	70.01	29.22	27.79	27.46	32.71	31.72	31.39
σ_{ow}	22.94	1.56	1.01	0.87	3.86	3.42	3.04
σ_{og}	20.58	20.58	20.58	20.58	21.06	21.03	21.02
S_o	26.49	7.08	6.20	6.01	7.79	7.27	7.33

It can be seen from Table 7 that interfacial tensions decreased after using these two surfactants for water-gas and water-condensate systems. But as the surfactant's concentration increased from 500 ppm to 3000 ppm, interfacial tensions decreased slightly, for example, from 3.86 mN/m to 3.04 mN/m in the nonionic surfactant containing brine systems. Also, comparing the anionic surfactant with the nonionic surfactant in the same solvent-brine systems, this anionic surfactant is more effective than the nonionic surfactant in reducing interfacial tensions. As an example, low IFT of 1.56 mN/m was obtained by using 500 ppm anionic surfactant in contrast to 3.86 mN/m by 500 ppm nonionic surfactant. However, for condensate-methane systems, interfacial tensions showed no change or a slight increase by using both surfactants. The anionic surfactant used in this study could not be dissolved in the condensate. In other words, this anionic surfactant has no effect on the interfacial tensions between condensate-methane and hence the same interfacial tension of 20.58 mN/m as shown in Table 7 was used. All of the data suggest that surfactants have their individual characteristics in different solvents thereby affecting the interfacial tensions to different extents.

Once interfacial tensions were determined, the oil spreading coefficient can be calculated according to Eq. (1) (Section 2.4). The calculated spreading coefficients are also presented in Table 7. In this particular condensate case, all the oil spreading coefficients determined from the experiments at ambient conditions are positive as displayed in Table 7. It also can be seen from Table 7 that the calculated spreading coefficients were reduced from original 26.49 mN/m to the average value of about 7 mN/m after the surfactants application. For anionic surfactant systems, the oil spreading coefficient decreases as the surfactant concentration is increased from 500 ppm to 3000 ppm. The declining trend of the oil spreading coefficient demonstrated that there is a possibility that the spreading coefficient could be changed from positive to negative, indicating

that the surfactants could enhance oil recovery in this strongly oil-wet system at ambient conditions.

4.2.3 Interfacial Tension and Spreading coefficient at Reservoir Conditions

Table 8 presents the results of interfacial tensions in condensate-brine and brine containing anionic surfactant systems at reservoir conditions of 2264 psia and 210 °F. Ambient-condition results were also listed in Table 8 for clearly comparing with reservoir-condition results. The concentration of 0 ppm represents the brine-condensate-gas system in the absence of anionic surfactant.

Table 8: Results of Interfacial Tensions and Spreading Coefficients at 2264 psia and 210 °F and Ambient Conditions

Parameter (mN/m)	0 ppm		500 ppm		1500 ppm		3000 ppm	
	Reservoir conditions	Ambient conditions	Reservoir conditions	Ambient conditions	Reservoir conditions	Ambient conditions	Reservoir conditions	Ambient conditions
σ_{wg}	43.87	70.01	34.80	29.22	12.70	27.79	10.07	27.46
σ_{ow}	9.10	22.94	1.22	1.56	Low*	1.01	Low*	0.87
σ_{og}	miscible*	20.58	miscible*	20.58	miscible*	20.58	miscible*	20.58
S_o	34.77	26.49	33.58	7.08	12.70	6.20	10.07	6.01

* The value of 0 was given to calculate the spreading coefficients.

From Table 8, it can be seen that for 0 ppm system, interfacial tensions for water-oil-gas (σ_{wg}, σ_{ow} and σ_{og}) at reservoir conditions are lower than those at ambient conditions, especially for interfacial tensions between condensate and methane (σ_{og}). At ambient conditions, the methane-condensate system has higher interfacial tension (σ_{og} =20.58 mN/m) as shown in Table 6. However, at reservoir conditions of 2264 psia and 210 °F, it was observed that methane had developed miscibility with condensate during the experiments. Figure 23 shows the images captured from the video of the experiments for methane and condensate at reservoir temperature 210 °F and different pressures (1450, 1650, 1750, 2000 psi).

| 1450 psi | 1650 psi | 1750 psi | 2000 psi |
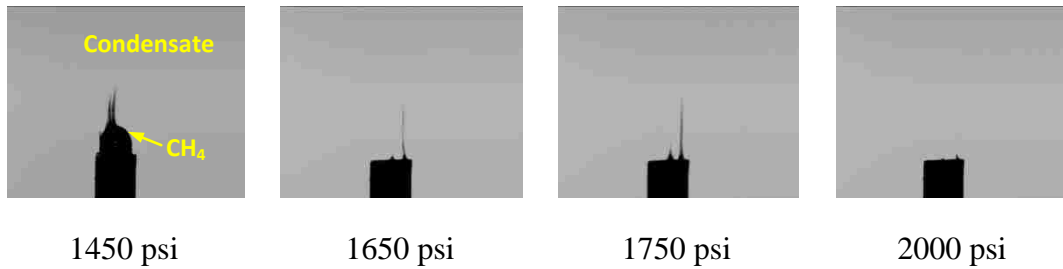
Figure 23: Images of Injecting CH_4 into Condensate at Different Pressures and 210 °F

When methane was introduced through the injection tip into the cell which was filled with condensate, at the relatively low pressure of 1450 psi, it can be clearly seen from the first image of Figure 23 that a methane bubble was formed although it quickly dissolved into the liquid condensate. As the pressure increased to 1650 psi and 1750 psi, it was hard to observe a methane bubble and only a light phase boundary between methane and condensate could be detected. At 2000 psi, gas and liquid phases disappeared to become a single phase as shown in the fourth image of Figure 23 clearly indicating that methane is miscible with condensate at reservoir conditions of 2264 psia and 210 °F.

Hence, the comparison of IFT results without anionic surfactant at ambient conditions and reservoir conditions strongly demonstrates the dependent of fluid-fluid interactions on pressure and temperature.

In the fluid-fluid systems in the presence of anionic surfactant, interfacial tensions decreased as the surfactant concentration increased at reservoir conditions. For example, interfacial tension between water and gas (σ_{wg}) decreased from 43.87 mN/m at 0 ppm to 34.80 at 500 ppm, 12.70 at 1500 ppm and 10.07 mN/m at 3000 ppm, quite similar to the ambient-condition observations, as can be found in Table 8. This indicates that this anionic surfactant is also a good choice to apply to this brine-condensate-gas system to effectively reduce the interfacial tension at reservoir conditions.

Note that in Table 8, at high surfactant concentrations of 1500 and 3000 ppm the values of 12.70 and 10.07 mN/m of IFT (σ_{wg}) at reservoir conditions are much lower than 27.79 and 27.46 mN/m at ambient conditions. However, for low concentration of 500 ppm, the IFT between gas and water (σ_{wg}) of 34.80 mN/m at reservoir conditions is higher than 29.40 mN/m at ambient conditions. Also, there is no significant difference between the gas/water IFT values of 27.79 mN/m at 1500 ppm and 27.46 mN/m at 3000 ppm at ambient conditions, however, the sharp decrease in IFT (σ_{wg}) from 34.80 to 10.07 mN/m at reservoir conditions still can be clearly noticed as the surfactant concentration increased from 500 ppm to 3000 ppm. The one possible explanation for these differences between both test conditions is that methane at reservoir conditions of 2264 psia and 210 °F exhibits strong supercritical properties and it behaves more liquid-like resulting in lower IFT. The other reason is that 500 ppm concentration is not sufficient for the surfactant to be effective at reservoir conditions. In other words, the availability of sufficient amount of surfactant molecules in the bulk solution contributes to the reduction of the interfacial tension. This implies that surfactant characteristics also depend on pressure and temperature.

All of the reservoir-condition oil spreading coefficients calculated from fluid-fluid interfacial tensions were positive for this particular condensate case but decreased with increasing surfactant concentration as shown in Table 8. The calculated spreading coefficients were reduced one order of magnitude in the presence of anionic surfactant except in the 500 ppm reservoir-condition case. The spreading coefficient at 500 ppm is 33.58 mN/m close to the original value (0 ppm) of 34.77 mN/m. This is also attributed to methane supercritical properties at reservoir conditions and surfactant properties which were affected by high temperature and high pressure. Similar to ambient-condition results, the declining tendency in oil spreading

coefficient induced by surfactants also suggests the potential of enhanced oil recovery in this strongly oil-wet system at reservoir conditions.

4.3   Effect of Surfactants on Wettability

For better analyzing the experimental visual observations and results, this section has been divided into two sections—during surfactant injection and after surfactant injection. Three surfactant concentrations of 500, 1500, 3000 ppm were tested in the experiments at both ambient and reservoir conditions. The following "during surfactant injection" section contains ambient-condition cases—two anionic surfactant cases (500 ppm and 1500 ppm) and two nonionic surfactant cases (500 ppm and 3000 ppm) and reservoir-condition anionic surfactant cases (500 ppm, 1500 ppm and 3000 ppm) to elucidate the dynamic behavior of the condensate drop between two substrates during surfactant injection period and how surfactants affected wettability.

In addition, the weakly oil-wet state in which contact angles range from 115 to 135° and strongly oil-wet state (135 ~ 180°) were defined in this study to better describe condensate drop behavior on the solid surface.

4.3.1   During Anionic Surfactant Injection at Ambient Conditions

From Table 7, it can be seen that the interfacial tension measured between condensate and synthetic brine without surfactants is 22.94 mN/m. It is reduced by one to two orders of magnitude when three levels of concentration 500, 1500, 3000 ppm of the anionic surfactant were used in the system. The total surfactant injection time is about 80 min at ambient conditions. During this anionic surfactant injection period, the dynamic behavior of the condensate drop between upper and lower substrates was similar for all these three surfactant concentrations. In general, it was observed that the drop was moving on the lower substrate and then floated away

to the upper surface to finally end up at the top of the cell. This process happened fast and it took only a few minutes to complete after starting anionic surfactant injection. The following sections give a detailed discussion on the basis of experimental observations and results in the two cases of 500 ppm and 1500 ppm brine containing surfactant.

4.3.1.1 During 500 ppm Anionic Surfactant Injection

Figure 24 illustrates the effect of 500 ppm brine containing anionic surfactant on the dynamic behavior of the condensate drop with time during certain time steps of the surfactant injection. The contact diameter on the lower surface, drop height and dynamic contact angles of the condensate drop on the lower substrate surface at different times are summarized in Table 9. Figure 25 depicts the change of the contact diameter and height of the drop with time during the 500 ppm anionic surfactant injection. The measured advancing and receding contact angles varied with time are displayed in Figure 26 and Figure 27.

It can be seen from Figure 24 that the big condensate drop moved rapidly (picture at t= 0s to t= 26.84 s) on the lower surface and it took only about 26 seconds after surfactant injection to float away to the upper substrate surface. The drop on the upper surface quickly remained suspended at the top of the cell, leaving little evidence of condensate interaction on the upper surface as is seen in pictures corresponding to 26.84, 41.681 and 80.082 s in Figure 24. Through the duration of 0 to 80.082 s, the contact diameter of the drop decreased as the drop varied from the big drop to the small drop on the lower surface (Figure 24 and Table 9). And the reduction in interfacial tension by the anionic surfactant is the main reason for decreasing the drop diameter during this period. The measured advancing angles fluctuated around 155° and the wetting state remained strongly oil-wet during this time, as can be seen in Table 9 and Figure 24.

79
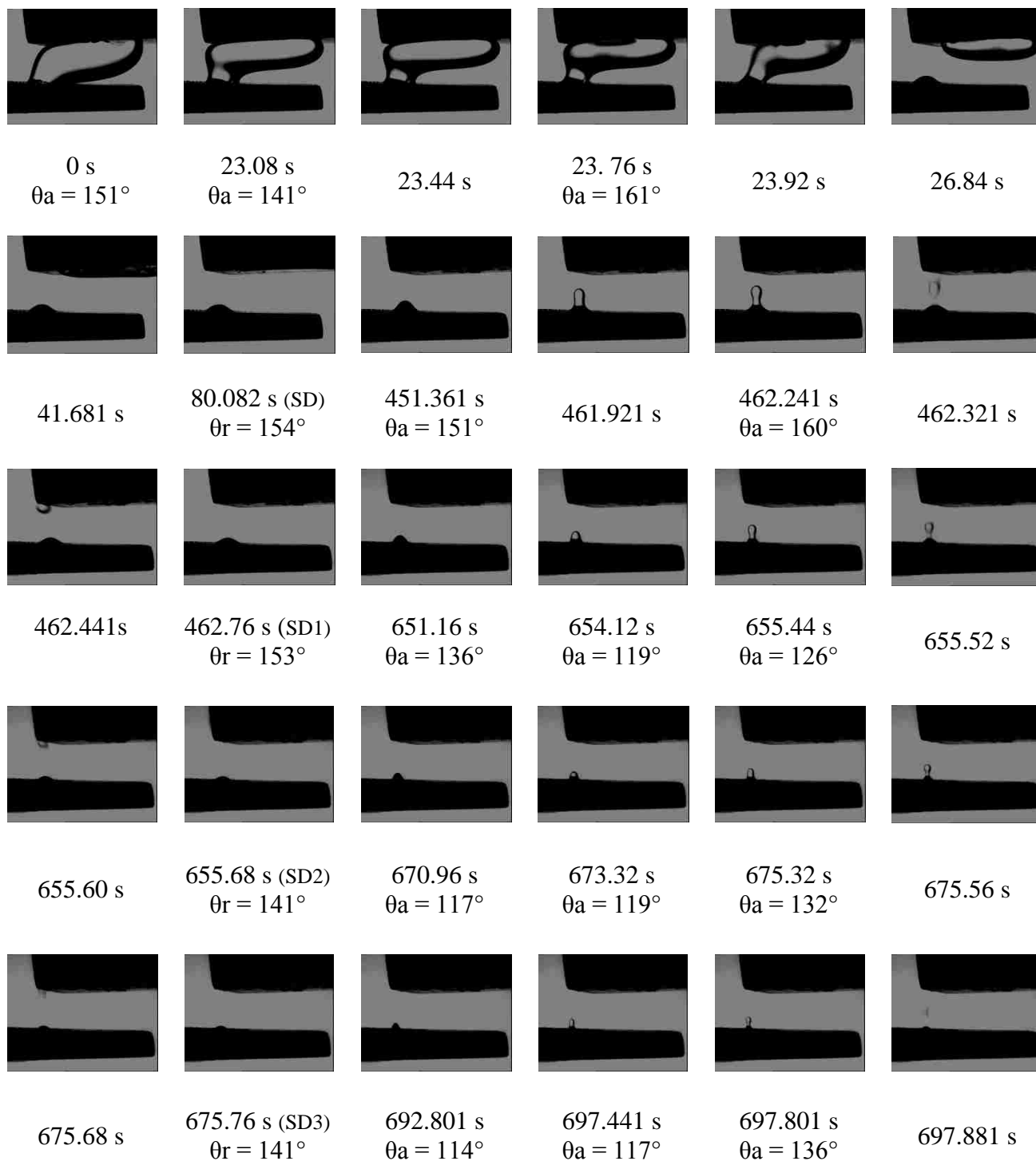
Figure 24: Photographic Depiction of Condensate Drop Dynamic Behavior during the Injection of 500 ppm Anionic Surfactant (SD= Small Drop)

Table 9: Quantitative Drop Dynamic Behavior on Lower Substrate during 500 ppm Anionic Surfactant Injection

Time, s	Dynamic Contact Angle, °		Height, cm	Contact Diameter (Lower Surface), cm	N_B	N_B'
	Advancing θa	Receding θr				
0	151		0.333	0.416	0.00	23.83
23.080	141		0.333	0.287	0.00	16.46
23.440	148		0.333	0.287	0.00	16.46
23.760	161		0.333	0.287	0.00	16.46
23.840	163		0.333	0.256	0.00	14.64
80.082		154	0.056	0.252	13.38	2.42
451.361	151		0.080	0.231	11.48	3.17
457.841	153		0.118	0.207	8.62	4.19
462.241	160		0.190	0.204	5.34	6.66
462.441		153	0.047	0.222	12.28	1.79
646.080	149		0.041	0.204	11.95	1.43
651.160	136		0.059	0.157	10.30	1.59
654.120	119		0.088	0.134	11.65	2.01
655.040	126		0.115	0.130	8.33	2.57
655.440	140		0.133	0.130	5.86	2.97
655.480	147		0.142	0.130	5.11	3.17
655.600		141	0.032	0.140	9.36	0.76
670.960	117		0.056	0.122	12.81	1.17
673.320	119		0.066	0.120	11.38	1.37
675.320	132		0.100	0.112	6.72	1.91
675.560	147		0.118	0.112	4.95	2.26
675.680		141	0.024	0.117	7.99	0.48
692.801	114		0.047	0.085	10.31	0.68
694.961	117		0.056	0.084	8.77	0.80
697.441	136		0.075	0.084	5.15	1.08
697.801	146		0.092	0.084	4.18	1.32
697.881		140	0.021	0.089	6.20	0.32

* Δρ of 0.26295 g/cm3 and σ of 1.5 mN/m were used in the Bond number calculations
N_B and N_B' were calculated using following equations:

$$N_B = \frac{\Delta \rho g (h - h_i) d}{\sigma \cos \theta}$$
$$N_B' = \frac{\Delta \rho g H d}{\sigma}$$
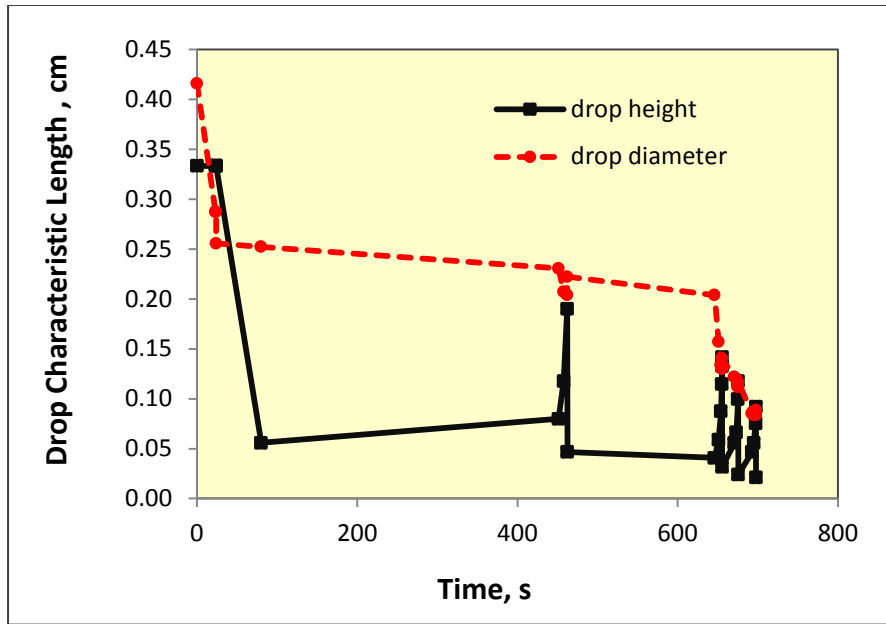
Figure 25: Variations of Condensate Drop Dimensions with Time on Lower Substrate during 500 ppm Anionic Surfactant Injection
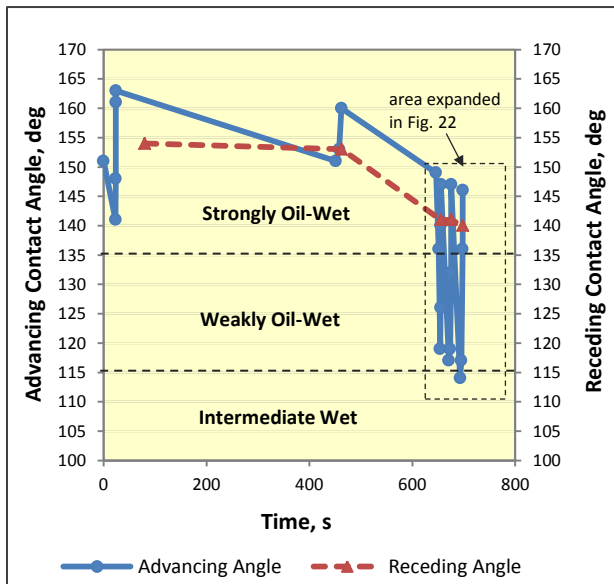
Figure 26: Variations of Dynamic Contact Angles with Time on Lower Substrate during 500 ppm Anionic Surfactant Injection
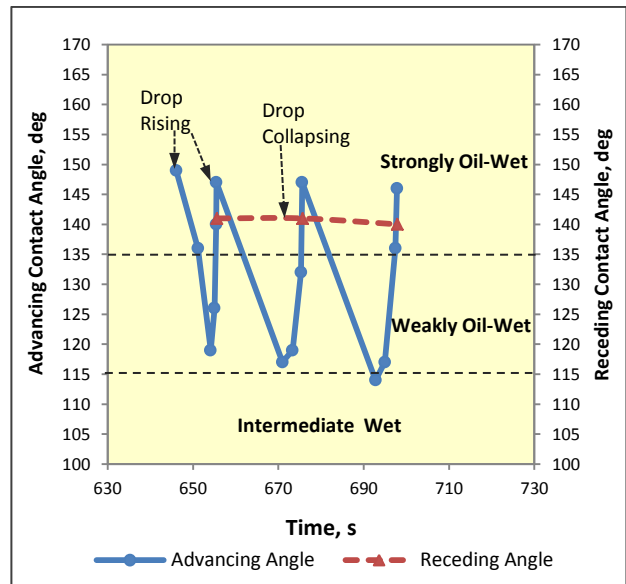
Figure 27: Variations of Dynamic Contact Angles with Time during 500 ppm Anionic Surfactant Injection (at Time Steps: 646-698 s)

Further analysis still focused on the small condensate droplet (SD) left behind on the lower surface as the surfactant continued to be injected into the cell. The small drop did not start

to move on the lower surface until the time of 451.361 seconds (about 7.5 minutes), because more and more surfactant molecules entered the cell and attempted to concentrate and adsorb on the interface which is either between the condensate and brine or between the condensate and quartz substrate. This is in addition to continuing decrease in oil/water interfacial tension. The adsorption of the surfactant on the surfaces led to the movement of the condensate drop along with the change of advancing angles. On the other hand, the adhesion force between condensate drop and the surface resulted in the drop adhering on the surface. Thus, part of the droplet SD detached from the surface due to the combination of forces and the drop SD became even smaller (SD1). The variation of drop height shown in Figure 25 demonstrates that the surfactant affects the interface between the condensate and brine causing the reduction in interfacial tension. The drop diameter decreased slightly and advancing angles remained fluctuating approximately around 153° (Table 9, Figure 25 and 26). The strongly oil-wet surface wettability still did not change in this interval from 451.361 s to 462.761 s. The smaller droplet (SD1) was inactive on the lower surface once again. The finding of drop movement and its corresponding shape changes (height and contact diameter) is resulting from the changes in interfacial tension and advancing (θ_a)/receding (θ_r) contact angle as the surfactant molecules enter the oil/water/surface interfaces. This is in agreement with the work of Li et al. (2004) who showed that the sessile crude oil drop on the rock slide changed its shape and became flattened due to dynamic IFT and contact angle phenomena when the crude oil was made in contact with alkaline-surfactant solution. They have also found that the wettability is slightly changed using an anionic surfactant-alkaline solution but permanently altered from water-wet to oil-wet by cationic surfactant-alkaline solution.

After another 3 minutes (at 651.16 s), the droplet SD1 took action on the lower substrate again owing to the continuous injection of the surfactant. A similar phenomenon occurred as before with droplet SD. SD1 then disintegrated into the smallest droplet SD2. In the same way SD2 repeated the whole process as SD1 did. Finally, it further reduced up to the smaller droplet SD3 and SD3 continued to duplicate the performance of the droplet SD2. The difference between SD1, SD2 and SD3 is that SD1 took shorter time 46.721 seconds (from 651.16 s to 697.881s of Figure 24) to transform to SD2 and SD3 due to the increase in the surfactant concentration in the cell. This repeatable and cyclical behavior of the condensate drop on the lower substrate can be clearly observed in Figure 24. It indicates that the surfactant activity at the solid surface does not start immediately, but affects the surface wettability gradually as the surfactant molecules diffuse to and interact at oil/rock interface.

The diameter of the droplet showed a decreasing trend with time in Figure 25. This means that the three-phase contact line did move on the lower surface. Carefully checking the diameter data in Table 9, it can be seen that the diameter of the droplet did not reduce at certain times. For instance, the diameter of 0.140 cm at 655.60 s is larger than 0.130 cm at 654.44 s. The possible explanation for this is that the gravity force exerted on the droplet pulled it down against the surface. The droplet has to be stretched and spread on the surface causing its diameter to increase. Corresponding to this spreading action, the contact angle switches to the receding angle at these particular times as shown in Table 9. Since the oil drop is spreading on the surface that was oil wet, the receding angles are also quite high. This leaving action of the drop allows more surfactant molecules to enter the oil/rock interface enabling further wetting alteration.

Also, it is worth noting here that the advancing contact angles distinctly changed during the period of 651.156 s to 697.881 s. Figure 27 gives the detailed plot of the advancing angles

with time in this short period. From Figure 27, the advancing contact angles cyclically changed three times as the droplet SD1 disintegrated to the smallest droplet SD3. The advancing angles varied from 149° to 119° for the first time. And the angles changed from the high values of 147° and 146° to the low values of 117° and 114° for the last two times. The alteration of advancing angles proves that the preferentially strongly oil-wet quartz surface has been changed to weakly oil-wet or intermediate-wet by the 500 ppm surfactant treatment. The similar dynamic behavior of crude oil was observed on the rock surface during surfactant injection into the oil-wet fractured reservoir (Ayirala et al., 2006), and the reservoir wettability was believed to alter from an initially strongly oil-wet state to less oil-wet or intermediate wet state induced by the surfactant.

4.3.1.2 During 1500 ppm Anionic Surfactant Injection

The photographic sequence of condensate drop behavior on the lower surface at certain time steps for 1500 ppm anionic surfactant injection, recorded by the video camera from the experiment, is given in Figure 28. And Table 10 describes the changes of the dynamic contact angles (advancing and receding), diameter and height of the condensate drop during this period. Variations of condensate drop characteristic lengths (diameter and height) and dynamic contact angles are plotted against contact time in Figure 29 and 30, respectively.

It is clear to see that the drop contact diameter on the lower substrate changed significantly from 0.755 cm at 0 s to 0.260 cm at 32.636 s as shown in Figure 28, 29 and Table 10. It indicates the significant movement of the three phase contact line on the lower surface due to surfactant injection. Also, the measured advancing contact angles altered from 145° to 110° (Table 10 and Figure 29). The time of 32.636 seconds consumed to complete this process is much faster than 670.96 seconds (about 11 minutes) in the 500 ppm surfactant injection. This

can be attributed to the higher surfactant concentration. The alteration of advancing angles indicates that the quartz substrate surface is no longer preferentially strongly oil-wet. And its wettability, as clearly shown in Figure 29, is changed by the 1500 ppm surfactant treatment to be intermediate-wet.

0 s θa = 145°	31.796 s θa = 163°	32.076 s	32.396 s θa = 151°	32.636 s θa = 110°	32.756 s θa = 118°
32.876 s θa = 147°	32.956 s	33.036 s θr = 156°	69.957 s θa = 159°	70.317 s	72.637 s θa = 156°
75.157 s θa = 121°	75.237 s	75.397 s θa = 142°	75.637 s	75.797 s θr = 154°	75.957 s
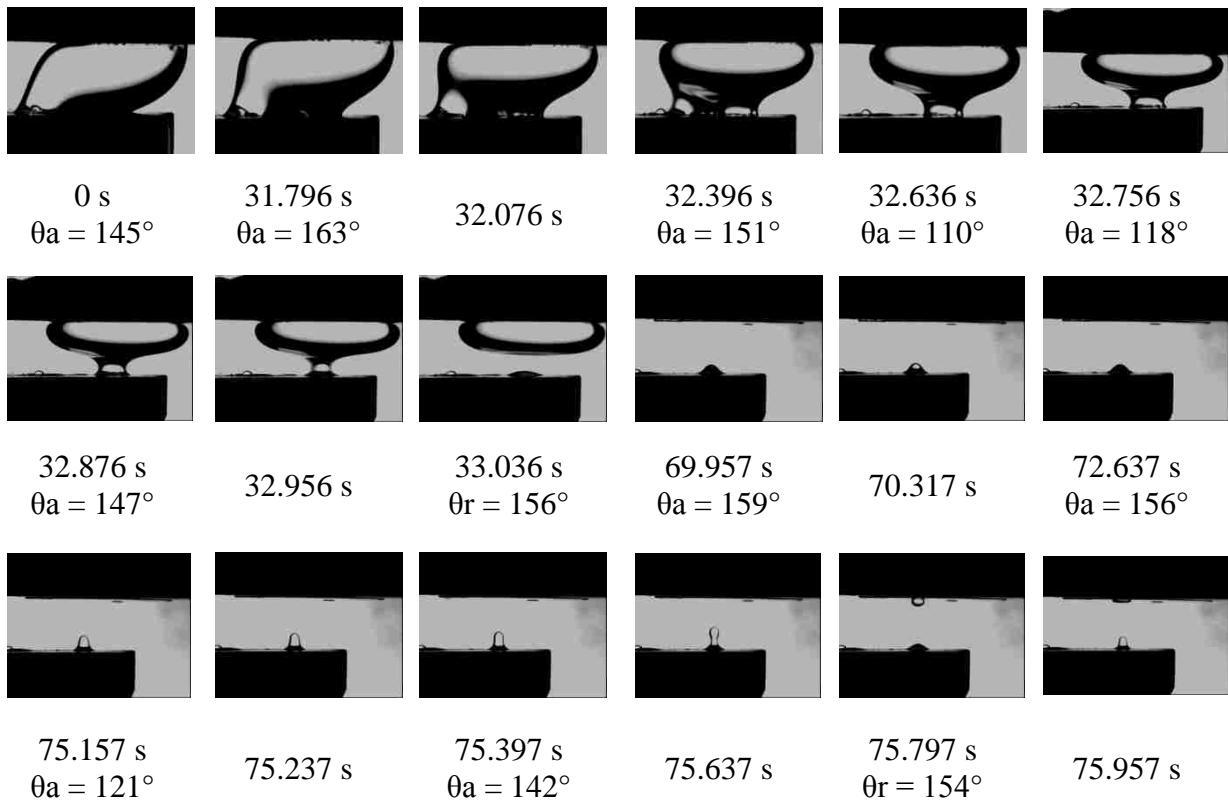
Figure 28: Photographic Depiction of Condensate Drop Dynamic Behavior during 1500 ppm Anionic Surfactant Injection

Next, the small condensate droplet left behind on the lower surface after the breakup of the large drop was further affected by the surfactant and the similar cyclical behavior of the droplet was observed as that in the case of 500 ppm surfactant injection. As the pictures of 69.957, 70.317 and 72.637 s in Figure 28 display, the droplet struggled on the lower surface to move on the surface. It rises up due to lowered IFT by the surfactant effect and then falls back on the lower surface by gravity. This up and down movement in position also can be seen in Table

10 and Figure 29 because the droplet contact diameter first decreased and then increased but its height followed the reverse trend. At the same time, the advancing contact angle alternated to the receding angle owing to the alteration of water /oil interface on the surface.

The subsequent dynamic behavior of the condensate droplet was similar to that in the 500 ppm surfactant injection case. With the increase of the surfactant concentration, the droplet was impelled to action again on the lower substrate. And this time it did not fail to change itself and disintegrate into a smaller droplet (the picture of 75.157 s through the picture 75.957 s in Figure 28). The measured advancing angles range from 160° to 121° revealed the alteration of the wettability from strongly oil-wet to weakly oil-wet (see Figure 30). As before, this process kept repeated for several times (Figures not shown) as more and more surfactant solution was injected and finally only a trace of condensate was left on the lower surface.

Figure 29: Variations of Condensate Drop Dimensions vs. Time on Lower Substrate during 1500 ppm Anionic Surfactant Injection
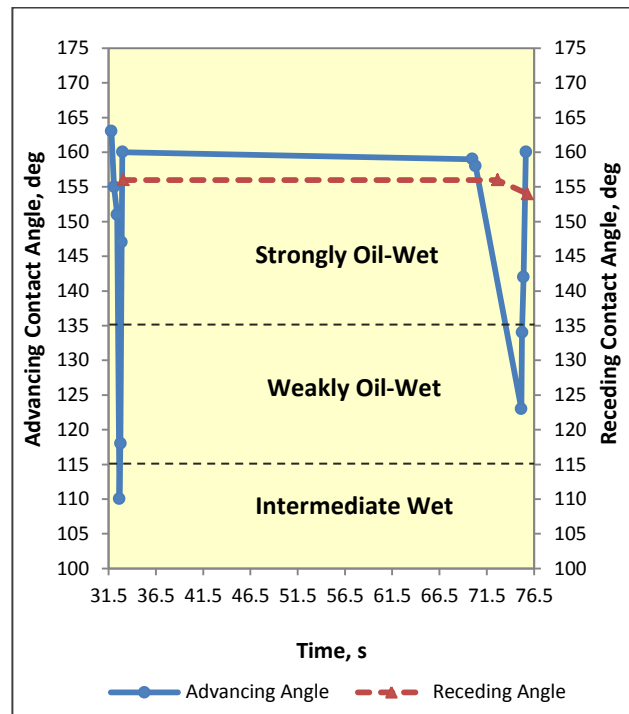
Figure 30: Variations of Dynamic Contact Angles with Time on Lower Substrate during 1500 ppm Anionic Surfactant Injection

Table 10: Quantitative Drop Dynamic Behavior on Lower Substrate during 1500 ppm Anionic Surfactant Injection

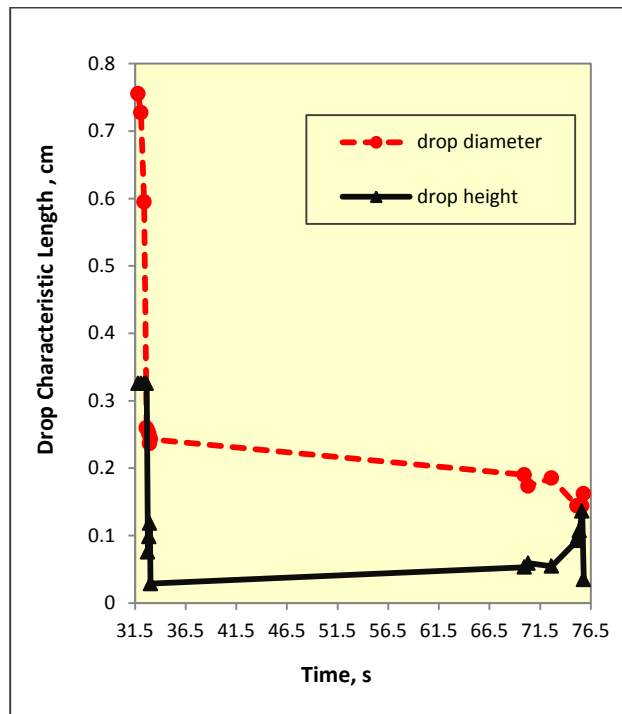| Time, s	Dynamic Contact Angle, °		Height, cm	Contact Diameter (Lower Surface), cm	N_B	N_B'
	Advancing θa	Receding θr				
0	145		0.326	0.755	0.00	42.28
31.796	163		0.326	0.755	0.00	42.28
32.076	155		0.326	0.727	0.00	40.71
32.396	151		0.326	0.595	0.00	33.31
32.636	110		0.326	0.260	0.00	14.53
32.756	118		0.076	0.256	23.44	3.34
32.876	147		0.098	0.251	11.70	4.25
32.956	160		0.118	0.236	8.97	4.80
33.036		156	0.029	0.243	13.57	1.20
69.957	159		0.053	0.190	9.54	1.73
70.137	158		0.059	0.174	8.58	1.76
72.637		156	0.055	0.185	9.44	1.74
75.157	121		0.092	0.144	10.59	2.28
75.237	134		0.098	0.144	8.08	2.43
75.397	142		0.108	0.144	6.84	2.66
75.637	160		0.136	0.144	4.98	3.37
75.797		154	0.035	0.162	9.01	0.97

* Δρ of 0.26298 g/cm^3 and σ of 1.5 mN/m were used in the Bond number calculations
N_B and N_B' were calculated using following equations:

$$N_B = \frac{\Delta \rho g (h - h_i) d}{\sigma \cos \theta} \qquad\qquad N_B' = \frac{\Delta \rho g H d}{\sigma}$$

4.3.2   During Nonionic Surfactant Injection at Ambient Conditions

In the three concentrations of 500, 1500, 3000 ppm of the nonionic surfactant cases, the slight movement of the condensate drop on the lower substrate was observed in two cases of lower concentrations 500 ppm and 1500 ppm surfactant injection. And for the highest concentration of 3000 ppm surfactant solution, the drop did change its location on the lower surface and floated away to the upper surface. However, part of the drop on the upper surface

strongly attached to the upper surface and did not dislodge. Two cases 500 ppm and 3000 ppm surfactant solutions are given as the examples to elucidate the process when the surfactant solutions were injected into the cell.

4.3.2.1 During 500 ppm Nonionic Surfactant Injection

The photographic sequence of condensate drop behavior on the lower surface is shown in Figure 31 for 500 ppm nonionic surfactant injection. And in Table 11 is presented the variations of the advancing contact angle, contact diameter and height of the condensate drop and Bond Number with contact time. Figure 32 and 33 illustrate the plots of condensate drop characteristic length (diameter and height) and advancing contact angle verse time.

0 s	18.441 s	33.401 s	59.802 s
133.400 s	193.081 s	264.962 s	358.991 s
481.00 s	489.641 s	656.020 s	778.961 s
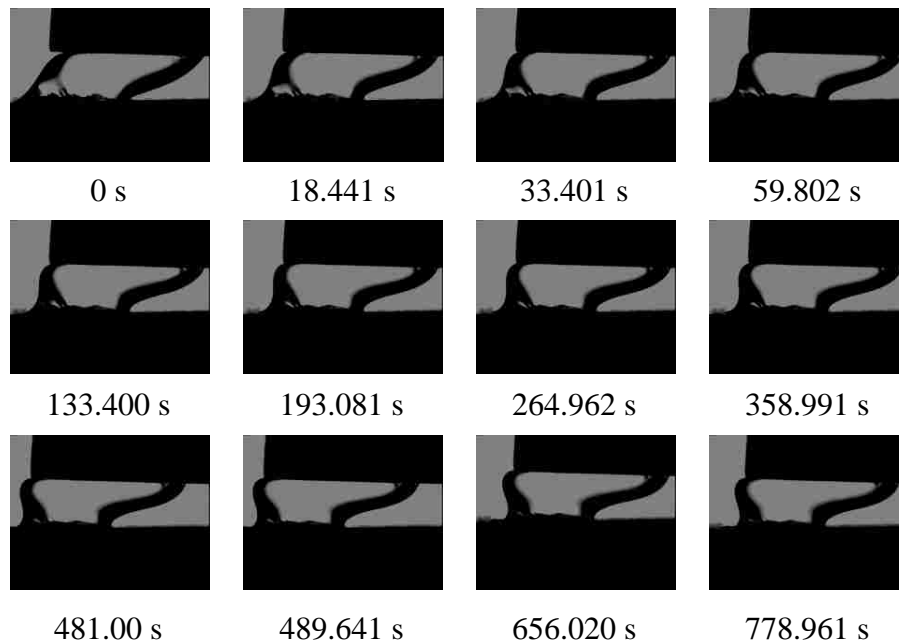
Figure 31: Photographic Depiction of Condensate Drop Dynamic Behavior during 500 ppm Nonionic Surfactant Injection

An obvious and direct observation from Figure 31 is that the condensate drop seemed stable between the two quartz substrates and no smaller droplet was formed during the surfactant injection period. In fact, a slight change of the drop position on the lower surface was found as shown in Table 11 and Figure 32. The diameter of the condensate drop decreased from initial

0.723 cm to 0.583 cm and gave the hint of the movement of the three-phase contact line. This also suggests that nonionic surfactant molecules still exhibited their adsorption property on the interface between condensate and quartz substrate and tried to substitute the condensate drop on the surface. However, the surfactant adsorption on the substrate surface was weaker than adhesion force between the condensate and the substrate so that the condensate drop maintained its position between the two surfaces.

Although the measured advancing contact angles varied corresponding to the change of drop diameter, the minimum advancing angle obtained was about 153° (Table 11 and Figure 33). The wettability of the quartz surface did not alter and remained strongly oil-wet as can be seen in Figure 33 during the 500 ppm nonionic surfactant injection.

Table 11: Quantitative Drop Dynamic Behavior on Lower Substrate during 500 ppm Nonionic Surfactant Injection

Time, s	Advancing Contact Angle θa, °	Contact Diameter (Lower Surface), cm	Height, cm	N_B	N_B'
0	153	0.723	0.272	0	13.12
18.441	158	0.720	0.272	0	13.06
33.401	162	0.705	0.272	0	12.78
59.802	165	0.705	0.272	0	12.78
133.40	160	0.682	0.272	0	12.36
193.081	164	0.673	0.272	0	12.21
264.962	165	0.673	0.272	0	12.21
358.991	158	0.648	0.272	0	11.75
481.000	155	0.611	0.272	0	11.09
489.641	159	0.595	0.272	0	10.78
656.002	153	0.583	0.272	0	10.57

* $\Delta\rho$ of 0.26303 g/cm^3 and σ of 3.86 mN/m were used in the Bond number calculations
N_B and N_B' were calculated using following equations:

$$N_B = \frac{\Delta\rho g(h-h_i)d}{\sigma\cos\theta} \qquad\qquad N_B' = \frac{\Delta\rho g H d}{\sigma}$$
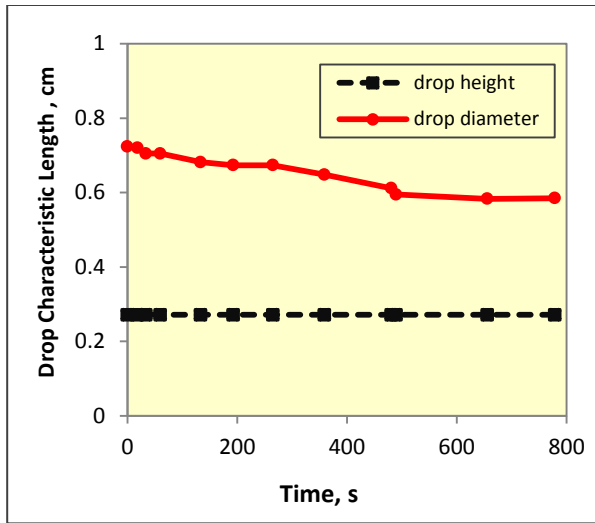
Figure 32: Variations of Condensate Drop Dimensions with Time on Lower Substrate during 500 ppm Nonionic Surfactant Injection
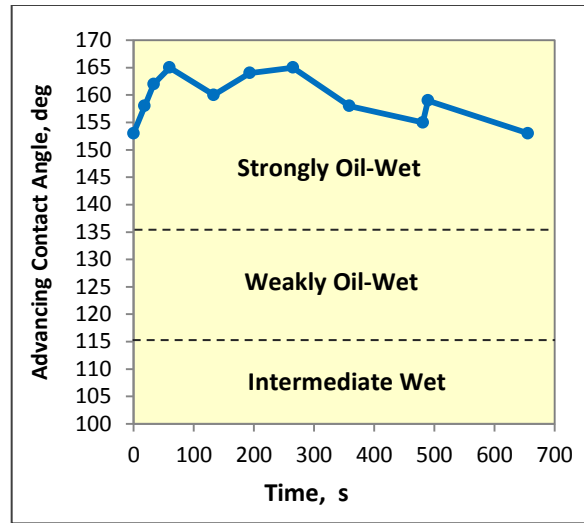
Figure 33: Variation of Dynamic Contact Angle with Time on Lower Substrate during 500 ppm Nonionic Surfactant Injection

4.3.2.2 During 3000 ppm Nonionic Surfactant Injection

Figure 34 demonstrates the photographic sequence of condensate drop behavior on the lower substrate for 3000 ppm nonionic surfactant injection. Table 12 summarizes the values of the dynamic contact angles, contact diameter and height of the condensate drop and Bond number at different time. And the curves of condensate drop characteristic length (diameter and height), and dynamic contact angles against contact time are displayed in Figure 35 and 36.

In this case, it can be plainly seen in Figure 34 that the big condensate drop moved on the lower surface and then sheared to two small drops. But this process began 419.641 seconds (almost 7 minutes) after the start of surfactant injection. Compared with 500 ppm and 1500 ppm anionic surfactant cases, this was much longer than about 20 to 30 seconds which were needed in these two anionic cases. Then the big drop took 51.481 seconds (picture 419.641 s through 471.442 s in Figure 34) to develop the smaller droplet on the lower surface. The time of 51.481 seconds is also much longer than 1.68 seconds in 500 ppm and 1.24 seconds in 1500 ppm

91

anionic surfactant cases, respectively, implying that the anionic surfactant is more effective than the nonionic surfactant in reducing interfacial tension and altering wettability.

| 0 s | 293.00 s | 419.641 s | 425.121 s | 430.041 s |

| 438.081 s | 454.282 s | 466.002 s | 468.962 s | 471.122 s |

| 471.442 s | 477.962 s | 778.002 s | 4707.760 s |
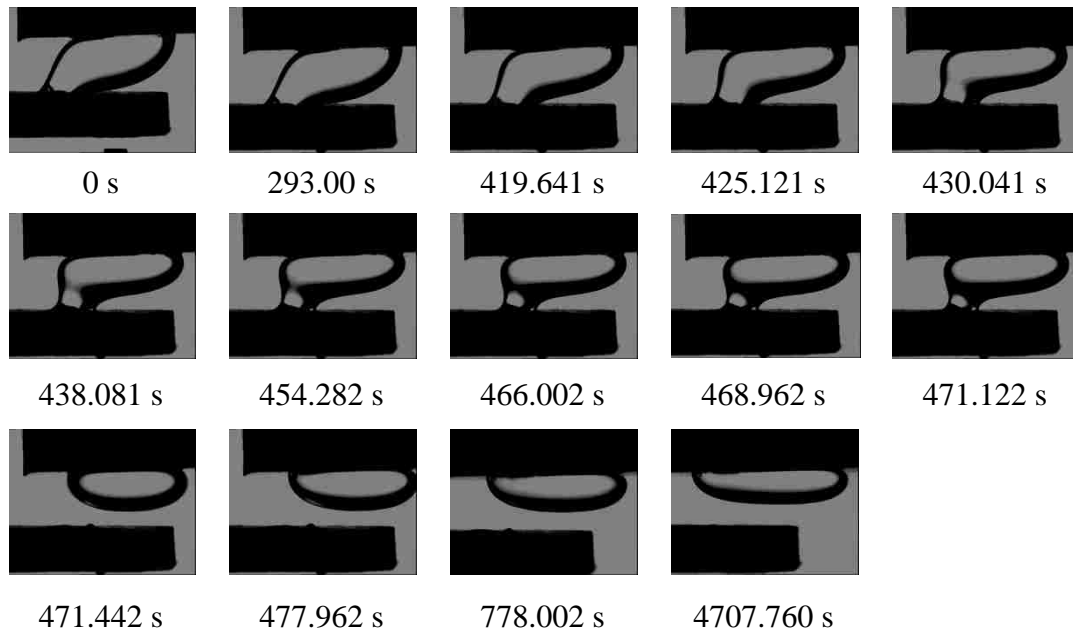
Figure 34: Photographic Depiction of Condensate Drop Dynamic Behavior during 3000 ppm Nonionic Surfactant Injection

Furthermore, Figure 35 displays the sharp change of the drop characteristic length from 0.381 cm to 0.039 cm for diameter and from 0.317 cm to 0.013 cm for height. This indicates the three-phase contact line moving significantly on the lower substrate. However, the distinct change of the condensate drop location resulted from the increase of the surfactant concentration and the adhesion of the condensate to the quartz surface still tends to be stronger than the surfactant adsorption. Thus, the small droplet on the lower surface did not rise up and float away to the upper surface like that observed in the cases of the anionic surfactant, and the droplet seems to be stable on the surface (in the pictures of 477.962 s and 778.002 s of Figure 34). However, the surfactant molecules still influenced the droplet as more surfactant entered the cell. This led to the diameter and height of the droplet slightly changing during this period as shown in Table 12 and Figure 35.

Table 12: Quantitative Drop Dynamic Behavior on Lower Substrate during 3000 ppm Nonionic Surfactant Injection

Time, s	Advancing contact angle θa, °	Contact Diameter (Lower Surface), cm	Height, cm	N_B	N_B'
0	151	0.381	0.317	0	10.25
293.000	163	0.381	0.317	0	10.25
419.641	157	0.350	0.317	0	9.42
425.121	160	0.338	0.317	0	9.08
430.041	162	0.338	0.317	0	9.08
438.081	164	0.321	0.317	0	8.62
454.282	162	0.296	0.317	0	7.95
466.002	162	0.280	0.317	0	7.53
468.962	164	0.280	0.042	6.79	1.00
471.122	166	0.268	0.042	6.43	0.96
471.442	151	0.081	0.025	2.29	0.17
477.962	155	0.079	0.025	2.29	0.17
778.002	155	0.073	0.024	2.30	0.15
4707.760	159	0.039	0.013	1.08	0.04

*Δρ of 0.26316 g/cm^3 and σ of 3.04 mN/m were used in the Bond number calculations. N_B and N_B' were calculated using following equations:

$$N_B = \frac{\Delta\rho g(h-h_i)d}{\sigma cos\theta} \qquad\qquad N_B' = \frac{\Delta\rho gHd}{\sigma}$$
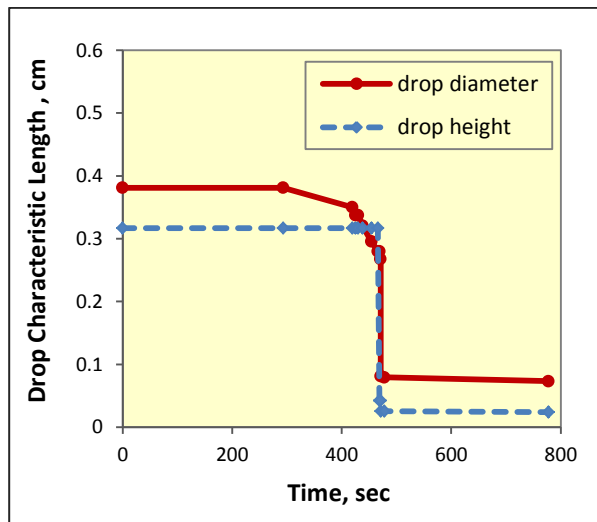

Figure 35: Variations of Condensate Drop Dimensions with Time on Lower Substrate during 3000 ppm Nonionic Surfactant Injection
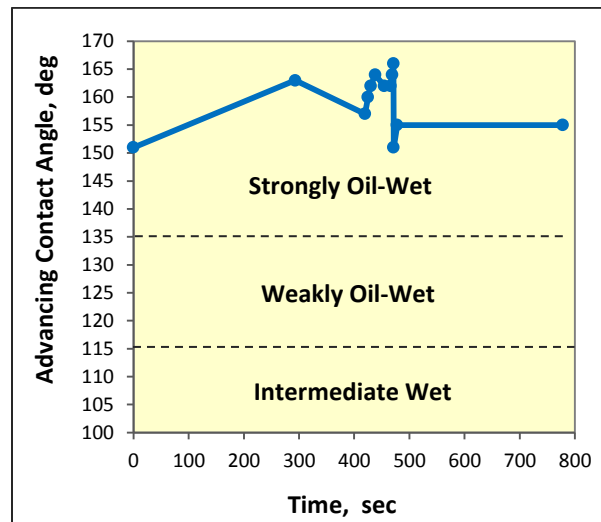

Figure 36: Variation of Dynamic Contact Angle with Time for Condensate Drop on Lower Substrate during 3000 ppm Nonionic surfactant Injection

The measured advancing contact angles also changed in response to the dynamic condensate drop behavior from the maximum value of 166° to the minimum 151° (Table 12 and Figure 36). It is observed from Figure 36 that no transition exists between strongly oil-wet and weakly oil-wet. The quartz surface still retained the strongly oil-wet nature during the 3000 ppm nonionic surfactant injection.

4.3.3 Summary of Results during Surfactant Injection at Ambient Conditions

Both the anionic and nonionic surfactants at three concentrations of 500, 1500 and 3000 ppm were examined at ambient conditions to investigate their wettability altering capability by measuring dynamic contact angles for this condensate reservoir. Figure 37 shows the effect of anionic and nonionic surfactants on interfacial tensions between condensate and synthetic brine and advancing contact angles. It can be seen from Figure 37 that interfacial tension was reduced by two orders of magnitude by the anionic surfactant and only one order of magnitude by the nonionic surfactant. Advancing contact angles measured in different concentrations of nonionic surfactant systems were higher than those in anionic surfactant systems. Larger advancing contact angles (>150°) shown in Figure 37 indicates that even using the high concentration (3000 ppm) of the nonionic surfactant could not alter the strong oil wettability. However, in all three anionic surfactant concentration cases, the wettability of the quartz surface was changed from strongly oil-wet to intermediate-wet as can be found in Figure 37. Hence, the anionic surfactant is more effective than the nonionic surfactant to alter the wettability in this condensate reservoir case.
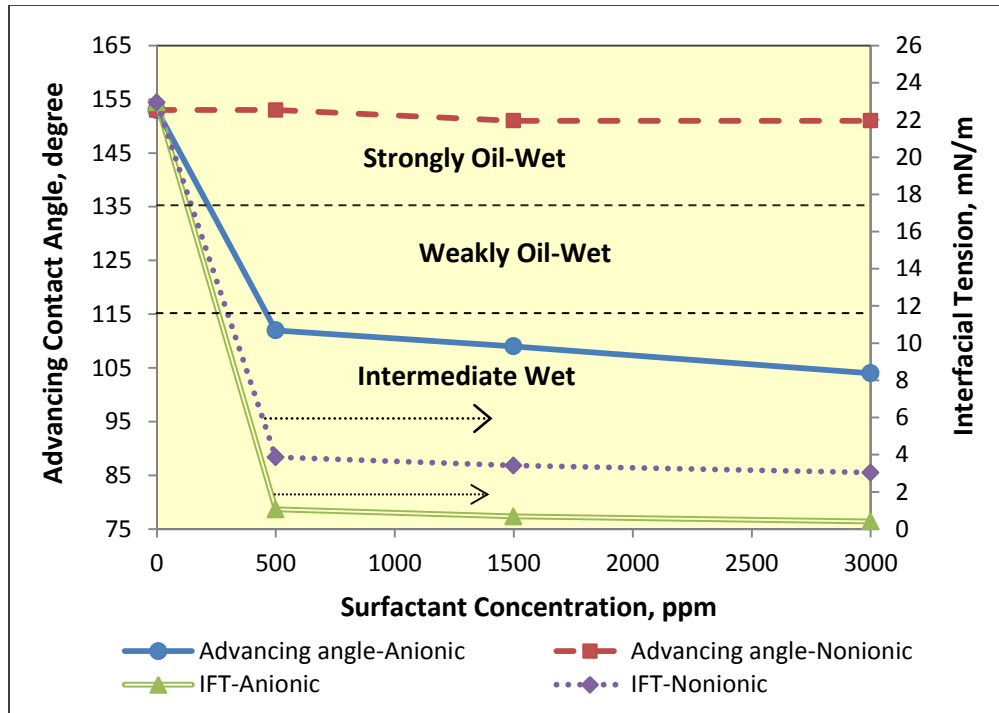
Figure 37: Effect of Anionic Surfactant and Nonionic Surfactant on Advancing Contact Angle and Interfacial Tension at Ambient Conditions

4.3.4 During Anionic Surfactant Injection at Reservoir Conditions

4.3.4.1 During 1500 ppm Injection

The photographic sequence of the dynamic condensate drop behavior on the lower surface over time during the 1500 ppm anionic surfactant injection at 2264 psia and 210 °F is displayed in Figure 38. Figure 39 depicts the change of the diameter and height of the drop with time during the 1500 ppm surfactant injection. The measured advancing contact angles varied with time and are shown in Figure 40.

From Figure 38, it can be seen clearly that the dynamic behavior of the big condensate drop on the lower substrate surface can be divided into two periods to analyze: the big condensate drop in between two substrates from 0 to 265.448 s; and the small drop on the lower substrate from 265.448 s to the end.
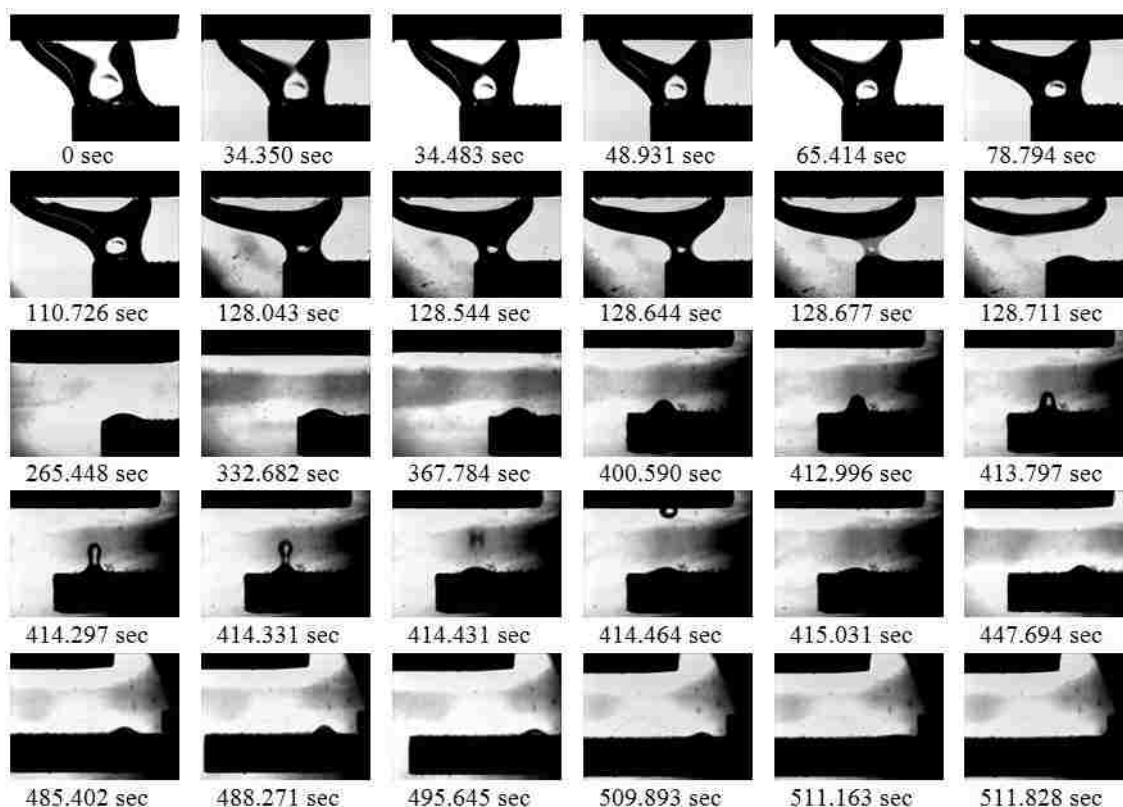
Figure 38: Photographic Depiction of Condensate Drop Dynamic Behavior during the 1500 ppm Anionic Surfactant Injection at 2264 psia and 210 °F

In the first period (0-265.448 s), the big condensate drop in between two substrates underwent movement on the lower surface, forming the drop neck and shearing into two small drops — slightly larger drop on the upper surface and smaller drop on the lower surface, quite similar to the observation at ambient conditions presented earlier. As more and more surfactant entered the cell, the upper condensate drop spread on the surface, floated away to the top of the optical cell due to the reduced interfacial tension (less than 1.22 mN/m) and then left a trace of condensate on the upper surface as shown in pictures at 128.711 to 265.448 s of Figure 38. The drop diameter measured in this period decreased from initial 0.51 cm to 0.25 cm as shown in Figure 39, indicating the movement of three phase contact line (TPCL) on the lower surface. The advancing contact angle corresponding to this period of drop movement (Figure 40) changed

96

from 153° to 120°. This demonstrates the wettability alteration from initially strongly oil-wet to intermediate wet.
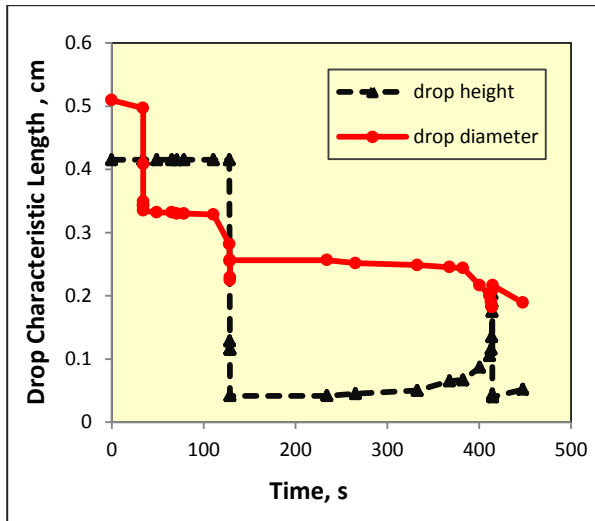

Figure 39: Variations of Condensate Drop Dimensions with Time on Lower Substrate during 1500 ppm Anionic Surfactant Injection at 2264 psia and 210 °F
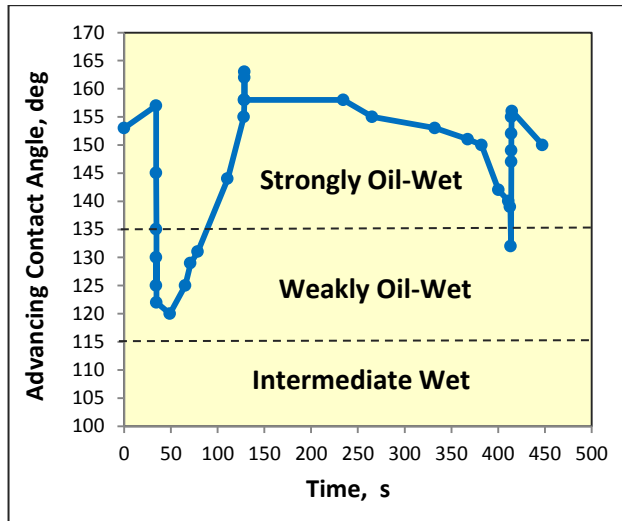
Figure 40: Variation of Advancing Contact Angle with Time for Condensate Drop on Lower Substrate during 1500 ppm Anionic Surfactant Injection at 2264 psia and 210 °F

Next period (from 265.448 s to the end), the dynamic behavior of the small condensate drop on the lower surface from 332.682 s to 415.031 s was also similar to the observations at ambient conditions discussed earlier. The small condensate drop on the lower surface kept rising up until the last part of the drop dislodged from the rest while the reminder collapsed back on the lower surface forming a smaller droplet, as displayed in pictures at 332.682 s through 415.031 s of Figure 38. This dynamic behavior of the condensate drop is the result of the combination of forces. Surfactant molecules adsorbed on the interface which was either between condensate and brine or between condensate and quartz substrate surface. This adsorption on the interface led to the movement of the drop on the surface and a decrease in cohesion force within the condensate phase. The buoyancy force was stronger than the cohesion force but still weaker than adhesion force resulting in part of the condensate drop leaving from the surface. The variation of the drop

height from low (0.067 cm) to high (0.203 cm) and then to low value (0.40 cm) and the movement of TPCL in this period as shown in Figure 39 also demonstrate that surfactant molecules affect the interfaces between condensate and brine as well as that between brine and rock surface and reduce the cohesive force within the condensate phase. The corresponding contact angle form 153° to 132° measured in this period (Figure 40) indicates the wettability altered from strongly oil-wet to weakly oil-wet.

Compared with the case of 1500 ppm anionic surfactant injection at ambient conditions, it took longer (287 seconds from 128.711s to 415.031s in Figure 38) for the small drop on the lower surface to rise up and disintegrate into a smaller droplet in the second period at reservoir conditions. The same process took about 34 seconds at ambient conditions. Also, at reservoir conditions this drop "rising-collapsing-rising" process only occurred once but, at ambient conditions, it happened several times until the whole drop floated away from the surface. Hence, at ambient conditions, the cycling dynamic behavior of the condensate drop on the lower surface was clearly observed especially in the case of 500 ppm surfactant injection. The one possible reason is that this anionic surfactant activity on the surface at reservoir conditions is less effective compared with its property at ambient conditions. The wettability was altered from strongly oil-wet to intermediate-wet at ambient conditions however at reservoir conditions the reservoir still has a weakly oil-wet nature even at a surfactant concentration of 1500ppm.

The other reason is the density difference ($\Delta\rho$) between condensate and brine containing surfactant solution. Table 13 lists the densities of 1500 ppm brine containing surfactant and condensate at both reservoir and ambient conditions. From Table 13, the condensate density of 0.89420 g/cm^3 at reservoir conditions due to compressibility of condensate is higher than 0.73439 g/cm^3 at ambient conditions; on the contrary, the density of 1500 ppm surfactant

solution at reservoir conditions is lower than that at ambient conditions. Therefore, the density

difference ($\Delta\rho$) at reservoir conditions is about 0.0777 g/cm^3 less than the difference of 0.265

g/cm^3 at ambient conditions. The higher condensate density at reservoir conditions of 2264 psia

and 210 °F indicates a stronger cohesion within the condensate phase. When the small drop

disintegrated into the smaller droplets, it was difficult for the buoyancy force to exceed cohesion

force due to the high density of condensate although surfactant molecules continued to affect the

fluid-fluid and rock-fluids interface.

Table 13: Densities of 1500 ppm Anionic Surfactant Solution and Condensate at Reservoir and
Ambient Conditions

Density, g/cm3	Reservoir Conditions	Ambient Conditions
$\rho_{1500ppm}$	0.97192	0.99953
$\rho_{condensate}$	0.89420	0.73439
$\Delta\rho$	0.07772	0.26514

Another interesting observation can be seen from Figure 38 that the smaller condensate

drop on the lower quartz surface started moving on the surface from the left side to the right side

starting from the time step of 332.682 s. Especially from the time step of 414.464 s to the

511.828 s in Figure 38, it can be clearly found moving on the surface until it was blocked from

being seen by the crystal holder. A possible explanation for this phenomenon, firstly, is due to

the low density difference between condensate and surfactant solution as explained in the above

paragraph. Secondly, the orientation of surfactant molecules on the lower surface influences the

dynamic behavior of the condensate drop. Figure 41 illustrates the schematic orientation of

surfactant molecules on the surface. As shown in Figure 41, the condensate drop was not located

in the center of the lower substrate. The space on the surface to the left of the drop is smaller

than the right space. In other words, more space on the right side of the quartz surface was

exposed to the brine. After surfactant injection, for the surface of the right-side of the condensate drop, a water-wet nature led to the surfactant molecules arranging themselves with hydrophobic tail away from the surface as shown in Figure 41. For the surface on the left-side of the drop, the surfactant orientation is also depicted in Figure 41. The left side of the substrate was exposed to the condensate drop because the condensate drop was placed close to the left edge of the quartz substrate. As the surfactant was introduced into the cell, on the left side of the lower surface, the surfactant molecules were oriented with the hydrophilic heads away from the surface due to the oil-wet nature of the surface. The small drop rose on the surface due to a large Bond number (Figure 56 in Section 4.4) but it could not float away owing to the small density difference between brine containing surfactant and condensate. It collapsed on the surface but not on the previous position because on the left side of the drop the surfactant molecules repelled it while on the right side they attracted it. Another possibility is the Marangoni flow effect caused by the interfacial tension gradient across the condensate drop phase. This created a force difference leading to the condensate drop moving on the surface from the left to the right in the manner of alternately rising and collapsing. Also, on the path in which the drop moved, a trace of condensate was left as can be seen in pictures 485.402 s through 511.828 s of Figure 38, which is caused by oil-wet nature of the surface.
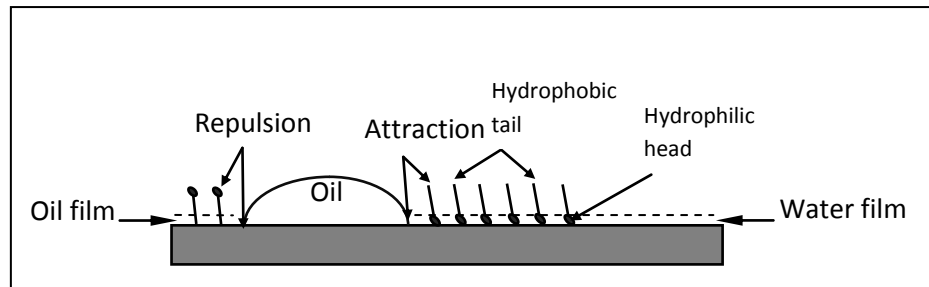

Figure 41: Schematic of Surfactant Orientation Mechanism on Lower Substrate Surface

4.3.4.2 During 500 ppm Injection

Figure 42 illustrates the effect of 500 ppm brine containing anionic surfactant on the dynamic behavior of the condensate drop with time during the surfactant injection period at reservoir conditions of 2264 psia and 210 °F. Variation of condensate drop characteristic length (diameter and height) and dynamic contact angles are plotted against contact time in Figure 43 and Figure 44, respectively.
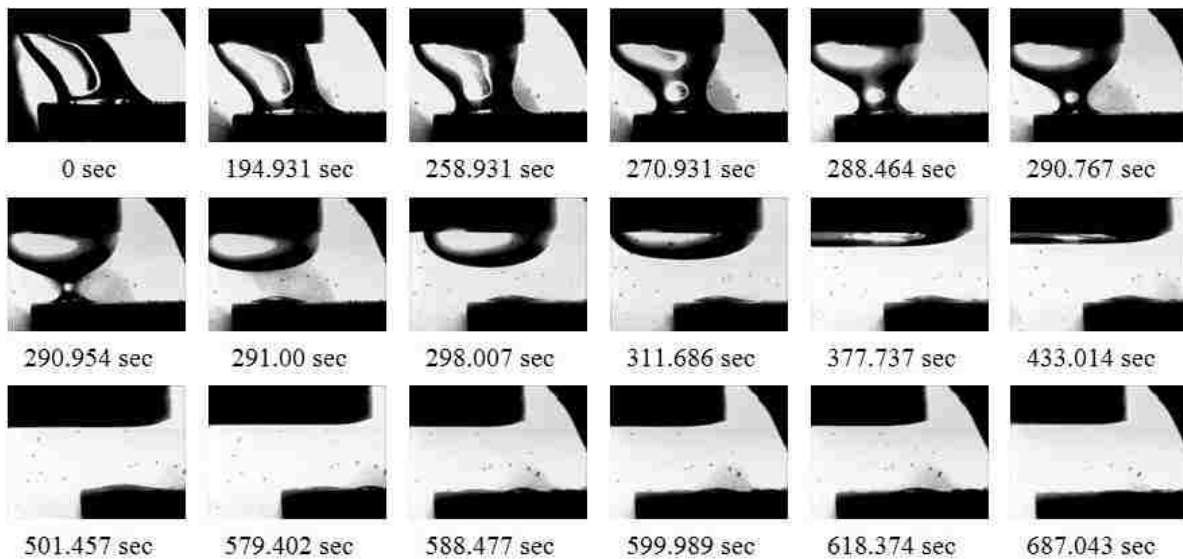
Figure 42: Photographic Depiction of Condensate Drop Dynamic Behavior during the 500 ppm Anionic Surfactant Injection at 2264 psia and 210 °F

In this 500 ppm surfactant injection case, it can be seen from Figure 42 that the big condensate drop moved on the lower quartz surface after starting to introduce anionic surfactant to the system. An obvious observation from Figure 42 is that before this large drop broke into two smaller drops (time step 290.954 s), the advancing contact angles were still large although the three phase contact line moved on the lower surface. This is evidenced by large values of the measured advancing contact angles and drop diameters in Figure 43 and Figure 44, respectively. In other words, during this period from 0 s to 290.954 s, a reduction in interfacial tension from

initial 9.10 at 0 ppm to 1.22 mN/m at 500 ppm (Table 6) between condensate and brine caused

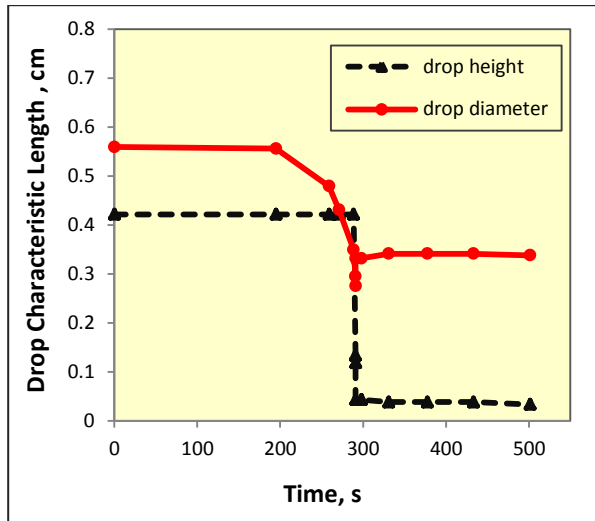by the surfactant is the main reason for the movement of TPCL.

Figure 43: Variations of Condensate Drop Dimensions with Time on Lower Substrate during the 500 ppm Anionic Surfactant Injection at 2264 psia and 210 °F
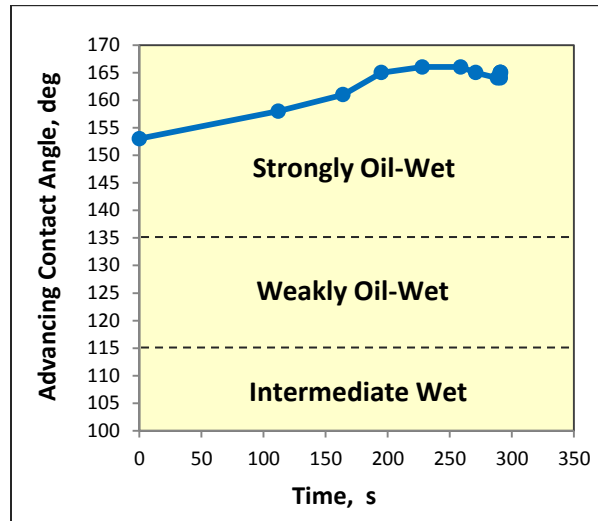
Figure 44: Variation of Advancing Contact Angle with Time for Condensate Drop on Lower Substrate during 500 ppm Anionic surfactant Injection at 2264 psia and 210 °F

After the time step 290.954 s, the big drop sheared into two smaller drops as shown in

picture at 291 s of Figure 42. The small condensate drop on the upper surface spread on the

upper surface and floated away to the top of the optical cell. On the upper surface at last only a

trace of condensate was left (see pictures 291 s through 501.457 s in Figure 42).

However, from Figure 42, another small condensate drop located on the lower surface

appeared stable on the surface for 3.5 minutes (291 s to 501.457 s). There was no obvious

process of alternate drop rising and collapsing similar to what occurred in the case of 1500 ppm

surfactant injection. However, as more surfactant molecules were injected into the HPHT optical

cell, the phenomenon of the small drop moving on the surface from the left to the right (579.402

s to 687.043 s of Figure 42) similar to that in1500 ppm case was observed. The reasons for this

102

movement are the same as in the previous 1500 ppm case: low density difference, surfactant molecules orientation on the surface and the Marangoni flow effect.

Although the measured advancing contact angles also varied with time, the minimum advancing angle obtained was about 153° (Figure 44). The wettability of the quartz surface was not altered and remained strongly oil-wet as displayed in Figure 44 during the 500 ppm anionic surfactant injection at reservoir pressure 2264 psia and temperature 210 °F. In the same concentration case at ambient conditions, it did change the wettability from strongly oil-wet to weakly oil-wet or intermediate wet. This indicates that this surfactant is less effective in altering wettability at reservoir conditions and its surface active properties were affected by pressure and temperature. It also further emphasized the facts that rock-fluid interactions depend on pressure and temperature and that such measurement should be made at reservoir conditions.

4.3.4.3 During 3000 ppm Injection

The photographic sequence of condensate drop behavior on the lower surface is demonstrated in Figure 45 for 3000 ppm anionic surfactant injection. Figure 46 and 47 illustrate the plots of condensate drop characteristic length (diameter and height) and advancing contact angle versus time.

In this 3000 ppm case, the experimental procedure of the surfactant injection was slightly different from above two cases. After completing DDDC experiment, the lower substrate was moved back laterally instead of immediately injecting surfactant into the HPHT optical cell, as shown in pictures "After DDDC" and 0 s of Figure 45. This movement created the equilibrium receding angle equaled to 65°. Then the 3000 ppm surfactant solution was introduced to the cell.

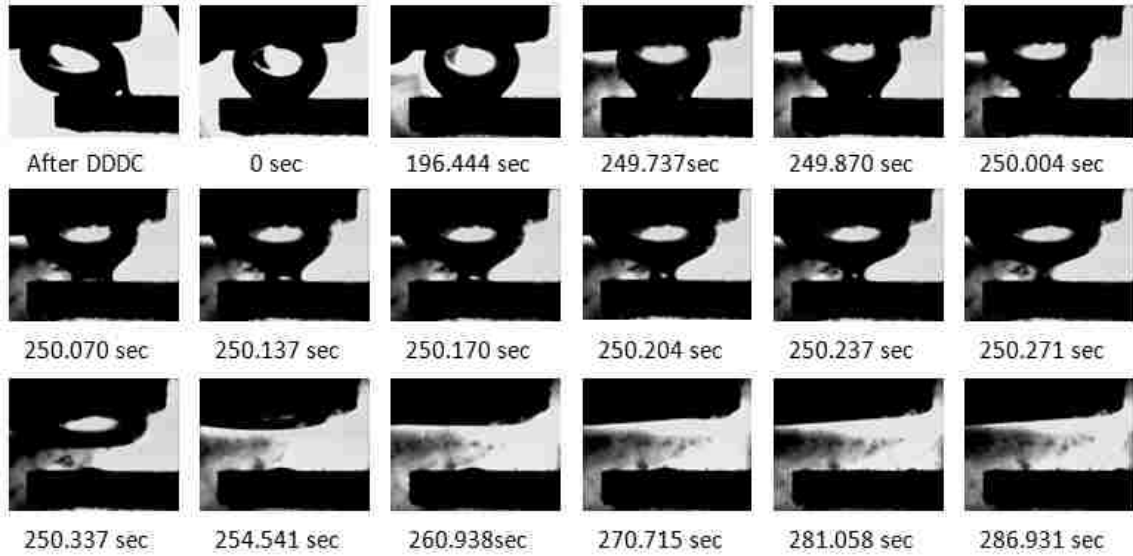| After DDDC | 0 sec | 196.444 sec | 249.737sec | 249.870 sec | 250.004 sec |
| 250.070 sec | 250.137 sec | 250.170 sec | 250.204 sec | 250.237 sec | 250.271 sec |
| 250.337 sec | 254.541 sec | 260.938sec | 270.715 sec | 281.058 sec | 286.931 sec |

Figure 45: Photographic Depiction of Condensate Drop Dynamic Behavior during the 3000 ppm Anionic Surfactant Injection at 2264 psia and 210 °F
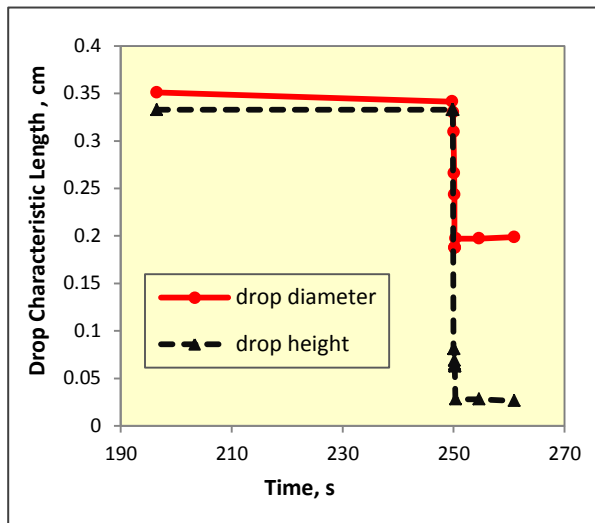
Figure 46: Variations of Condensate Drop Dimensions with Time on Lower Substrate during the 3000 ppm Anionic Surfactant Injection at 2264 psia and 210 °F
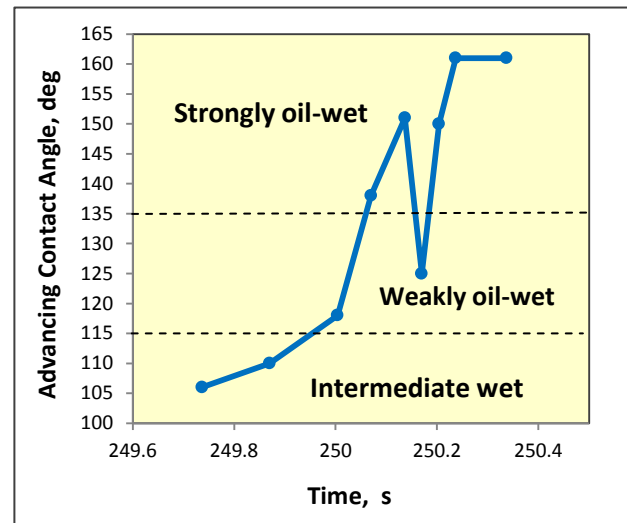
Figure 47: Variation of Advancing Contact Angle with Time for Condensate Drop on Lower Substrate during 3000 ppm Anionic surfactant Injection at 2264 psia and 210 °F

From Figure 45, the big condensate drop quickly broke into two small drops especially after the drop neck was formed at time step 250.004 second and it took only 0.3 second (from 250.004 s to 250.337 s) due to higher surfactant concentration. During this period, the drop

104

moved on the lower surface resulting in a movement of TPCL (corresponding to a decrease of drop height and diameter) and a change of advancing contact angles as can be seen in Figure 46 and 47. The alteration of advancing angles indicates that the quartz substrate surface is no longer preferentially strongly oil-wet by nature. And its wettability clearly shown in Figure 47 is altered by the 3000 ppm surfactant treatment to be intermediate-wet or weakly oil-wet.

After the time step of 250.337 s, the small drop on the upper surface spread on the upper surface and floated away to the top of the optical cell as well due to the low interfacial tension induced by the surfactant. Obviously alternate drop rising and collapsing was not observed for the smaller droplet on the lower surface. And this small droplet behaved in a similar manner to the before mentioned 500 and 1500 ppm cases. It moved on the lower surface from the left to the right as shown in pictures 270.715 s to 286.931 s of Figure 45. This movement is also attributed to low density difference, surfactant molecules orientation on the surface and the Marangoni flow effect.

4.3.4.4 Summary of Results at Reservoir Conditions

The anionic surfactant at three concentrations of 500, 1500 and 3000 ppm was tested to investigate its wettability altering capability by measuring dynamic contact angles for this particular condensate reservoir at reservoir conditions (2264 psia and 210 °F). The effect of this anionic surfactant on interfacial tensions (condensate-water and CH_4-water), spreading coefficient and advancing contact angles at reservoir conditions is plotted in Figure 48. It can be seen from Figure 48 that in the low concentration (500 ppm) case the values of IFT, spreading coefficient and advancing contact angle are much higher than those in the 1500 ppm and 3000 ppm cases. This indicates that this anionic surfactant at low concentration has less influence on both fluid-fluid interactions and rock-fluid interactions at reservoir conditions.
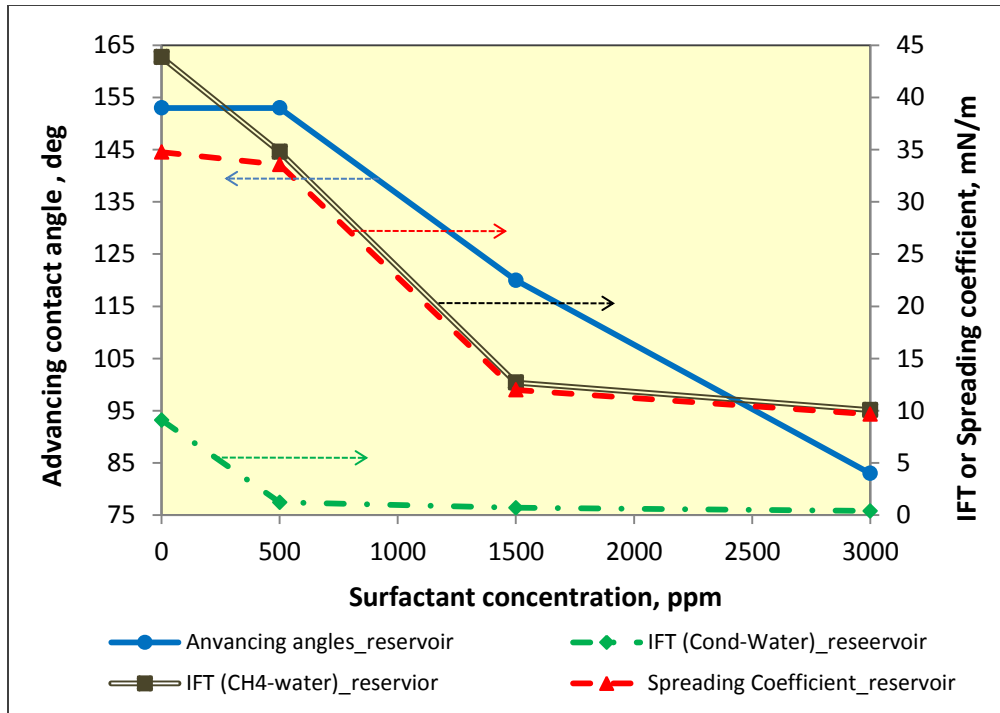
Figure 48: Effect of Anionic Surfactant on Interfacial Tension, Spreading Coefficient and Advancing Contact Angle at Reservoir Conditions of 2264 psia and 210 °F
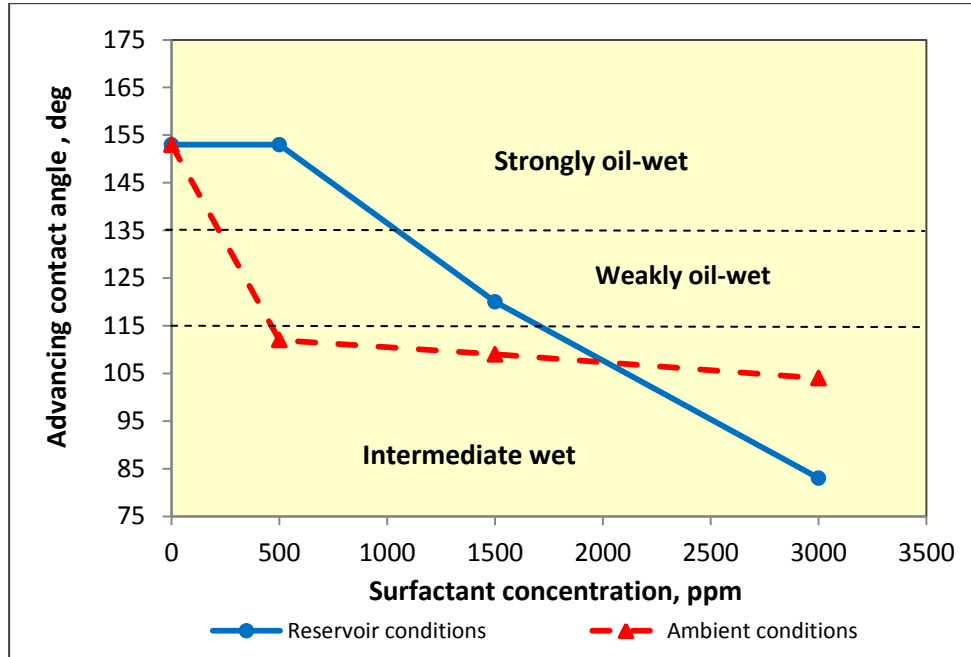

Figure 49: Effect of Anionic Surfactant on Advancing Contact Angle at Ambient and Reservoir Conditions (2264 psia and 210 °F)

106

Figure 49 shows the comparison of the effect of the anionic surfactant on advancing contact angles at ambient and reservoir conditions. As can be seen in Figure 49, at ambient conditions, in all three surfactant concentration cases, the reservoir wettability was altered from strongly oil-wet to weakly oil-wet or intermediate-wet. However, at reservoir conditions, the low concentration 500 ppm of anionic surfactant solution was not found to change reservoir wettability. As the surfactant concentrations increased to 1500 and 3000 ppm, it was clearly observed from Figure 49 that the anionic surfactant altered the wettability of quartz surfaces from strongly oil-wet to weakly oil-wet or intermediate-wet. The difference between these two conditions indicates that the effectiveness of the anionic surfactant on altering wettability at reservoir conditions is less than that at ambient conditions for this particular reservoir case. This proves that surfactants exhibit their specific characteristics at different pressure and temperature conditions. It also demonstrates that rock-fluids interactions depend on pressure and temperature as well.

4.3.5   After Surfactant Injection at Ambient and Reservoir Conditions

After surfactant injection, the optical cell was full of the specific concentration of brine containing surfactant at ambient and reservoir conditions of 2264 psia and 210 °F. At both conditions, in all three anionic surfactant solution cases, almost nothing or only a trace of condensate drop was found staying on the upper and lower quartz surfaces. For the two lower concentrations (500 and 1500 ppm) nonionic surfactant cases at ambient conditions, the condensate drop kept staying between the two surfaces, and the only difference between the original drop and the final drop is the drop shape due to surfactant effect. For the highest concentration (3000 ppm) nonionic surfactant case, a very small condensate droplet can be

observed on the lower substrate surface and a small drop remained on the upper surface (see the picture 4707.760 s of Figure 34).

Further experiments were conducted to investigate the quartz-condensate interaction after surfactant injection for both ambient and reservoir conditions. The first test was to bring down the upper surface and let the trace of condensate drop on the two surfaces merge once again. The second test was that the lower surface which had the condensate trace (referred to as surface A) was turned upside down and a condensate drop was injected and placed in the same position on the surface A. The last test was carried out to examine the surface B which is the other surface of the lower substrate which had not been in contact with the condensate. Another condensate drop was placed on this unexposed surface.

The observations for the surface A and B obtained from ambient and reservoir conditions experiments are similar. As an example, after 1500 ppm anionic surfactant injection at 2264 psia and 210 °F, the dynamic behavior of condensate drop on lower surface A is shown in Figure 50. The interesting observation is that the two droplets could not mingle into one (not shown in Figure 50) or the new condensate drop was unable to be placed on the surface A to touch the old droplet as can be seen in Figure 50.

| 8.609sec | 8.676 sec | 8.742 sec | 8.809 sec | 10.044sec |

Figure 50: Dynamic Behavior of Condensate Drop on Lower Surface A after 1500 ppm Anionic Surfactant Injection at 2264 psia and 210 °F

Figure 51 presents the consecutive photographs extracted from the surface B test after surfactant injection at ambient conditions. Pictures taken at 3.040 s through 7.040 s illustrate the

condensate drop behavior on the lower surface B in the 500 ppm anionic surfactant system. Pictures 1.800 s to 19.161 s and pictures 4.800 s to 17.321 s represent the case of the 3000 ppm nonionic surfactant system. It should be noted here that pictures 1.800 s to 19.161 s and pictures 4.800 s to 17.321 s were obtained from two time recordings in the experiment.   It can be seen from Figure 51 that the condensate drop had no ability to adhere to the surface even though the tip of the needle was inserted into it to hold it in place in both the systems. Once the tip was removed from the drop, the drop immediately floated away to the top of the cell as shown in Figure 51. Similar phenomena and surfactant adsorption mechanisms have been elaborated and used by Ayirala et al. (2006) to analyze the effect of surfactants on wettability in an oil-wet fractured reservoir. Hence, a brief explanation of the mechanism of the drop behavior is given below.

| 3.040 s | 3.480 s | 3.600 s | 5.600 sec | 6.640 s | 7.040 s |

500 ppm Anionic Surfactant System

| 1.800 s | 10.560 s | 19.121 s | 19.161 s |

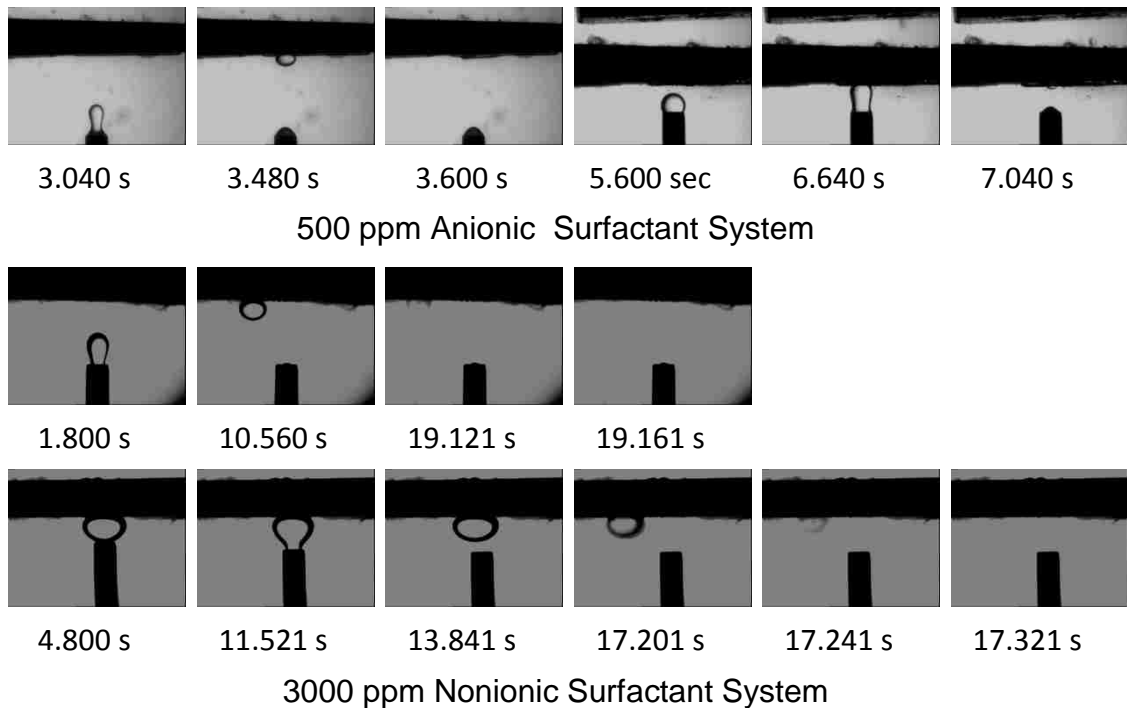| 4.800 s | 11.521 s | 13.841 s | 17.201 s | 17.241 s | 17.321 s |

3000 ppm Nonionic Surfactant System

Figure 51: Dynamic Behavior of Condensate drop on Lower Surface B after Surfactant Injection at Ambient Conditions

The surface A was initially exposed to condensate and a film of condensate was formed on the surface. Figure 52 schematically displays the proposed mechanism of this phenomenon for the second test of surface A. After surfactant injection, surfactant molecules adsorbed on this film and orientated themselves with the hydrophobic tails in the condensate film and the hydrophilic heads away from the surface as shown in Figure 52. When the new condensate drop was introduced into the cell for the second test, surfactant molecules oriented themselves on the condensate surface in the same way as they did on the lower surface A (Figure 52). As the drop approached the surface, an electrostatic repulsion force took place between the hydrophilic heads of surfactant molecules adsorbed on condensate drop and the rock surface began to wet. This led to the drop being unable to come in contact with the surface. And the same mechanism can be applied to the first test of surface A. Also, due to the repulsion between hydrophilic heads of surfactant molecules absorbed on the two rock surfaces, it was impossible for the two condensate drops to mix together.
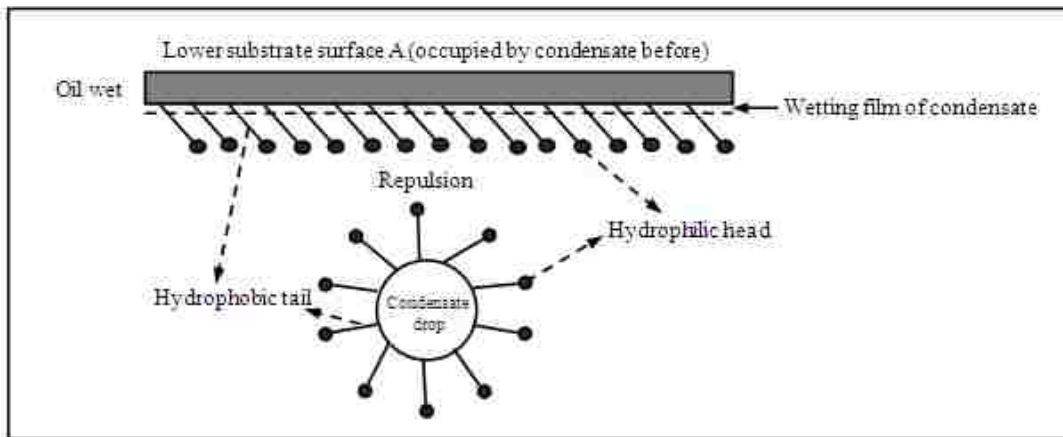

Figure 52: Schematic of Surfactant Orientation Mechanism on Lower Substrate Surface A

Figure 53 illustrates the possible mechanism of surfactant action on the surface B. The surface B was not previously occupied by condensate. It was clean and only exposed to the brine containing surfactant. Hence, the surface initially had been covered with a thin water film and its

nature should be water-wet as can be seen in Figure 53. The surfactant molecules were oriented with hydrophobic tail away from the surface, which was the reverse of the former two tests. It is clear that the hydrophilic head groups of surfactant molecules adsorbed on the condensate drop would be attracted by hydrophobic tail groups adsorbed on the surface B. Thus, at first the drop can be easily adhered to the surface. As more and more condensate molecules occupied the surface and displaced the water molecules, the water-wet surface was altered to oil-wet. Consequently, the surfactant molecules reoriented themselves to respond to the change of the surface nature with hydrophilic heads away from the surface. The force transition from attraction to repulsion between the surface and the condensate drop caused the drop to detach from the surface and float to the top of the cell.
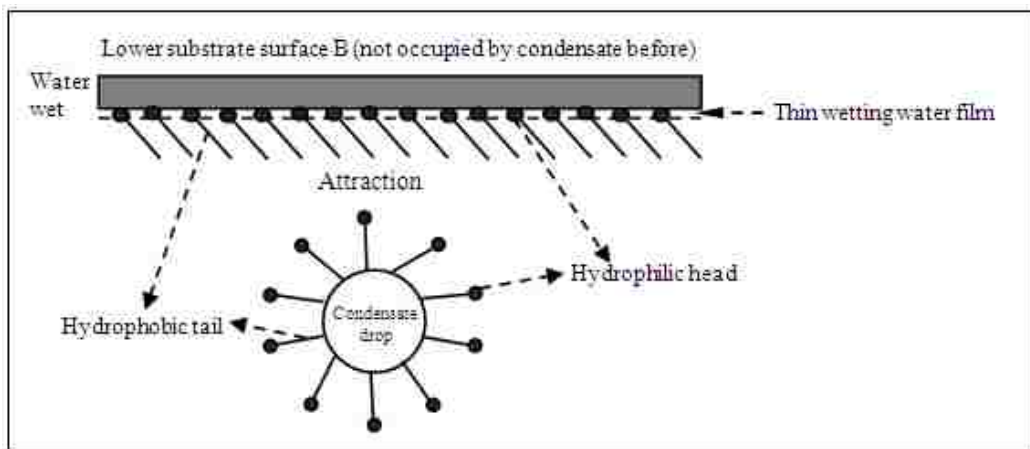

Figure 53: Schematic of Surfactant Orientation Mechanism on Lower Substrate Surface B

It should be noted here that a slight difference occurs between anionic surfactant cases and nonionic surfactant cases while testing the interactions on surface B. In anionic surfactant cases, once the condensate drop reached the surface, it could not keep the regular drop shape and immediately deformed to a condensate film on the surface. It is this condensate film, not the drop, that departed from the surface as can be noticed in pictures 3.600 s and 7.040 s of Figure 51 in the 500 ppm anionic surfactant system. However, pictures 10.560 s and 13.841 s of Figure 51

111

show that the condensate drop still can maintain the regular drop shape in the 3000 ppm nonionic surfactant system. The drop moved fast on the surface and finally left the lower surface B. A good explanation for this observation is that these two types of surfactants have different effects on brine-condensate interfaces. In other words, different interfacial tensions in these two systems cause the different behavior of the condensate drop. As shown in Table 5, the IFT in the anionic system are lower than those in the nonionic system. Lower interfacial tensions in anionic systems contribute to the deformation of the condensate drop. Therefore, surface active properties of surfactant molecules at the brine-condensate interface and the rock- liquid (brine or condensate) interface control the ability of the condensate drop on the rock surface.

Finally, the absent of wettability reversals to native wettability state during the experiments and the reduction in IFT with increasing surfactant concentration at all concentrations showed that the concentration of the surfactant did not approach the critical micelle concentration (CMC) due to the absence of significant bilayer adsorption of the surfactant on the rock surface. It can be concluded that all the surfactant concentrations used in this work were below the CMC of the surfactant at both ambient and reservoir conditions.

4.4   Calculated Bond Number

The calculated Bond Number N_B and N_B' based on Eq. (4) and Eq. (2) for the four ambient-condition cases were given in Table 7, 8, 9 and 10. Figure 54 and 55 show the Bond Numbers, N_B and N_B', of the ambient-condition cases during 500 ppm and 1500 ppm anionic surfactant injection. And the right plot in Figure 54 displays the variation of both the Bond numbers with time at the time steps 644-656 s. The trends of Bond Number N_B and N_B' computed for three 500, 1500 and 3000 ppm reservoir-condition cases are similar. Therefore, 1500 ppm anionic surfactant case at reservoir conditions as an example was discussed here and the plots of the Bond number N_B and N_B' against time for this case are shown in Figure 56.

As can be seen in Figure 54, both the Bond numbers, N_B and N_B', show the cyclical trends. It provides the evidence that the surfactant gradually affects the dynamic behavior of condensate drop on the surface. Significant difference between N_B and N_B' as shown in right picture of Figure 54 is that the Bond number N_B calculated using contact angle is larger than N_B' which does not use the contact angle. Especially at the time 655.60 s, N_B' approached a value of 0.76 (less than unity), but N_B is 9.36 much higher than unity. Based on the conclusion of Hirasaki and Zhang (2004), the condensate drop should be stable if considering the N_B' of 0.76. However, the movement of the drop on the surface could still be visually observed in Figure 24 after 655.60 seconds. This condensate drop dynamics could be better described by the Bond number N_B, since it was more than unity indicating the unstable drop on the surface.
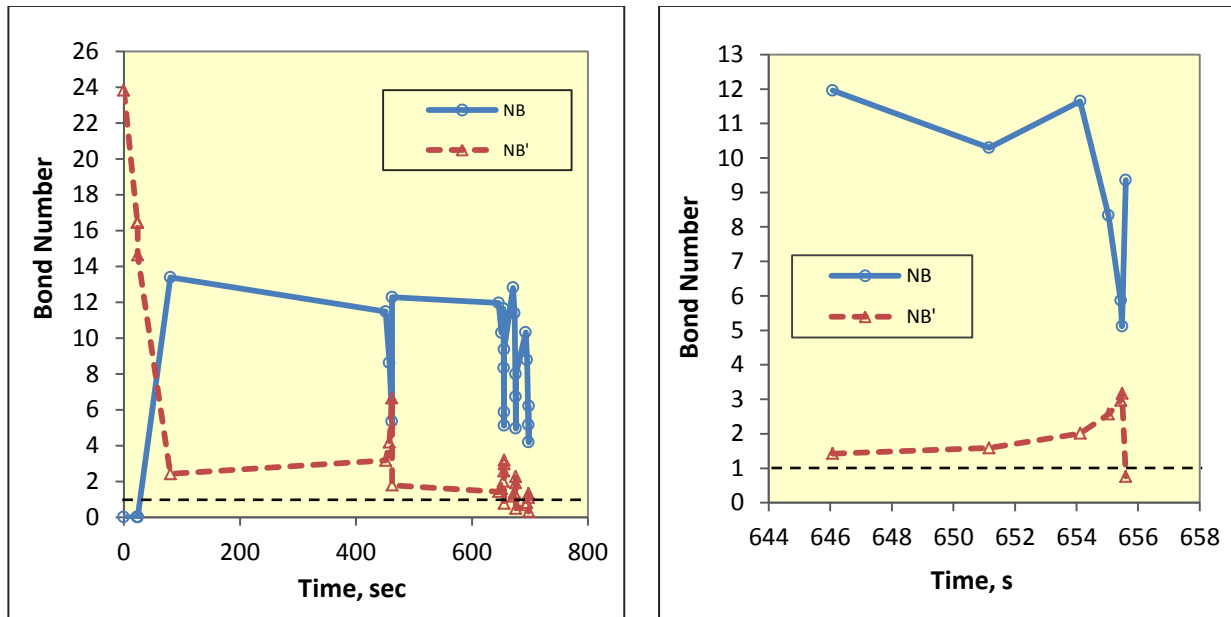

Figure 54: Variation of Bond number with Time for Condensate Drop on Lower Substrate during the 500 ppm Anionic Surfactant Injection at Ambient Conditions (right: at time steps 644-656 s)
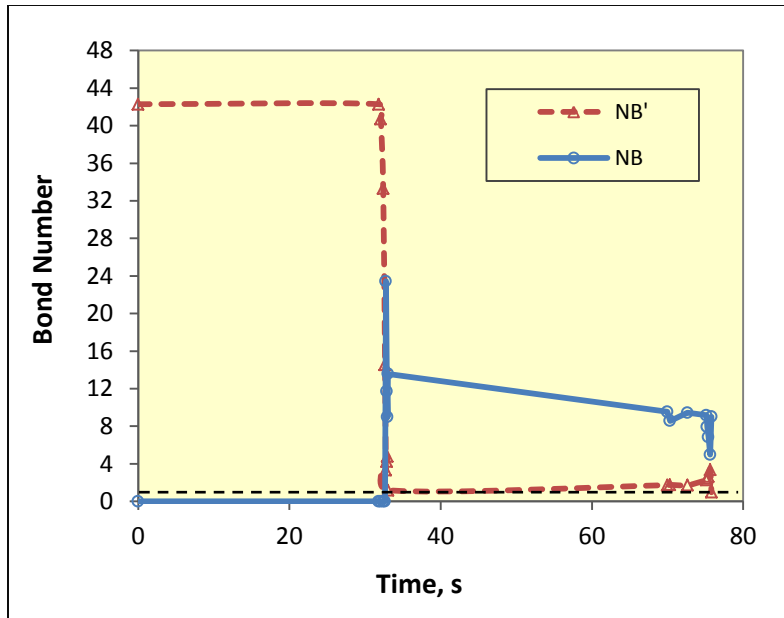
Figure 55: Variation of Bond number with Time for Condensate Drop on Lower Substrate during the 1500 ppm Anionic Surfactant Injection at Ambient Conditions
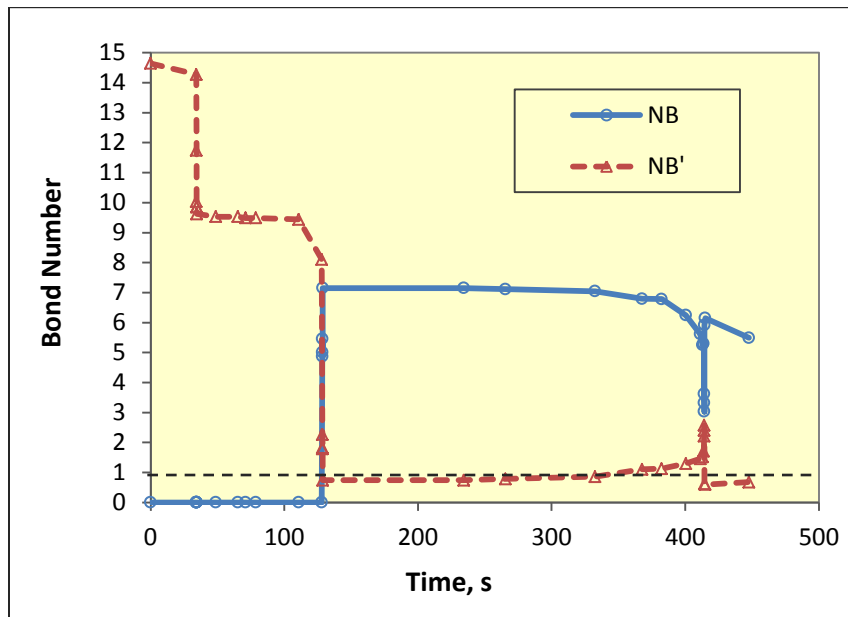

Figure 56: Variation of Bond number with Time for Condensate Drop on Lower Substrate during the 1500 ppm Anionic Surfactant Injection at 2264 psia and 210 °F

From Figure 55 and 56, it can be seen that the trends of the Bond numbers N_B and N_B' for both ambient conditions and reservoir conditions at 1500 ppm anionic surfactant injection cases

are similar to the case of 500 ppm surfactant injection at ambient conditions. The Bond number N_B' is equal to 0.97 (less than 1) but N_B is 9.07 at the time of 75.797 seconds as shown in Figure 55 and Table 8 for ambient-condition 1500 ppm case; while the Bond number N_B' of reservoir-condition 1500 ppm case, for example, is 0.74 (<1) at time step 128.711 s (in Figure 56) and N_B is 7.15 at the same time step. According to the values of the Bond Number N_B (greater than 1), it indicates an unstable state on the surface. This is consistent with the visual observations recorded during the experiments. From Figure 28 and Figure 38, it can be found that the drop rose up once again after 0.16 second for the ambient-condition case and 204 seconds for the reservoir-condition, respectively. It clearly points out that still some more time is needed for the condensate drop to stabilize on the lower substrate. This confirms that the criterion that the drop should be stable at Bond numbers less than unity appears to be true only for the Bond number formulation including contact angle term.
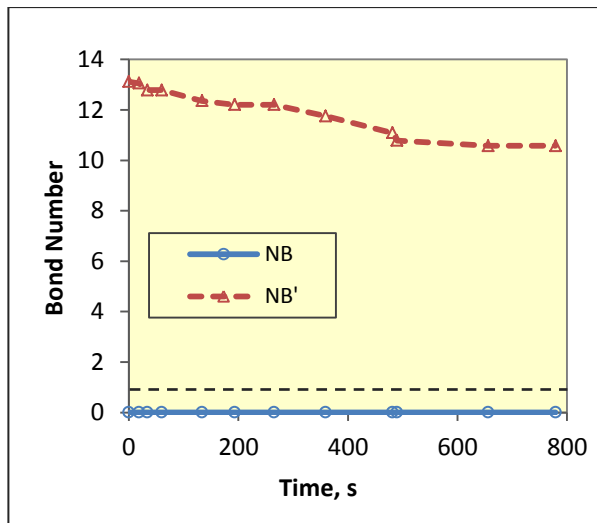

Figure 57: Variation of Bond Number with Time for Condensate Drop on Lower Substrate during the 500 ppm Nonionic Surfactant Injection at Ambient Conditions
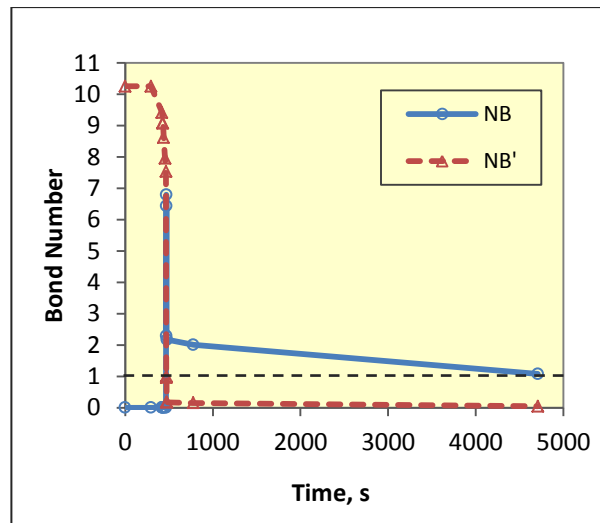
Figure 58: Variation of Bond Number with Time for Condensate Drop on Lower Substrate during the 3000 ppm Nonionic Surfactant Injection at Ambient Conditions

Figure 57 and 58 illustrate the variation of the Bond Number N_B and N_B' against contact time at ambient conditions during 500 ppm and 3000 ppm nonionic surfactant injection. From Table 9 and Figure 57, the Bond number N_B is equal to zero since the drop is always in equilibrium between the two substrates during injecting 500 ppm nonionic surfactant solution. This indicates that the condensate drop is stable on the surface. However, in this case the Bond number N_B' has opposite characteristics. It always has a higher value (more than 10) as shown in Table 11 and Figure 31 indicating the drop's instability on the surface. This is not true because until the surfactant injection process was accomplished (about 80 minutes) the drop was observed in Figure 31 to be still on the surface just as it was in 778.961 s. This confirms that N_B' (without contact angle) is not represented of the phenomenon occurring.

For 3000 ppm ambient-condition nonionic surfactant injection case, it can be noticed from Table 12 and Figure 58 that after the time step 468.692 s the Bond number N_B' is less than unity suggesting that the droplet is stable on the surface; nevertheless, the values of N_B are larger than one which indicates that the drop is unstable during this period (from 468.692 s and 778.002 s) and needs more time to become stable. This is proved by the later observations in Figure 34 that until the time step 4707.760 s (about 79 minutes) the Bond number N_B becomes close to the unity (1.08), indicating that the droplet should be stable on the lower substrate. After 80 minutes surfactant injection, the droplet became a very small drop and appeared stationary on the lower surface as can be seen in Figure 34.

Hence, these two nonionic surfactant injection cases give the further evidence that the Bond number formulation containing contact angle provides a better characterization of dynamic capillary/gravity phenomenon.[1]

---

[1] The material in Chapter 4.1-4.4 was previously presented at the conferences: SPE/DOE Improved Oil Recovery Symposium held in Tulsa, OK, USA, April 24-28, 2010, and SPE International Symposium on Oilfield Chemistry held in The Woodlands, Texas, USA, April 11-13, 2011.

4.5   Surfactant-Induced Flow Behavior at Ambient Conditions [2]

Unsteady state relative permeability measurements were conducted before and after surfactant treatment to investigate the effects in gas relative permeability and oil (condensate) recovery in Berea sandstone rock-condensate-synthetic brine system. Surfactant-induced wettability effect was also investigated by using the relative permeability measurements, mainly oil-water relative permeability ratio and fractional flow curves.

Initial water saturation, residual oil saturation and endpoint relative permeabilities were measured through coreflood experiments along with pressure and recovery profiles. These were then history matched using a coreflood simulator to obtain the relative permeability and oil-water relative permeability ratio curves. The history match of recovery and pressure drop obtained from the simulator as well as the resulting relative permeability curve is shown in Appendix. Craig's rules of thumb in Table 14 were applied to interpret wettability changes in this study.

Table 14: Craig's Rules of Thumb Used for Wettability Interpretation (Ayirala, 2002)

Criterion	Water-wet	Oil-wet
Initial water Saturation, S_{wi}	>0.25	<0.15
Water saturation at cross-over point	>0.5	<0.5
Endpoint relative permeability to water at S_{or}	<0.3	>0.5
Endpoint relative permeability to oil at S_{wi}	>0.95	<0.7~0.8

4.5.1   Relative Permeability and Wettability Measurements for Berea Rock-Condensate-Synthetic Brine System

The history match of condensate recovery and pressure drop obtained from a coreflood simulator (See section 3.5) during the waterflood in the absence of surfactant (0 ppm) in Berea

---

sandstone rock-condensate-synthetic brine system at room temperature of about 68°F is shown in Figure 59 and Figure 60. The comparison of simulation and experimental results for endpoints is listed in Table 15. It can be seen from Figure 59, 60 and Table 15 that a good history match was obtained. The resulting relative permeability curves obtained from the simulator are shown in Figure 61.
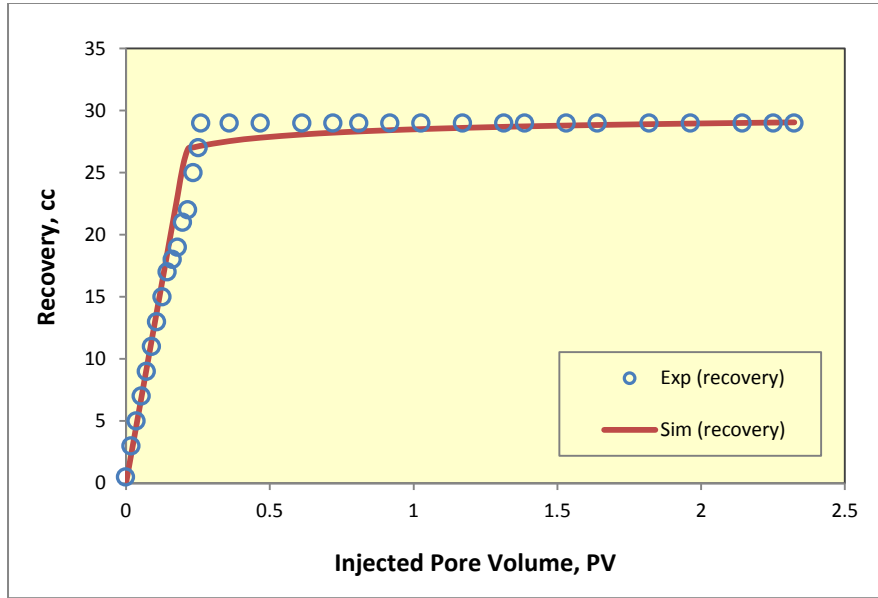

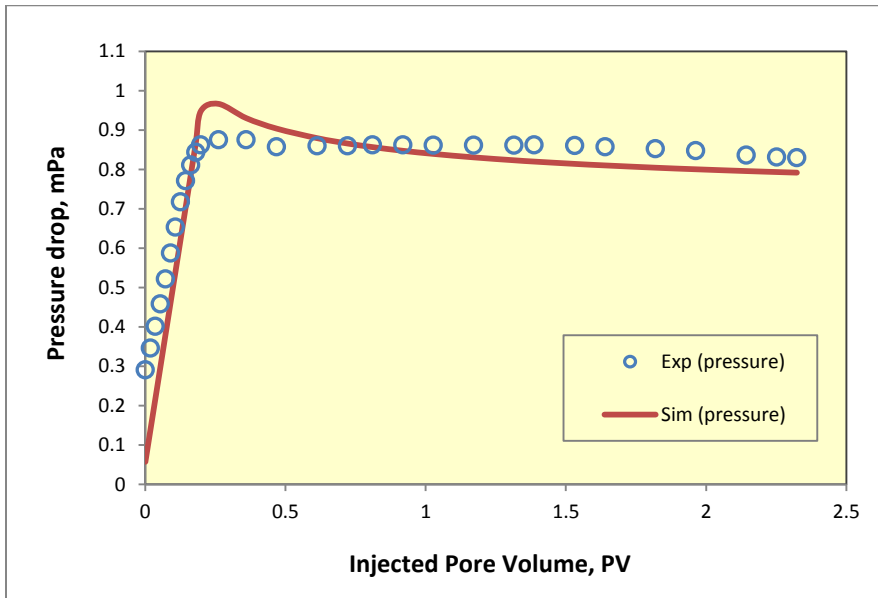Figure 59: History Match of Condensate Recovery for Base Case (0ppm, No Surfactant)

Figure 60: History Match of Pressure Drop for Base Case (0ppm, No Surfactant)
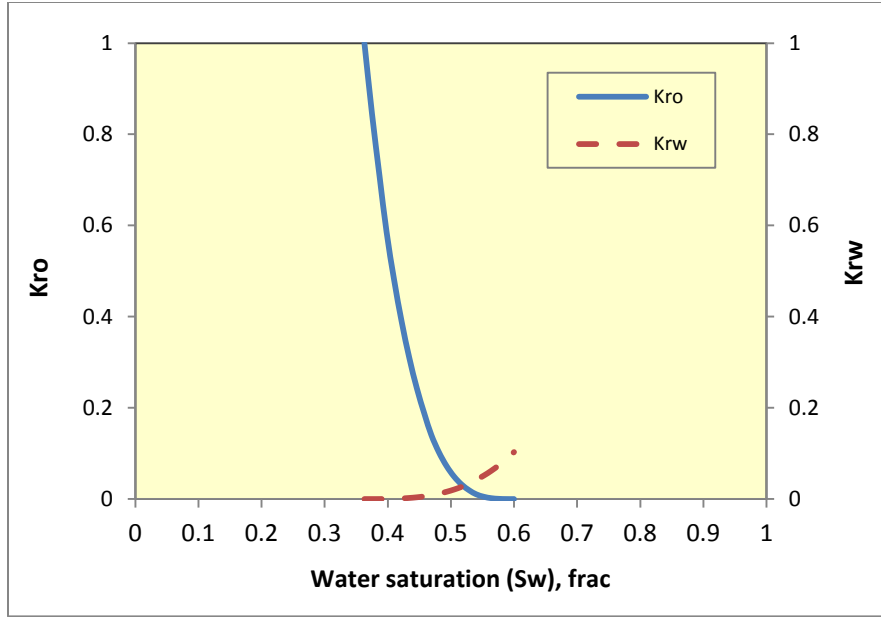
Figure 61: Oil-Water Relative Permeabilities for Base Case (0 ppm, No Surfactant) Obtained from a Coreflood Simulator

Table 15: Summary of Experimental and Simulation Waterflood Results for Base Case (0 ppm) at Both Room and Reservoir Temperatures

Temperature (°F)	Recovery (%OOIP)	Experimental				Simulation				
		Swi	Sor	Kro	Krw	Swi	Sor	Kro	Krw	Sw (X-Over point)
68	35.8	0.372	0.403	1.0	0.109	0.363	0.401	1.0	0.103	0.52
210	40.6	0.465	0.326	1.0	0.143	0.46	0.321	1.0	0.135	0.63

According to Craig's rules of thumb (Table 14), the relative high initial water saturation of 0.363 (>0.25), low endpoint water relative permeability 0.103 (<0.3), high endpoint oil relative permeability of 1.0 (>0.95), and the slightly higher crossover point water saturation 0.52 (>0.5) in Figure 61 for this base case (0 ppm, no surfactant) indicate the weakly water-wet characteristics of this Berea rock-condensate-synthetic brine system.

Table 16 presents the oil (condensate)-water interfacial tensions (IFT) and the advancing contact angles measured using DDDC technique for this rock-fluids system at various anionic

surfactant concentrations. As shown in Table 16, the advancing contact angle of 153° was obtained for the quartz-condensate-synthetic brine system in the absence of surfactant, which indicates the strong initial oil-wet nature of the system. Thus the wettability inferred from the contact angle measurements is significantly different from that derived from the corefloods. This discrepancy between them appears to be due to insufficient aging time on rough rock (core) surfaces and the pore structure change caused by fines migration as explained below.

Table 16: Summary of Waterflood Results, Oil-Water Interfacial Tensions and Contact Angles in Berea Rock-Condensate-Synthetic Brine System at Various Anionic Surfactant Concentrations

Surfactant Concentration (ppm)	Recovery (%OOIP)	IFT (σ_{ow}) (mN/m)	Advancing Contact Angles (degree)
0	35.8	22.94	153
1500	59.1	1.01	109
3000	51.8	0.87	104

In DDDC contact angle experiments, smooth quartz surfaces were used to measure the water-advancing contact angle. The aging time of 24 hours was sufficient to attain solid-fluids equilibrium and the system showed a strongly oil-wet state. However, in coreflood experiments, Berea rock is not only rough but also mineralogically heterogeneous.

The chemical composition of Berea sandstone cores, which is provided by the supplier's (Cleveland Quarries) website, consists mainly of silica (about 93%). Alumina (Al_2O_3) in the core is about 3.86% and the remaining 3% constitutes ferric oxide, ferrous oxide, magnesium oxide and calcium oxide. The composition of Berea cores shows the presence of impurities. Although the non-silica minerals only account for about 7% in Berea cores, their structure is loose with large surface area resulting in roughness and heterogeneity on the rock surface.

The roughness of rock surface can affect both contact angle and wetting state. Vijapurapu et al. (2002) reported that the water-advancing contact angles on silica-based surfaces showed a declining trend with increasing surface roughness and the water-advancing contact angle decreased from 166° on smooth glass to 58° on rough quartz for Yates crude oil system. Thus, roughness of pore walls of Berea rock appears to be the main reason for the observed results. This also demonstrates that more aging time should be given to reach solid-fluids equilibrium in coreflood experiments to account for the effect of surface roughness.

Furthermore, during the single-phase experimental period, when the core was initially saturated with synthetic brine (low salinity of about 3100 ppm, Table 3 in section 3.1.1) and flow was established with brine to measure the absolute permeability, a small amount of light yellow fine solid particles has been observed to be entrained in the flowing fluids and transported through the core to the production burette. This experimental observation gives evidence that fines migration occurred in this sandstone core. Fines migration in the single-phase flow has been studied by several researchers (Mungan, 1965, Gruesbeck and Collins, 1982, Khilar and Fogler, 1983, and Sarkar and Sharma, 1990). And fines migration was believed to be the most important mechanism of permeability reduction in porous media due to clay particles dislodging from the pore walls, migrating in the flowing direction and then blocking the pore throats. It was also believed by some researchers that fines migration played a key role in enhanced oil recovery for low salinity brine flood (Tang and Morrow, 1999). In addition, the strong impact of rock pore structure on relative permeability resulting in an apparent contrast between the DDDC results and the coreflood results was also proved by the other two published cases - Crossfield Cardium sandstone oil reservoir system and Beaverhill Lake carbonate oil reservoir system reported in the literature (Rao, 2002). This shows the limitations of interpreting wettability from relative

permeability using Craig's rules of thumb to discern wettability. It also confirms the suggestion by Anderson (1987) that it is preferable to measure wettability independently rather than to rely on Craig's relative permeability rules alone to characterize wettability.

4.5.2 Effect of Temperature on Condensate Recovery, Relative Permeability and Wettability for Berea Rock-Synthetic Brine-Condensate

Before performing surfactant flood experiments, the effect of temperature on relative permeability and wettability was tested for base case (0 ppm surfactant case). When the initial conditions of the core were ready for waterflood step, the core was aged at reservoir temperature of 210 °F for 3 to 5 days. Then the waterflood experiment was conducted to investigate the temperature effect. Table 15 also summarized experimental and simulation results obtained from waterfloods performed using Berea sandstone, which was aged at reservoir temperature. A good history match was also given by the coreflood simulator as can be seen in Figure A4-A6 of Appendix. The effects of temperature on relative permeability and relative permeability ratios are shown in Figure 62 and Figure 63, respectively. The effect of temperature on condensate recovery is presented in Figure 64.

It can be seen from Figure 62 and Table 15 that as the aging temperature is increased from room temperature 68 °F to reservoir temperature 210 °F, the cross-over point (x-axis) water saturation is shifting from the left (0.52) to the right (0.63). Also, from Figure 63, it clearly can be seen that the relative permeability ratio (K_{rw}/K_{ro}) curves are gradually shifting to the right. Both of these observations indicate that the wettability of this rock-fluids system is altered from weakly water-wet to water-wet.

Furthermore, as can be seen in Table 15 and Figure 64, the oil (condensate) recovery increased from 35.8% at room temperature to 40.6% at reservoir temperature. The two tests were conducted quite similarly except for the aging temperature between them. Hence, this marginal

increment of about 5% in oil recovery could be attributed to slight wettability alteration from a state of weakly water-wet to a water-wet state caused by the elevated temperature. This further substantiates the importance of the proper conditions for coreflood experiment.
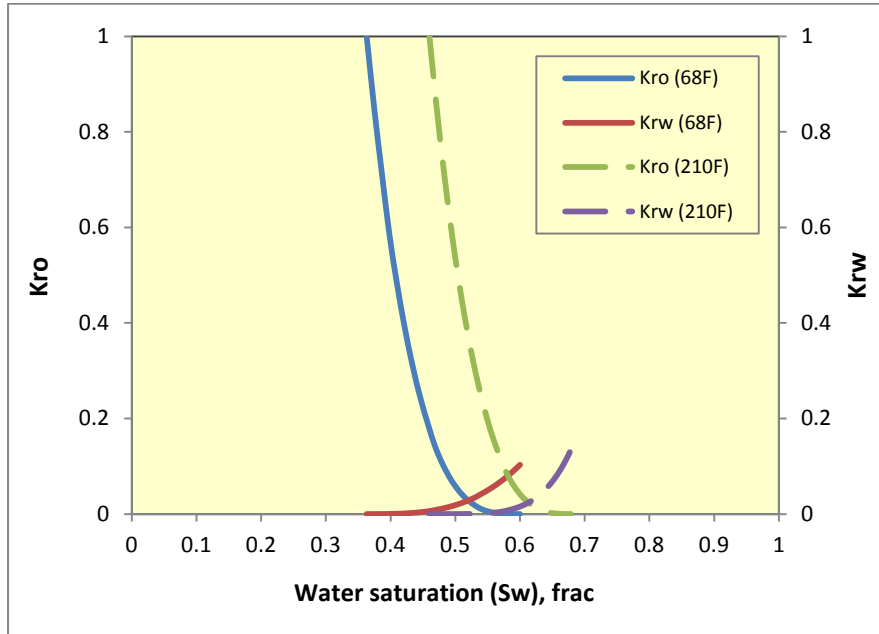

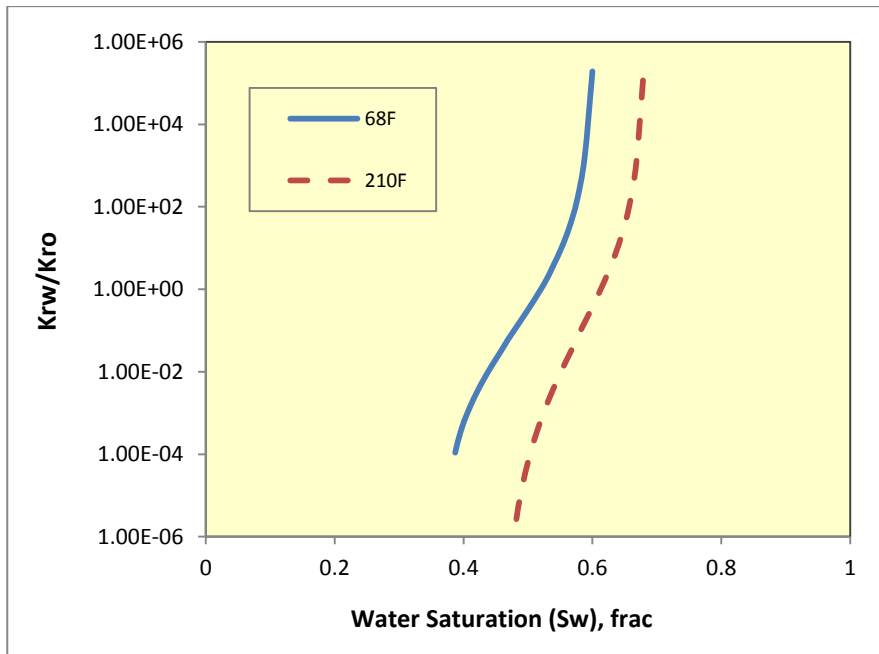Figure 62: Effect of Temperature on Relative Permeability

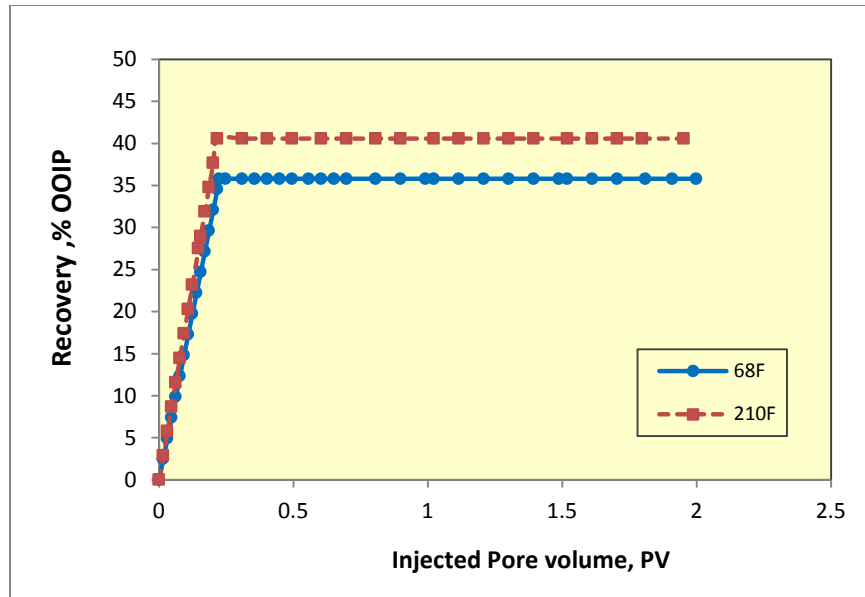Figure 63: Effect of Temperature on Relative Permeability Ratios

Figure 64: Effect of Temperature on Condensate Recovery

4.5.3 Effect of Anionic Surfactant on Condensate Recovery and Gas Relative Permeability

The summary of experimental and simulation results including recovery, saturation and endpoint relative permeabilities for waterflood of condensate in Berea rock at various anionic surfactant concentrations is shown in Table 17. The crossover points of relative permeability curves are also included in Table 17. A good history match given by the simulator still can be seen in Figure A7-A12 of Appendix.

Table 17: Comparison of Experimental and Simulator Results for Waterflood in Berea Core at Various Anionic Surfactant Concentrations

Cases	Recovery (%OOIP)	Experimental				Simulation				
		Swi	Sor	Kro	Krw	Swi	Sor	Kro	Krw	Sw (X-Over Point)
0ppm	35.8	0.372	0.403	1.0	0.109	0.363	0.401	1.0	0.103	0.52
1500ppm	59.1	0.469	0.217	1.0	0.094	0.460	0.207	1.0	0.0943	0.64
3000ppm	51.8	0.341	0.318	1.0	0.105	0.340	0.313	1.0	0.0989	0.54

124

Table 18: Summary of Gasflood Results and Spreading Coefficient in Berea Rock-Condensate-Synthetic Brine-Gas System at Various Anionic Surfactant Concentrations

Cases (ppm)	Krg	Krg Improvement (%)	Condensate Recovery (%OOIP)	Water Recovery (%)	Liquid Recovery (%)	S_{Lrg}	S_{org}
0	0.135	/	8.64	41.6	30.23	0.698	0.349
1500	0.246	82.2	10.22	50.2	46.51	0.535	0.128
3000	0.194	43.7	3.53	61.5	48.06	0.519	0.233

The results for the tertiary gas displacements in this system at various surfactant concentrations are presented in Table 18. The improvement listed in the third column of Table 18 is calculated as the ratio of the difference of gas relative permeability after the surfactant treatment (1500 ppm and 3000 ppm) cases and untreated case (0 ppm) to the untreated (0 ppm) gas relative permeability. Liquid recovery in Table 18 is the ratio of the total liquid (water and condensate) volume to the pore volume of the core. The water volume produced in this gasflood process over the water volume left in the core at the end of waterflood is defined as the water recovery. S_{Lrg} and S_{org} represent the residual liquid saturation and residual condensate saturation in the core at the end of gasflood. Figure 65 depicts the effect of anionic surfactant concentration on oil (condensate) recoveries which were normalized against their respective original oil (condensate) in place (OOIP) and gas relative permeability.

From Figure 65 and Table 17, it can be seen that the condensate recovery increased from 35.8% OOIP at 0 ppm surfactant concentration to the highest value of 59.1% OOIP at the 1500 ppm concentration and then decreased to 51.8 % at 3000 ppm concentration, indicating that surfactant treatment is beneficial for enhanced condensate recovery. Also, the gas relative permeability shows a similar trend as can be seen in Figure 65 and Table 18. In other words, it increased to the maximum value of 0.246 at 1500 ppm and then declined to 0.197 at 3000 ppm.

The improvements in gas relative permeability after surfactant treatment shown in Table 18 are 82.2% at 1500 ppm and 43.7% at 3000 ppm. This also demonstrates the benefit of surfactant treatment from improving gas flow.
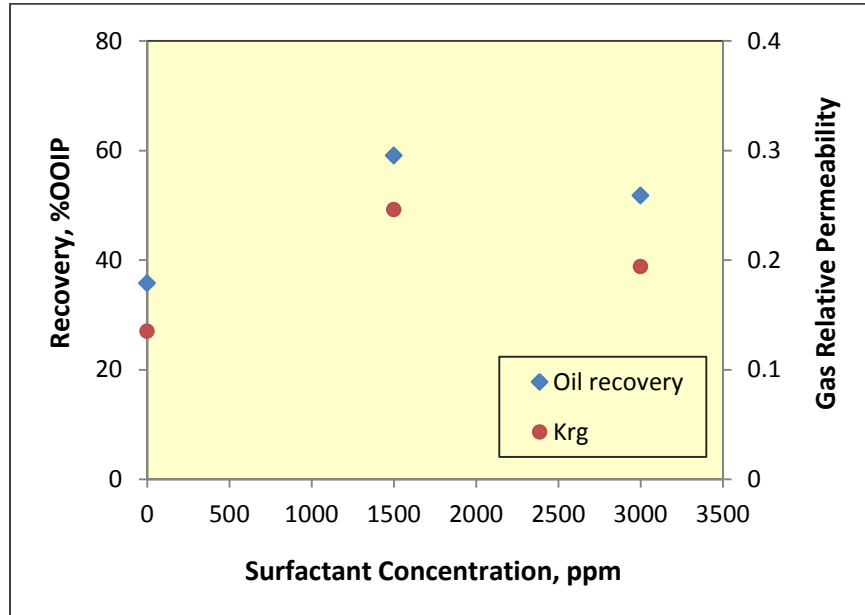

Figure 65: Effect of Anionic Surfactant Concentration on Recovery and Gas Relative Permeability

In addition, it can be clearly noted in Figure 65 that the highest oil recovery and gas relative permeability were obtained at low surfactant concentration (1500 ppm). This is a very important result because the application of low surfactant concentrations in the field can make the treatment more cost-effective.

Compared with the 1500 ppm surfactant treatment case, a slight drop in condensate recovery and the reduction in the improvement in gas relative permeability were obtained at 3000 ppm surfactant concentration as shown in Figure 65 and Table 18. One of the possible explanations is that oil/water emulsion was formed during 3000 ppm surfactant solution injection. This emulsion was not observed until about 4.2 PV brine containing surfactant was flooded into the core. Also, this emulsion did not break up after one week, suggesting it was

stable. However, no emulsion was found during the entire 1500 ppm surfactant flood. The other possible reason is that this higher concentration (3000 ppm) appears to be near critical micelle concentration (CMC) of the surfactant. The bilayer surfactant adsorption probably occurred and led to partial wettability reversal towards the native wettability state (Somasundaran and Zhang, 2006), and thus reduced the oil recovery.

4.5.4 Effect of Anionic Surfactant on Relative Permeability and Wettability

The ratios of oil-water relative permeabilities in this study are used to interpret the wettability changes induced by the anionic surfactant. This method has been used in the published literature to infer wettability states (Anderson, 1987; Rao, et al, 1992). Figure 66 depicts the condensate recovery history at various surfactant concentrations. The effect of surfactant concentration on water-oil relative permeability is represented by the variations in relative permeability ratios (K_{rw}/K_{ro}) as displayed in Figure 67. Figure 68 shows the effect of the anionic surfactant on fractional water flow.
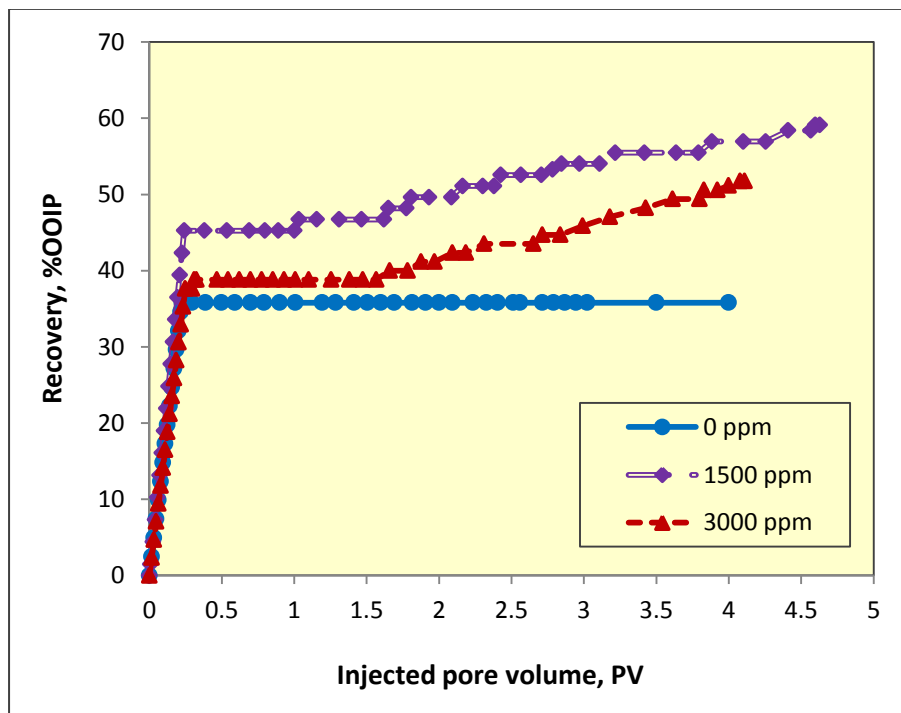

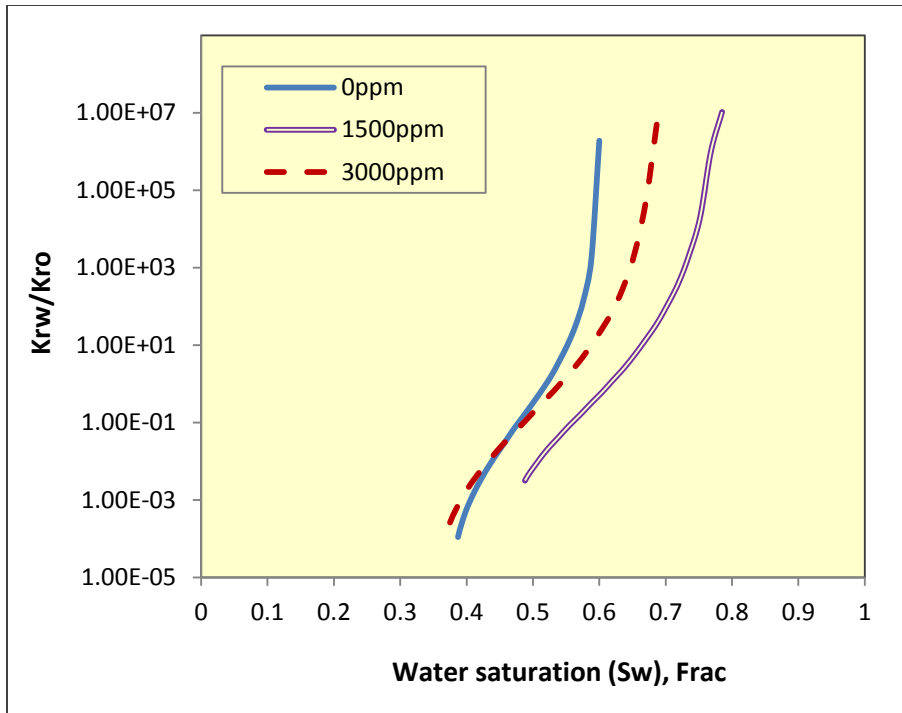Figure 66: Effect of Anionic Surfactant Concentration on Condensate Recovery

Figure 67: Effect of Anionic Surfactant Concentration on Relative Permeability Ratios
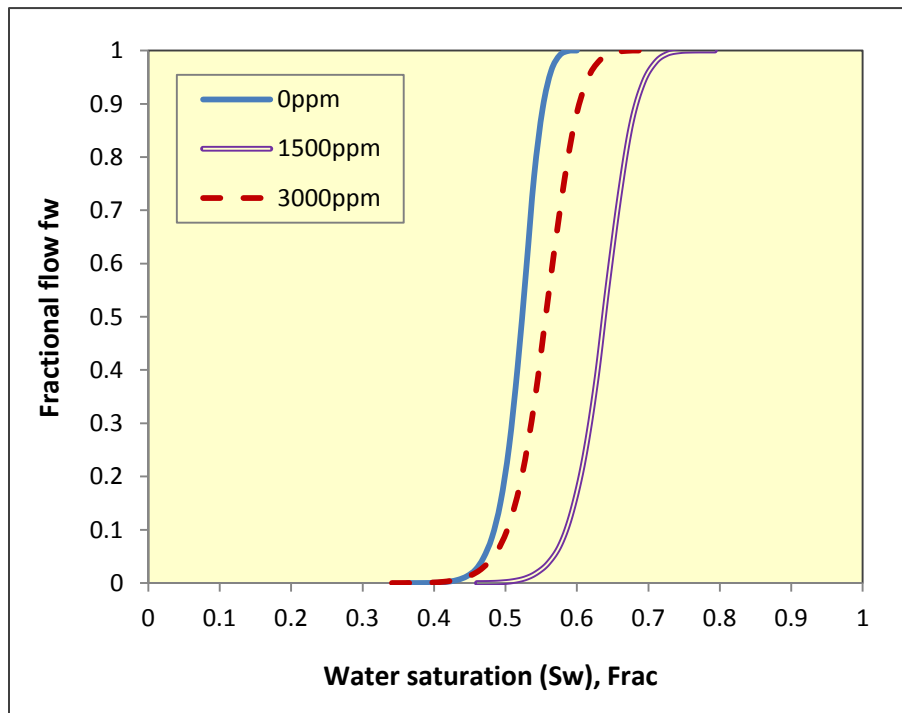

Figure 68: Effect of Anionic Surfactant Concentration on Fractional Water Flow

It can be seen from Figure 66 that there is no significant condensate production after breakthrough for 0 ppm case and the condensate recovery is about 35.8% OOIP. However, corresponding to 1500 and 3000 ppm surfactant treatment cases, both condensate recoveries of 45.3% and 38.8% exceed the recovery of 35.8% in the base case at breakthrough time. After breakthrough, the recovery of 1500 ppm case, as an example, is gradually increased by more than 20% over 0 ppm case at 4PV water injection as shown in Figure 66.

From the plot of water-oil relative permeability ratio (K_{rw}/K_{ro}) against water saturation (Figure 67), it can be observed that oil-water relative permeability ratio curves are gradually shifting to the right after using surfactant. This kind of relative shift to the right in relative permeability ratio curves is indicative of a change in the rock wettability from water-wet to intermediate wet induced by this anionic surfactant (Rao, et al. 1992, 2006). In addition, it should be noted that, there is a smaller rightward shift in relative permeability ratio curves for 3000 ppm case compared to 1500 ppm case. This resulted from two opposite effects: one is due to formation of oil-water emulsion which shifts the relative permeability curves to the left; the other is the development of intermediate wet nature which shifts the relative permeability curves to the right. And Figure 67 shows the final rightward shift for 3000 ppm case, clearly indicating that surfactant-induced wettability alteration to intermediate wet seems to have overcome the effect of the oil/water emulsion. A similar shift from left to right can be noticed in the fractional water flow curves as shown in Figure 68. The advancing Contact angle measured in the presence of the surfactant changed from 153° at 0 ppm to 109° at 1500 ppm and 104° at 3000 ppm (Table 16). This corroborates well with surfactant flood results that the wettability was altered to intermediate wet in this rock-fluids system.

The oil-water interfacial tensions measured with this anionic surfactant decreased from 22.94 mN/m at 0 ppm to 1.01 at 1500 ppm and 0.87 mN/m at 3000 ppm as can be seen in Table 16. This indicates that about two orders of magnitude reduction in oil-water interfacial tension caused by anionic surfactant was obtained in this condensate system. Lowering of interfacial tension can increase the oil recovery, however, significant improvements in oil (condensate) recovery caused by oil-water interfacial tension reduction require four to five orders of magnitude reduction in interfacial tension (Klins, 1984). Mungan (1966) investigated the effect of interfacial tension on the displacement of a nonwetting by a wetting liquid without changing wettability and found that decreasing IFT from 40 to 0.5 dyne/cm resulted in only 8.1% additional recovery after breakthrough. In contrast, additional higher condensate recovery of about 20% after breakthrough (Figure 66) was observed due to surfactant usage in this Berea rock-condensate-brine system. Therefore, the wettability alteration to intermediate wettability is the principal mechanism responsible for significant enhanced oil recovery in this system.

4.5.5 Effect of Anionic Surfactant on Tertiary Recovery and Spreading Coefficient

Immiscible gas (N_2) was flooded into the core after the brine flood or surfactant flood process. In all cases, the water phase was first observed to flow out of the core implying that gas first displaced water, because water saturation in the core was high caused by the preceding waterflood. The oil (condensate) was next displaced by gas, and gas breakthrough occurred shortly after oil breakthrough. Similar observations can be found elsewhere and the double-drainage mechanism was considered to be responsible for these phenomena (Oren and Pinczewski, 1994).

The condensate recovery for this tertiary process also approached the maximum value of 10.2% OOIP at 1500 ppm and the lowest condensate recovery of 3.5% OOIP was obtained for 3000 ppm treatment (Table 18). The reduction in this tertiary recovery at 3000 ppm is still

primarily associated with high surfactant concentration and formation of oil-water emulsion in previous waterflood step. During the gas flood for 3000 ppm treatment case, the collected water phase displaced by gas in the production burette was observed to show a slightly cloudy appearance. It indicates that small amount of oil was dispersed as small droplets in water phase and formed oil-in-water emulsion and thus reduced the collected condensate volume in the production burette.

Water and liquid recoveries increased while residual liquid saturation decreased as the surfactant concentration increased from 0 ppm to 3000 ppm, as shown in Table 18. In other words, more liquid including condensate and water were produced from the core after surfactant treatment, implying that condensate blockage and the water accumulation near the well bore region were mitigated. This further substantiates that surfactant treatment can effectively improve gas relative permeability in this Berea rock-fluids system by remedying the condensate buildup and blockage near the wellbore.

Table 19: Interfacial Tensions and Spreading Coefficients for Brine/Surfactant-Condensate-Gas Systems

System	σ_{wg} , mN/m	σ_{ow} , mN/m	σ_{og}, mN/m	S_o, mN/m
0ppm	70.01	22.94	20.58	26.49
1500ppm	27.79	1.01	20.58	6.20
3000ppm	27.46	0.87	20.58	6.01

Table 19 gives the measured interfacial tensions in brine (with or without the anionic surfactant)-condensate-gas systems. The calculated oil spreading coefficients based on Eq. (1) (Section 2.4) are also listed in Table 19. It shows that oil spreading coefficient for all three cases is positive although it decreased from 26.49 mN/m at 0 ppm to 6.01 mN/m at 3000 ppm, indicating that the spreading coefficient remained positive throughout. Therefore, surfactant-

induced wettability alteration appears to have a more pronounced influence on improving gas relative permeability than the spreading coefficient in this Berea rock-fluids system.

4.5.6 Practical Implications of Surfactant Treatment

Historically, condensate liquids have been considered more valuable than the gas because the condensates are composed mainly of light hydrocarbons. This price differential made gas cycling a common practice. Gas cycling or the injection of dry gases (N_2, CO_2 or CH_4) was applied to the gas condensate reservoirs to remedy the condensate blockage problems. In this method, the reservoir pressure was maintained above the dew point pressure owing to the vaporization of condensate by gas injection, leading to an increase in gas productivity (Luo et al., 2001; Eikeland and Hansen, 2007; Al-Abri et al., 2009). A CO_2 huff-n-puff injection was investigated and found that it could improve gas well productivity (Zhang et al., 2006; Odi, 2012). Although this remedial technique can reduce the impairment effects of condensate buildup around the well, it has limited and short-term success because the condensate bank forms again with time when the pressure near the wellbore falls below the dew point pressure.

However, injecting surfactant into the wellbore zone or huff-n-puff surfactant injection can provide long-term strategy for increased productivity due to surfactant-induced wettability alteration. In the oil-wet reservoirs, surfactant-induced wettability alteration to either weakly oil-wet or intermediate wet is beneficial for field implementation. Due to lowering of the adhesion forces between the liquid condensate and the rock surface which, in turn, would enable the gas phase to flow more easily though the pores displacing the condensate ahead of it. The removal of liquid bank through this process also results in the improvement in gas relative permeability and gas productivity. It should be recognized, of course, that the surfactant type (ability to cause

favorable wettability alteration), surfactant concentration and determination of original reservoir wettability are critical in determining the economic success of this process in the field.

4.6 Effect of Brine Salinity and Composition[3]

4.6.1 Interfacial Tension in Condensate and Different Synthetic Brine Systems

Interfacial tensions for multi-component (low and high salinity) brine/condensate systems obtained from experiments are summarized in the Table 20. In this study, synthetic reservoir brine with totally dissolved solids (TDS) of 2700 ppm is also in the range of the low salinity water. Table 21 gives the measured interfacial tensions in single-salt brine/condensate systems at two salinities (3100 and 93,300 ppm).

Table 20: Interfacial Tension and pH of Condensate/Multi-Component Brine Systems

Type of Brine	Brine Salinity, ppm	Interfacial Tension, mN/m	pH
Low Salinity	0	29.79	7.1
	300	27.60	6.0
	700	27.28	6.0
	1300	32.80	7.40
Synthetic Reservoir Brine	2700	33.92	7.34
High Salinity	26,800	33.65	7.11
	52,800	25.67	6.8
	77,910	32.02	6.22
	125,500	26.28	6.5

From Table 20, it can be seen that the interfacial tension between condensate and different salinity multi-component brines varied from about 26 mN/m to 34 mN/m. The highest interfacial tension of 34 mN/m occurs in condensate/synthetic reservoir brine case and the lowest of around 26 mN/m in 52,800 ppm brine case. In general, the interfacial tensions in low salinity

---

[3] The material in Chapter 4.6 was previously presented at the conference: 8th International Symposium on Contact Angle Wettability and Adhesion held at Université Laval, Québec City, Québec, Canada, 13-15 June, 2012.

brine cases (0~2700 ppm) appears to be slightly more than those in high salinity brine cases (26,800 ppm ~125,500 ppm) as shown in Table 20.

Table 21: IFT and pH of Condensate/Single-Salt Brine System at Two Salinities

Type of Brine	Brine Salinity, ppm	Single Component used	Interfacial Tension, mN/m	pH
Low Salinity	3100	NaCl	28.03	6.3
		$CaCl_2$	33.66	5.5
		$MgCl_2$	33.40	5.6
		$AlCl_3$	29.02	3.2
		$FeCl_3$	28.92	2.6
High Salinity	93,300	NaCl	27.61	7.1
		$CaCl_2$	33.39	5.8
		$MgCl_2$	32.73	5.3
		$AlCl_3$	27.66	2.5
		$FeCl_3$	27.09	2.2

For single-salt brine/condensate systems at two salinity levels, it can be found from Table 21 that the interfacial tension varied from the lowest of about 27 mN/m in condensate/93,300 ppm $AlCl_3$ brine case to the highest of about 34 mN/m in condensate/3100 ppm $CaCl_2$ brine case. Low salinity single-salt brine/condensate cases generally have slightly higher interfacial tensions compared to high salinity single-salt brine/condensate cases. Also, in divalent cation (Ca^{2+}, Mg^{2+}) brine/condensate cases, the higher interfacial tensions of about 33mN/m were obtained (Table 21) for both low salinity and high salinity cases in contrast with monovalent cation (Na^+) and trivalent cation (Al^{3+}, Fe^{3+}) brine/condensate cases.

Therefore, the interfacial tensions in these nineteen cases did not show any significant difference due to brine composition changes and varied from 26 mN/m to 34 mN/m.

4.6.2 Measured pH in Condensate-Brine Systems

Measured pH using Thermo Orion pH meter (model 410 A plus) purchased from Thermo Scientific for multi-component brine systems and single-salt brine at two salinities systems are also listed in Table 20 and Table 21.

From Table 20, it can be seen that the pH measured in multi-component brine systems is around 6 to 7, indicating a neutral condition. However, in single-salt brine systems, pH varies from neutral (6~7) in low and high salinity Na^+ brine cases to weak acid about 5.5 in divalent cation (Ca^{2+}, Mg^{2+}) brine cases and then to acid (2~3) in trivalent cation (Al^{3+}, Fe^{3+}) brine cases as clearly shown in Table 21. The increasing acidity of brine with increasing cationic valence (+1 to +3) can be attributed to the chemical nature of these cations present in solution.

The plots of interfacial tension against the pH of brine in different multi-component brine systems and single-salt brines at two salinity levels systems are given in Figure 69 and Figure 70. In different saline multi-component brine systems, there is no apparent trend in the interfacial tensions which can be observed in Figure 69. Interfacial tensions were distributed randomly from 26 to 34 mN/m in the neutral pH conditions (6~7). Interfacial tensions in single-salt brine at 3100 and 93,300 ppm systems showed an initial increase and a later decrease with increasing pH as may also be seen in Figure 70. The peak interfacial tension of around 34 mN/m exists at weakly acidic conditions which correspond to divalent cation (Ca^{2+}, Mg^{2+}) brine (3100 ppm and 93,300 ppm) systems. Under neutral (Na^+ brine) and slightly strong acidic (Al^{3+} and Fe^{3+} brine) conditions, the values of interfacial tension are close to about 27~29 mN/m.

Although measured pH either kept at almost neutral conditions in different salinity multi-component brine systems or varied from neutral to acidic conditions in single-salt brine systems, interfacial tensions in all nineteen cases were in the range of 26 to 34 mN/m demonstrating no significant difference among all the cases. Hence, no general trend or direct observation and

relationship between pH of solutions and interfacial tensions were obtained within the range of brine compositions studied.
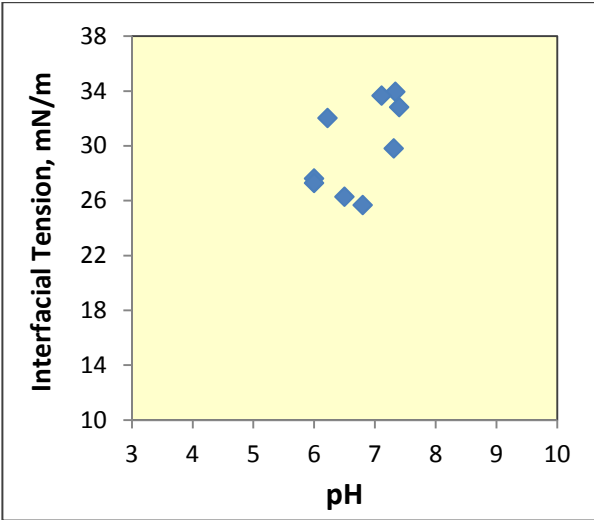

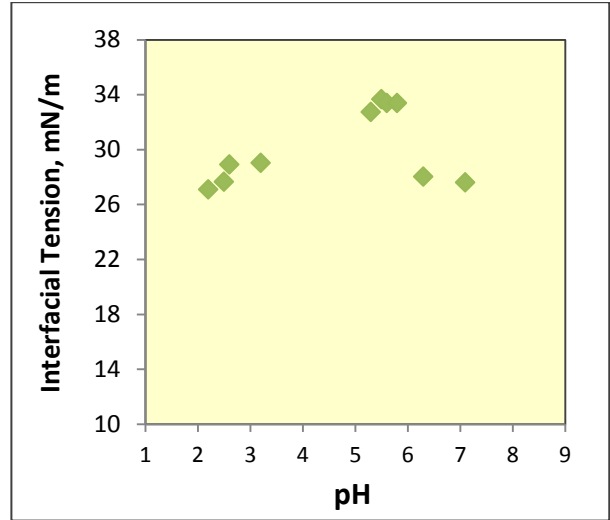Figure 69: Interfacial Tension against pH in Condensate- Multi-Component Brine Systems

Figure 70: Interfacial Tension against pH in Condensate-Single-Salt Brine Systems

4.6.3   Effect of Brine Salinity/Composition and the pH of Brine on Wettability

To investigate the effect of brine salinity (multi-component brines) or brine composition (single-salt brines) on wetting behavior, a series of experiments were conducted using DDDC technique to measure advancing contact angles in condensate-brine-quartz system. Wettability in terms of contact angle was classified by Anderson (1986a) as water-wet in range of 0~75º, intermediate wet 75~115º and oil-wet 115~180º. Also, in this study, the contact angle ranging from 55 ~ 75º is defined as weakly water-wet, 0~55º as strongly water-wet. And the angle from 115 ~ 135º is weakly oil-wet, from 135~180 º is strongly oil-wet.

Table 22 and Table 23 list the results of advancing contact angles obtained from DDDC technique in multi-component (low and high salinity) brine experiments and single-salt brines with two levels of salinity (low and high) experiments. The images of advancing contact angle

136

for all the cases as displayed in Table 22 and Table 23 were extracted from the experiments using a digital video camera.

Table 22: Effect of Brine Salinity (Multi-Component Brine) on Dynamic Contact Angles and Adhesion Number

Type of Brine	Brine Salinity, ppm	Receding Contact Angle (from Sessile Drop), deg			Advancing Contact Angle (from DDDC) θa, deg		Adhesion Number, N_a
		θr, 0hr	θr, 24hr				
Low Salinity	0	60	72		164		1.270
	300	62	96		165		0.861
	700	43	58		149		1.387
	1300	60	71		155		1.232
Synthetic Reservoir Brine	2700	87	98		166		0.831
High Salinity	26,800	65	70		155		1.248
	52,800	90	102		162		0.743
	77,910	116	120		167		0.474
	125,500	96	108		163		0.647

It can be seen from Table 22 that for nine brine salinity cases including synthetic reservoir brine big advancing contact angles varied from 149 to 166° by DDDC contact angle measurement were obtained, indicating a strongly oil-wet nature for all the cases. This can be visually observed in Table 22. The images of advancing contact angles clearly demonstrated the strong adhesion of the condensate drop on the quartz surface forming large water-advancing contact angles as the low quartz crystal was horizontally shifted to the left side.

As may be also seen in Table 23, in single-salt brine at low salinity (3100 ppm) systems the measured advancing contact angles using DDDC technique varied from 138 to 163º. And they changed from 144 to 164º in high salinity (93,300 ppm) single-salt brine cases. Therefore, a strongly oil-wet behavior was also presented in single-salt brine at two salinity levels (3100 and 93,300 ppm). The images of advancing contact angle in Table 23 obtained from the experiments also provided the visual evidence of oil-wet nature in all single-salt cases.

Table 23: Effect of Brine Composition (Single-Salt Brine) on Dynamic Contact Angles and Adhesion Number

Type of Brine, ppm	Component	Receding Contact Angle (from Sessile Drop), deg			Advancing Contact Angle (from DDDC) θa, deg		Adhesion Number, N_a
		θr, 0hr	θr, 24hr				
Low Salinity (3100)	NaCl	82	109		160		0.614
	CaCl$_2$	90	103		159		0.709
	MgCl$_2$	104	112		163		0.582
	AlCl$_3$	53	67		150		1.257
	FeCl$_3$	45	52		138		1.359
High Salinity (93,300)	NaCl	88	107		164		0.669
	CaCl$_2$	87	99		159		0.812
	MgCl$_2$	87	107		160		0.647
	AlCl$_3$	89	95		153		0.804
	FeCl$_3$	61	82		144		0.948

Hence, both brine salinity (multi-component brine) and brine composition (single-salt brine) did not show a pronouncing effect on the wetting characteristics in this condensate-brine-quartz rock system.

The curves of dynamic contact angles (advancing and receding angle) varied with measured pH in both different salinity multi-component brine and single-salt brine systems are presented in Figure 71 and Figure 72. Under neutral pH conditions or weakly/strongly acidic conditions, the advancing contact angles for all nineteen cases as shown in Figure 71 and Figure 72 are large, fluctuating in the range of about 140 to 165º. This demonstrates that the pH of brine has no distinct impact on the advancing contact angles and the wettability in this condensate–brine–quartz rock system.
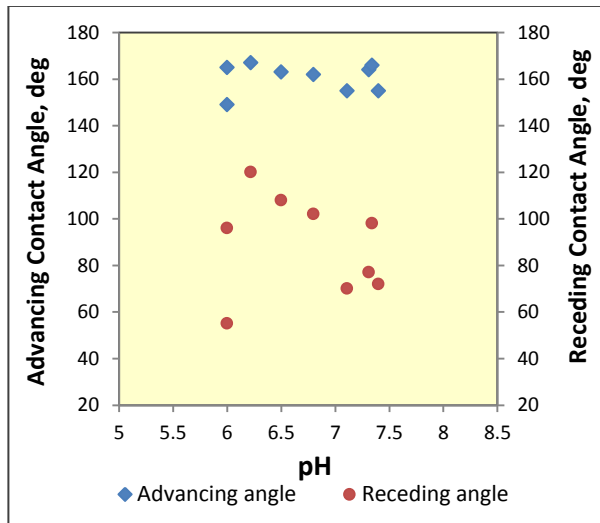
Figure 71: Dynamic Contact Angle against pH in Condensate- Multi-Component Brines
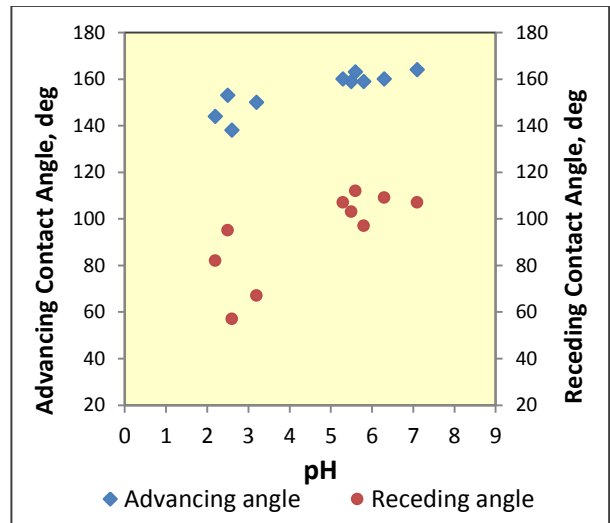
Figure 72: Dynamic Contact Angle against pH in Condensate-Single-Salt Brines

4.6.4 Effect of Brine Salinity/Composition and the pH of Brine on Spreading

Sessile drop method was used in this study to measure water-receding contact angles in condensate-brine-quartz system to explore the effect of brine salinity (multi-component brines) or brine composition (single-salt brines) on spreading behavior. The results of receding contact

angle and the images of receding contact angle at 24 hr for both multi-component brine system and single-salt brine system are also displayed in Table 22 and Table 23. Receding contact angles at 0 hr and 24 hr in both Tables mean the measured angles at the times of just placing the condensate drop on the crystal surface and aging the drop for 24 hours, respectively.

For this representative condensate-brine-quartz system, the most interesting observation is the large water-receding contact angles like 109º (3100 ppm NaCl brine) obtained for all nineteen cases as can be seen in Table 22 and Table 23. It also can be found in both Tables that the initial water-receding angles were smaller than those after 24 hours aging. This indicates the spreading of the condensate drop on the quartz surface against brine.

| 0hr, θr=62º (d/di=1.0, h/hi=1.0) | 2min, θr=77º (d/di=1.09, h/hi=0.86) | 5min, θr=83º (d/di=1.11, h/hi=0.84) | 3hr, θr=96º (d/di=1.22, h/hi=0.82) | 24hr, θr=96º (d/di=1.22, h/hi=0.82) |
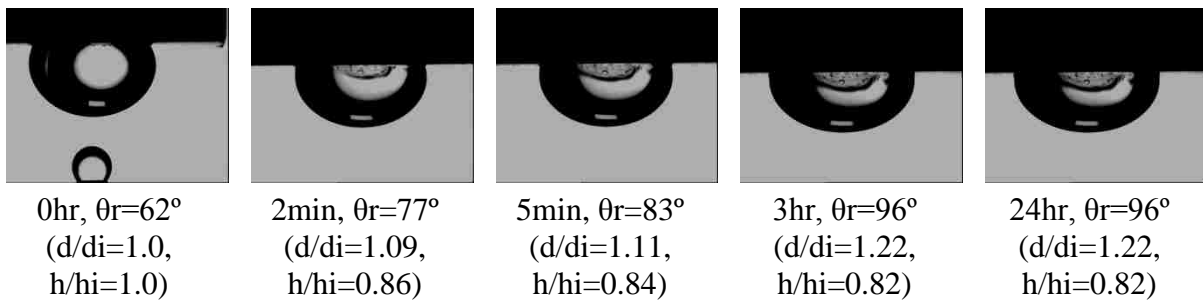
Figure 73: Sessile Drop Contact Angle with Time for Condensate-Quartz-300 ppm Multi-Component Brine

| 0hr, θr=87º (d/di=1.0, h/hi=1.0) | 3min, θr=99º (d/di=1.08, h/hi=0.92) | 15min, θr=101º (d/di=1.11, h/hi=0.85) | 19hr, θr=103º (d/di=1.126, h/hi=0.83) | 24hr, θr=107º (d/di=1.129, h/hi=0.82) |
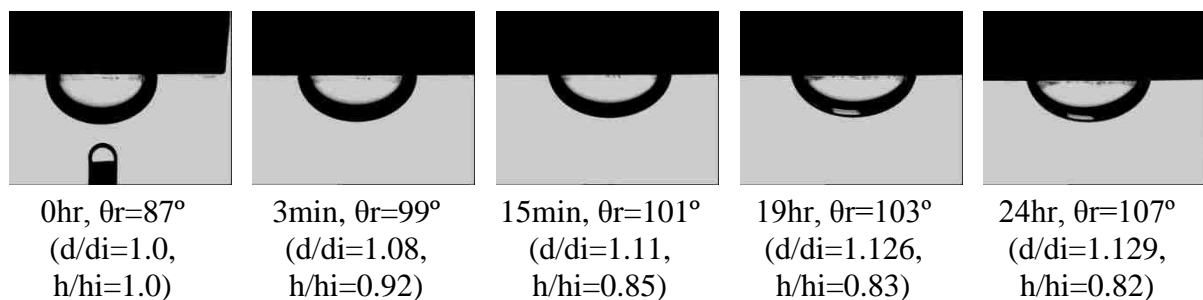
Figure 74: Sessile Drop Contact Angle with Time for Condensate-93,300 ppm $MgCl_2$ Brine-Quartz

The examples of the drop spreading process with time are depicted in Figure 73 and Figure 74, where drop profiles were captured by the digital video system at short intervals during

the experiments of a condensate drop resting on a smooth quartz surface immersed in 300 ppm synthetic multi-component brine and 93,300 ppm $MgCl_2$ brine. In both Figures, receding contact angles measured by sessile drop method, the dimensionless diameter/height of the sessile drop which is defined by the ratio of the drop diameter/height to the initial (0 hr) diameter/height of the sessile drop were also given. Figure 75 illustrates the variation of drop shape due to spreading on the solid surface based on image analysis of the photographs of Figure 73 and Figure 74.
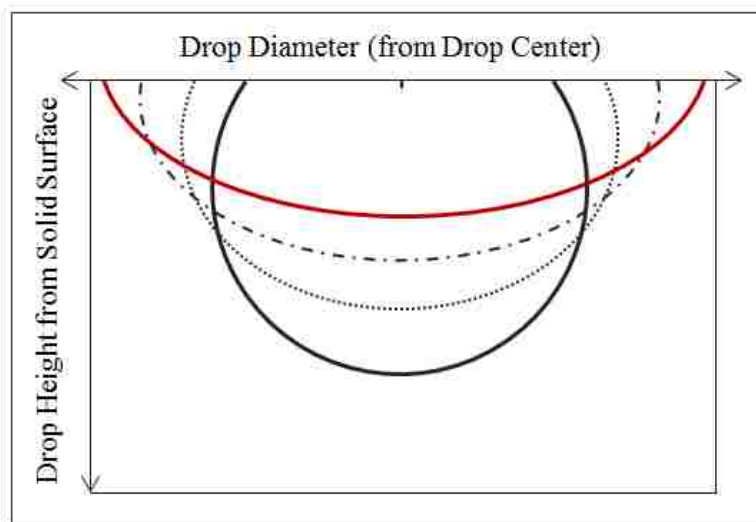
Figure 75: Variation of Sessile Drop Shape due to Spreading on the Solid Surface

An increase in dimensionless drop diameter and reduce in dimensionless drop height as can be clearly observed in Figure 73 and Figure 74 prove that the drop was spreading on the surface. As soon as the condensate drop was placed on the quartz surface it began to spread on the surface creating a pancake-like appearance with large receding angles such as 107º in 93,300 ppm $MgCl_2$ brine case (Figure 74) even up to 120º in 77,910 ppm brine case (Table 22). This phenomenon is schematically displayed in Figure 75. In some cases, this spreading process occurred so fast that it only took a few minutes the receding angles changed from initial small

angle to the big one. For example, in the 300 ppm brine case, the initial receding angle of 62º altered to 83º in five minutes as shown in Figure 73. Further, in some cases, after a few hours such as 3 hours in 300 ppm brine case, the spreading process approached stabilization and the angle was stable at the value of 96º; while in other cases, it took slightly longer time to reach equilibrium. In 93,300 ppm $MgCl_2$ brine case, as an example, after 19 hours of aging on the quartz surface, the condensate drop still slowly spread on the surface as indicated by a receding contact angle changing from 103º at 19 hr to 107º at 24 hr (Figure 74).

As can be seen from Table 22, in low salinity (less than 2700 ppm) and medium salinity (26,800 ppm) multi-component brine cases, sessile drop experiments showed that the receding angles varied from 58º to 98º. However, in high salinity multi-component brine cases, the receding contact angles were in the range of 102º to 120º. Hence, the receding contact angles obtained in high salinity multi-component brine systems were larger than those in low and medium salinity multi-component brine systems.

In single-salt brine at low salinity (3100 ppm) system, the large equilibrium receding contact angles (103~112°) were obtained for Na^+, Ca^{2+} and Mg^{2+} brines; while 52° and 67° of receding angles were obtained corresponding to Al^{3+} and Fe^{3+} brines as can be seen in Table 23. And the equilibrium receding angles obtained for all the single-salt brines at high salinity of 93,300 ppm systems were ranged from 82° to 107°.

Receding contact angles against measured pH in multi-component brine cases and single-salt brine cases also plotted in Figure 71 and Figure 72. Either larger (120°) or smaller (58°) receding contact angles obtained under neutral conditions (6~7 of pH) in multi-component brine system as shown in Figure 71 implies the insignificant effect of the pH of brine on the receding contact angles and spreading in this condensate–brine–quartz rock system. However, the smaller

receding angles like 52° were obtained at the pH of about 2 to 3 in multivalent single-salt brines cases (Al^{3+} and Fe^{3+}) as can be noticed in Figure 72. It indicates that the pH of single-salt brines might have significant influence on the receding angles.

4.6.5 Adhesion Number

Adhesion Number N_a was defined as the ratio of the adhesion force to the capillary force. The following equation has been used to approximately determine Adhesion Number (Rao, 2003):

$$N_a = \gamma_{ow} (Cos\ \theta_r - Cos\ \theta_a)/\gamma_{ow} = Cos\ \theta_r - Cos\ \theta_a \qquad (7)$$

where γ_{ow} is oil-water interfacial tension, θ_r and θ_a are receding and advancing contact angles. From Eq. (7), Adhesion Number is simplified as the difference between cosines of receding and advancing contact angles. It expresses the extent of adhesion force with respect to capillary force.

The calculated Adhesion Number N_a based on Eq. (7) for all nineteen cases is listed in Table 22 and Table 23. Figure 76 and Figure 77 illustrate the plot of adhesion number against the equilibrium receding contact angle (θ_r at 24 hr) for both multi-component brine and single-salt brine systems, respectively. The linear trend lines (R^2 of about 99%) were obtained for both systems as also shown in Figure 76 and Figure 77, indicating that for both systems adhesion number is dependent on receding contact angles. This is reasonable because for these nineteen cases large advancing angles about 140° to 165° were obtained. The cosine of advancing angle is almost constant in Eq. (7) and thus the Adhesion Number N_a is the function of receding contact angle θ_r. It can also be seen from Figure 76 and Figure 77 that Adhesion Number decreases with increasing receding angle. In other words, the condensate spreading on the rock surface with a large receding angle resulted in small Adhesion Number. For example, the receding angle is 120° and Adhesion Number is 0.474 in 77,910 ppm multi-component brine case; while Adhesion

Number is 1.387 with a receding angle of 58° in 700 ppm multi-component brine case as shown in Table 22 and Figure 76. Small Adhesion Number as a result of a large receding angle signifies the presence of weak adhesion force but strong capillary force between condensate and rock surface in the system.
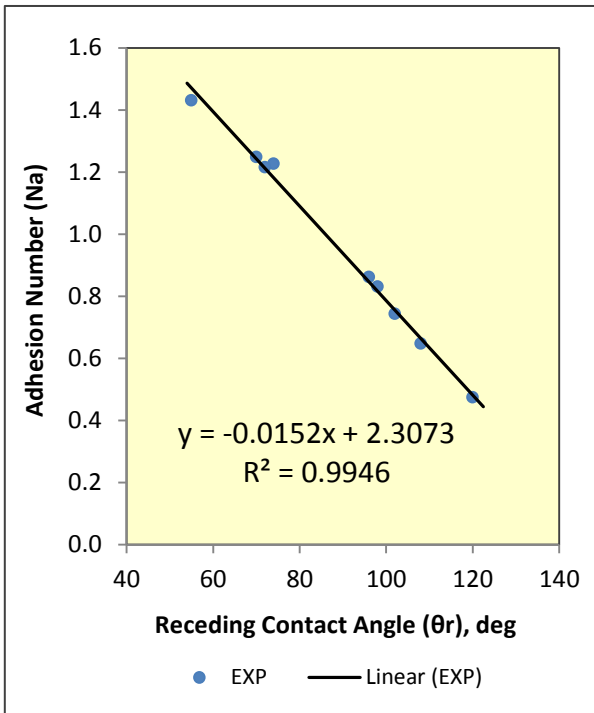
Figure 76: Adhesion Number against Receding Contact Angle in Multi-Component Brine Systems
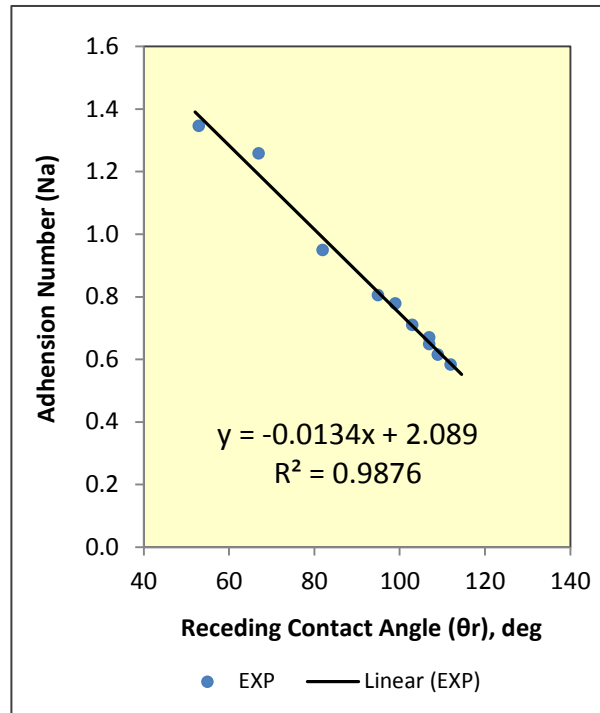
Figure 77: Adhesion Number against Receding Contact Angle in Single-Salt Brine Systems

This indicates that spreading on the rock surface has an advantage for the condensate to form a thin film on the entire rock surface and create an oil-path for it to drain through, migrate towards the producing well and thus enhance condensate recovery. However, high capillary force gives the adverse effect because it can cause strong capillary retention. Vizika and Lombard (1996) also reported that the lowest oil recoveries were obtained due to strong capillary retention

in oil-wet porous media, although in this condition oil remained continuous through wetting films.

4.6.6   Receding Contact Angle with Interfacial Tension in Multi-Component Brines

Figure 78 displays the plot of receding contact angle with interfacial tension in multi-component brine system.
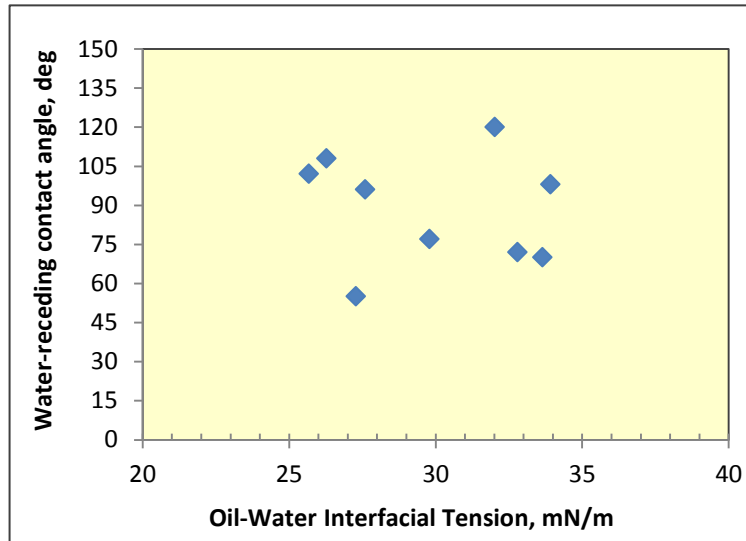
Figure 78: Receding Contact Angle versus Condensate-Water Interfacial Tension in Multi-Component Brine Systems

The receding contact angles distribute randomly against condensate-water interfacial tensions as shown in Figure 78. Also, the dilution of multi-component brines did not cause significant IFT change as discussed in the preceding section. Large interfacial tension (about 26~34 mN/m shown in Figure 78) obtained demonstrates the high surface energy resulting in much more stabilization of condensate in condensate/multi-component brine systems. When the IFT of oil decreased below Zisman-type critical spreading tension (Zisman, 1964), the oil spread on the solid surface with high receding contact angles (Vijapurapu and Rao, 2004). This phenomenon is referred to Zisman-type plot and Zisman-type spreading characteristic. However, Zisman-type plot and Zisman-type spreading characteristic were not observed in this study. The

probable reason is that, compared to crude oil, the condensate has less heavy ends (Table 2) and thus has the stronger stability in brine, resulting in interfacial tension of condensate above the critical spreading tension induced by brine dilution.

4.6.7 Preliminary Analysis of Spreading Mechanism

In this study, contact angle data obtained from the sessile drop experiments showed that the condensate drop spread on the quartz surface with large receding contact angles. This raises a question as to whether the condensate drop was spread on a film of water wetting the quartz surface or was it spreading on the quartz surface itself by de-stabilizing the water film. Hence, the stability of thin wetting water films on the rock surface is the key to analyze the three-phase (rock-condensate-brine) interactions.

The presence of thin wetting water films and their stability has a profound effect on spreading, adhesion and wettability of a surface by a fluid in competition with another fluid. The stability of the thin wetting films of water on the rock surface is affected by several factors such as brine composition, brine pH, electrostatic potential on the rock surface, the applied capillary pressure and temperature (Derjaguin et al., 1978; Hall et al., 1983; Hirasaki, 1991; Gupta and Sharma, 1991; Rao, 1999). The stability of thin films is expressed in terms of disjoining pressure, which is the force that tends to disjoin or separate two interfaces. A negative disjoining pressure means attraction between two interfaces.

Disjoining pressure results from intermolecular or interionic forces described by the DLVO theory, which has been applied to the colloid systems to explain their stability (Derjaguin et al., 1987, 1989). In this theory, three interfacial forces, including double layer repulsion or attraction, London van der Waals attraction, and poorly characterized short-range "non-DLVO" forces such as hydration and steric repulsion, were considered to take effect together on interfaces between rock and fluids (Ryan and Elimelech, 1996). The electrical double layer

forces arise from the overlap of diffuse clouds of ions (double layer) that accumulate near charged surfaces to balance the surface charge. They will be either repulsive or attractive depending on the charges of interacting surfaces and their strength can be affected by chemistry of surrounding solution. For example, if the interacting surfaces are like-charged, the double layer forces will be repulsive and vice versa. The van der Waals forces caused by electrostatic attraction between temporary fluctuating dipoles in the molecules are long-range forces and always attractive. They exist between all matter and thus are an important component of the surface forces in thin films. The van der Waals forces strongly depend on the nature of interacting material and will not be affected by surrounding solutions. The short-range "non-DLVO" repulsive forces are not well understood so far, however, it is believed that these forces are intermolecular structural forces and often attributed to some form of hydration or steric repulsion. The short-range repulsive forces are also believed to be very strong at separation distances less than a few nanometers (Ryan and Elimelech, 1996).

For silica, the surface becomes negatively charged when the pH is increased above 2 to 3.7, while calcite does not become negatively charged until the pH is greater than 8 to 9.5. Hence, in water near neutral pH, silica is negatively charged and tends to adsorb organic bases, while calcite is positively charged and tends to adsorb organic acids (Anderson, 1986a). The negatively charged quartz surface is attributed to the dissociation of silanol groups and forms electrical double layer with H^+ and OH^- from water (Iler, 1979):

$$SiOH \leftrightarrow SiO^- + H^+$$

Electric double layers are also formed at the interface between an aqueous phase and an oil (condensate) phase. Some researchers have shown that the charge on oil/brine interface depends on brine pH and it appears that the adsorption of OH^- ions gives rise to a significant

surface-charge density if the oil phase has no polar constituent (Hall et al., 1983; Takamura and Chow, 1985; Buckley et al., 1989). In terms of their findings, at low pH, oil has positive charges (dominated by ionized bases); while oil charge reduces as pH increases until it approaches zero at the isoelectric point and then transfers to strongly negative at high pH values (dominated by ionized acids). This charge alteration from positive to negative has been found in many oils and the isoelectric point occurs at the pH range of 2 to 6 dependent on oil composition.

In this study, during the sessile drop experiments, the quartz surface (silica) was first immersed in aqueous phase. The hydrophilic nature of quartz surface causes the formation of stable thin water films on the surface. Further, according to the above findings, if the pH of the aqueous solution is in the range of 5 to 7, the quartz/water interface is negatively charged and condensate/brine interface also has negative charges. As a consequence, the electrostatic repulsion arising from similar electric charge and potential at interacting interfaces would take place between quartz surface and condensate drop in terms of the DLVO theory. And the thin water film on the quartz surface is stabilized by the repulsive forces.

From the observations of the sessile drop experiments, in low salinity (3100 ppm) single-salt Na^+, Ca^{2+} and Mg^{2+} brine cases, the oil (condensate) drop immediately adhered to the surface and then spread on the quartz surface as it was placed on the surface, resulting in a large receding contact angle such as 109° in Na^+ brine case and 112° in Mg^{2+} brine case (Table 23). These phenomena of condensate drops adsorbing and spreading on the surface indicate that the thin water films on the surface were destabilized due to changes in surface forces. In low salinity Na^+, Ca^{2+} and Mg^{2+} brines, the pH varied from 5.5 to 6.3 (Table 21), suggesting the repulsive forces between the like-negatively charged quartz/brine and oil/brine interfaces. But in the presence of cations of Na^+, Ca^{2+}, Mg^{2+} in aqueous phase, the cations can shield the same

negative charges of condensate drops and quartz surfaces and thus compact the double layers formed between them. The net repulsive interaction forces and potential between condensate drops and quartz surfaces then decrease. Meanwhile, the attractive London-van der Waals forces become more dominant compared to the double layer repulsion forces. The excess van der Waals attraction results in the rupture of the thin wetting films and thus adsorption of the condensate drop on the quartz surface. Similar observations were found in the work of Cao et al. (2009, 2010) where colloid (virus) adsorption on the sand grains was increased with the addition of the monovalent NaCl salt.

In addition, for divalent cations of Ca^{2+}, Mg^{2+}, except van der Waals attractive forces, cation bridges formed between like-charged condensate drop and quartz surface are also responsible for attracting the condensate drop on the surface (Buckley et al., 1998).

It can be seen from Table 22 that in the deionized water (DIW) without any ions (0 ppm, pH=7.1in Table 20) the receding contact angle measured is about 72°, smaller than those in low salinity (3100 ppm) single-salt Na^+, Ca^{2+} and Mg^{2+} brine cases. The spreading behavior was also found not to be as dramatic compared with these three cases. This is the consequence of the electrostatic repulsive forces between the condensate/DIW and DIW/quartz interfaces due to similar negative charges on both interfaces.

An unexpected observation could be noticed in the low salinity (3100 ppm) multivalent (Al^{3+} and Fe^{3+}) brine cases. It was slightly difficult to place the condensate drop on the quartz surface during the experimental process. When the drop touched the surface, it flew away from the surface. After several repeats, the condensate drop was finally put on the surface but it did not spread on the surface like a pancake which occurred in Na^+, Ca^{2+}, Mg^{2+} cases. And low receding angles of about 67° and 52° for Al^{3+} and Fe^{3+} brine cases were obtained as shown in

149

Table 23. The pH values for these two brines, shown in Table 21, are 3.2 and 2.6 suggesting acidic conditions, which are caused by the hydrolysis of cations of Al^{3+} and Fe^{3+} in water. Multivalent Al^{3+} and Fe^{3+} are hydrated cations which first attract H_2O molecules and form hydration and then hydrolyze in water to produce H_3O^+. This acid hydrolysis gives the low pH values. The reactions for hydration and hydrolysis of Al^{3+} and Fe^{3+} are given in below.

Hydration: $Fe^{3+} + 6H_2O \rightarrow Fe(H_2O)_6^{3+}$ or $Al^{3+} + 6H_2O \rightarrow Al(H_2O)_6^{3+}$

Hydrolysis: $Fe(H_2O)_6^{3+}{}_{(aq)} + H_2O_{(l)} \rightleftarrows H_3O^+{}_{(aq)} + Fe(H_2O)_5(OH^{2+})_{(aq)}$

$Al(H_2O)_6^{3+}{}_{(aq)} + H_2O_{(l)} \rightleftarrows H_3O^+{}_{(aq)} + Al(H_2O)_5(OH^{2+})_{(aq)}$
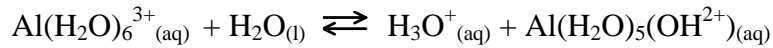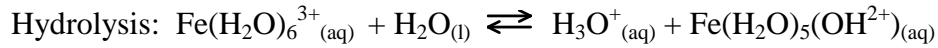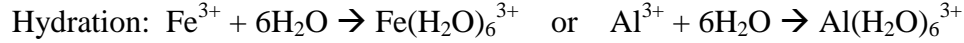
Although cations Al^{3+} and Fe^{3+} can provide more positive charges to balance the opposite charged interacting interfaces, the short-range repulsive forces owing to hydration of these strongly hydrated cations based on the DLVO theory are more pronounced than van der Waals attractive forces between condensate drops and quartz surfaces. The net repulsion accounts for the stability of the thin water films on the surface and thus causes low receding contact angles. This is in agreement with the work of Pashley (1984) who pointed out that the presence of more strongly hydrated trivalent ions augments the short-range repulsion.

In high salinity (93,300 ppm) single-salt Na^+, Ca^{2+}, Mg^{2+} brine cases, the large receding angles of about 99° to 107°, as shown in Table 23, were obtained, similar to the observations of the low salinity (3100 ppm) cases. However, in high salinity multivalent Al^{3+} and Fe^{3+} brine cases, the experimental observations are different from those in low salinity brine cases. Condensate did spread on the quartz surface and the large receding angles of 82° for Fe^{3+} and 94° for Al^{3+} were also obtain in these two brines as can be seen in Table 23. Overall, in all of high salinity single-salt brines, large receding contact angles obtained indicate the destabilization of the thin wetting films on the quartz surface. Hall et al. (1983) investigated the dependence of

the wetting-film thickness on electrolyte concentration and pore size, and found that wetting-film thickness decreased as the electrolyte concentration in brine increased according to their calculations from overlapping electrical double-layer theory. In other words, at higher electrolyte concentrations, the electric potential between the interacting interfaces is decreased, and this reduces the repulsive force between them, destabilizing the films of smaller thickness. These findings of Hall et al. (1983) support that in high salinity single-salt brine cases, the concentration of ions becomes a dominant factor responsible for the decrease in the repulsion between condensate drops and quartz surfaces. This reduced repulsion results in the rupture of the thinner wetting films, spreading of the drop on the surface and thus large receding contact angles.

In multi-component brine systems, the pH for low and high salinity multi-component brines is about 6 to 7, almost neutral conditions. The receding contact angle results (Table 22) show that although the condensate/brine/ quartz rock interactions in multi-component brine systems are more complex than those in single-salt brine systems, the spreading behavior of condensate drop in high salinity brines is more distinct than that in low brine salinity brines.

In high salinity multi-component brine cases (52, 800 ppm, 77,910 ppm and 125,500 ppm), it can be obviously observed from Table 22 that large receding angles of 102°~120° were obtained from the experiments. This agrees with the results in high salinity single-salt brine cases, which also have large receding angles. The high concentration of ions in these brines is also crucial to be in charge of the rupture of the thin aqueous films on the surface and large receding angles.

The receding contact angles varied from 58° to 98° in low salinity (300~2700 ppm) multi-component brine cases and 70° in medium salinity (26,800 ppm) multi-component brine

case. The results are more complex than those in low salinity single-salt brines. In the cases with small receding contact angles, the repulsive forces between the condensate drop and quartz surface are predominant causing the stability of the thin wetting films on the surface; while the attraction is more striking in large receding angle cases. The mechanism of the fluctuating repulsive and attractive forces may be the cause for the uncertainties of the poorly characterized short-range "non DLVO" forces in the presence of strongly hydrated multivalent cations of Al^{3+} and Fe^{3+} in low salinity multi-component brines.

The underlying mechanism accounting for the variation of the receding angles in multi-component brine systems, especially in low salinity brines cannot be elucidated simply by contact angle measurements. Other experimental measurements such as zeta-potential, acid and base number should be further investigated to explore and fully understand the key mechanisms behind the spreading behavior observed in multi-component brine systems.

5. CONCLUSIONS AND RECOMMENDATIONS

5.1 Summary of Findings and Conclusions

Surfactants and brine salinity and composition were tested in this study to evaluate their effect on interfacial tension, fluid-fluid spreading coefficient, wettability and relative permeability to mitigate condensate blockage problems in gas-condensate reservoirs. The significant conclusions of this study are summarized below.

5.1.1 Effect of Surfactants on Wettability

1. The reservoir wettability was determined through measuring contact angles using the DDDC technique. The advancing contact angles of 151° and 153° at ambient and reservoir conditions demonstrated that this representative sandstone condensate reservoir has a strongly oil-wet nature under both conditions. This observation negates the generally held notion that the heavy ends in crude oils are responsible for rendering oil-wet characteristics to reservoirs.

2. The dynamic contact angle measurements with and without anionic and nonionic surfactants (500, 1500, 3000 ppm) at ambient conditions indicate that the initially strongly oil-wet nature of this particular reservoir rock-brine-condensate was altered by the anionic surfactant to weakly oil-wet or intermediate-wet nature. However, the reservoir wettability was not modified by the nonionic surfactant which remained strongly oil-wet.

3. Based on DDDC contact angle measurements at reservoir conditions, the surfactant-induced wettability alteration did not occur in the 500 ppm case with the anionic surfactant. As the surfactant concentrations increased to 1500 and 3000 ppm, it was observed that the anionic surfactant altered the reservoir wettability from strongly oil-wet to weakly oil-wet or intermediate-wet for this particular reservoir case. It reiterates that the rock-fluid interactions

153

depend on pressure and temperature and the consequent need to make such measurements at actual reservoir conditions.

4. The fluid-fluid and rock-fluid interactions and their dependence on type and concentration of surfactants examined in this study at both ambient and reservoir conditions have demonstrated the potential of the beneficial effects of wettability alteration and spreading coefficient reduction in resolving condensate blockage problems.

5.1.2 Effect of Surfactants on IFT and Spreading Coefficient

1. At ambient conditions, anionic and nonionic surfactants reduced the interfacial tension in brine-condensate (σ_{ow} from 22.94 to 3 mN/m) and brine-methane systems (σ_{wg} from 70.01 to 28 mN/m) and had less influence on lowering interfacial tension in condensate-methane systems (σ_{og} =20.58 mN/m).

2. At reservoir conditions, the nonionic surfactant had poor thermal stability and was therefore rejected for use in further experimentation. The anionic surfactant also decreased the interfacial tensions in brine-condensate (σ_{ow} from 9.10 to 1 mN/m) and brine-methane systems (σ_{wg} from 43.87 to 10.72 mN/m). In condensate-methane systems, however, methane developed miscibility with condensate at reservoir pressure and temperature ($\sigma_{og} = 0$ mN/m).

3. Positive spreading coefficients were obtained with and without surfactants (anionic and nonionic) at ambient and at reservoir conditions (anionic), but the spreading coefficients did decrease in magnitude after surfactant application under both conditions. This declining trend indicates that the use of the surfactants in this strongly oil-wet condensate reservoir could improve condensate recovery and gas relative permeability. However, compared to the role played by wettability alteration, spreading coefficient played a relatively minor role in enhancing gas relative permeability in this condensate reservoir case.

5.1.3 Effect of Surfactants on Relative Permeability and Recovery

1. The anionic surfactant treatment in this Berea rock-condensate-synthetic brine was effective in enhancing both the condensate recovery and gas relative permeability. The improvements in condensate recovery and gas relative permeability were up to 23% OOIP and 82% at 1500 ppm surfactant concentration, respectively. This implies that the low surfactant concentration can be effective make the surfactant treatment more economical in the field.

2. The gradual rightward shift in relative permeability ratio curves induced by surfactant demonstrated the wettability alteration to intermediate-wet in this rock-fluids system. The advancing contact angles measured in this system also substantiate the wettability shift to intermediate-wet due to the ability of this anionic surfactant.

3. A change in the temperature for aging period from ambient temperature (68 °F) to reservoir temperature (210 °F) resulted in a marginal increment of oil (condensate) recovery of up to 5% original oil in place (OOIP) in this Berea sandstone rock-condensate-synthetic brine. This can be attributed to slight wettability alteration induced by the temperature increase.

5.1.4 Effect of Brine Salinity

1. Condensate-brine interfacial tensions measured in different salinity multi-component brine and single-salt brine systems varied from 26mN/m to 34mN/m. Wettability was determined by DDDC technique for both multi-component and single-salt brine systems. Large advancing angles of about 140° to 165° obtained in this study for all nineteen cases show a surprisingly strongly oil-wet nature of a gas-condensate fluid. No significant change in interfacial tension and wettability for all cases implies that brine salinity and composition have very little influence within the ranges studied.

2. The pH of brine was measured for all cases. In multi-component brine systems, the pH is about 6 to 7. In single-salt brine systems, the pH of brine varied between 2 to 3 for multivalent brines (Al^{3+}, Fe^{3+}) but 5 to 7 for divalent brines (Ca^{2+}, Mg^{2+}) and monovalent brine (Na^+). Although the pH changed, no particular effect on condensate-brine interfacial tension and wettability was observed.

3. The variation of brine salinity and brine composition yielded an unexpected observation in that the condensate drop spread on the rock surface resulting in a large receding contact angle. This spreading behavior was more pronounced in high salinity brine (both multi-component and single-salt) systems.

4. Stability of the thin aqueous films is responsible for the adsorption and spreading of the condensate onto the quartz surface.

5.1.5   Key Mechanisms from Observed Results

1. The dynamic behavior of condensate drops was visually observed on the quartz surface during surfactant injection and after surfactant injection at reservoir conditions. The possible explanation for the observed dynamic behavior was given on the basis of their relative affinity to the rock-liquid (brine or condensate) and brine-condensate interfaces.

2. The dimensionless Bond number was used to explain the dynamic capillary/gravity effect on condensate drops on the lower substrate at ambient and reservoir conditions. It was shown that the Bond number which includes the contact angle term quantitatively better interprets the rock-fluids interactions at both conditions.

3. The coreflood results show the weakly water-wet nature for this rock-fluids system. However, the wettability of this rock-fluids system inferred from DDDC contact angle measurements is strongly oil-wet. These contradictory wettabilities appear to be related to

rock pore structure caused by insufficient aging time in corefloods as well as fines migration observed in the experiments. The results show the wettability interpretation from relative permeability data is subject uncertainties due to the dependence of relative permeability on factors other than wettability. It further points out, as has been established in the literature, that making an independent wettability measurement such as reproducible contact angle measurements is more important than that determined from relative permeability data.

4. A reduction of two orders of magnitude in oil-water interfacial tension was obtained with this anionic surfactant in this rock-fluids system, which is insufficient for enhancing condensate recovery. This clearly proves that the predominance of wettability alteration mechanism over reduction of interfacial tension and spreading coefficient is the principal reason to modify multiphase flow characteristics and oil (condensate) recovery in this Berea sandstone rock.

5.2   Recommendations for Future Work

1. To use the chemicals to create the core with artificial strongly oil-wet nature, then use the same surfactants to test the effect of surfactants on wettability, spreading, and enhanced oil recovery and gas productivity;

2. To measure Zeta potential to determine the interaction with quartz or sandstone in the presence of different saline solutions;

3. To measure polar components in the condensate, both acidic and basic;

4. To Test the effect of the dual-salt brines with various salinities (ex. Na^+ + Al^{3+}/ Fe^{3+}, Ca^{2+}/Mg^{2+} + Al^{3+}/Fe^{3+}) on water-advancing and receding contact angles;

5. To conduct the similar experiments to examine brine salinity/composition effect under the real reservoir conditions;

6. To perform compositional simulations on the basis of experimental results to evaluate the economics of surfactant treatment;

7. To perform similar contact angle measurements in a crude oil instead of condensate system, using brines with various salinities and quartz surface to compare the results of both condensate and crude oil systems.

`

REFERENCES

1. Abdel-Wali, A. A.: "Effect of Simple Polar Compounds and Salinity on Interfacial Tension and Wettability of Rock/Oil/Brine System," *Journal of King Saud University-Engineering Science*, 1996, 8(2): 153-163.

2. Abel, W., Jackson, R.F. and Wattenbarger, R. A.: "Simulation of a Partial Pressure Maintenance Gas Cycling Project with a Compositional Model, Carson Creek Field, Alberta," *Journal of Petroleum Technology*, Jan., 1970, p. 38.

3. Afidick, D. Kaczorowski, N. J. and Bette, S.: "Production Performance of Retrograde Gas Reservoir: A Case Study of the Arun Field," paper SPE 28749, presented at the SPE Asia Pacific Oil and Gas Conference, Melbourne, Australia, Nov. 7-10, 1994.

4. Agbalaka, C.C., Dandekar, A. Y., Patil, S. L., Khataniar, S. and Hemsath, J. R.: "Coreflooding Studies to Evaluate the Impact of Salinity and Wettability on Oil Recovery Efficiency," *Transport in Porous Media* 76(1):77-94.

5. Al-Abri, A., Sidiq, H. and Amin, R.: "Enhanced Natural Gas and Condensate Recovery by Injection of Pure $SCCO_2$, Pure CH_4 and Their Mixtures: Experimental Investigation," paper SPE 124145, presented at the SPE Annual Technical Conference and Exhibition held in New Orleans, Louisiana, USA, 4-7 October, 2009.

6. Al-Anazi, H. A., Pope, G. A., Sharma, M. M., and Metcalfe, R. S.: "Laboratory Measurements of Condensate Blocking and Treatment for Both Low and High Permeability Rocks," paper SPE 77546, presented at the SPE Annual Technical Conference and Exhibition, San Antonio, TX, 29 Sep.-2 Oct., 2002.

7. Al-Anazi, H. A., Walker, J. G., Pope, G. A., Sharma, M. M, and Hackney, D. F.: "A Successful Methanol Treatment in a Gas-Condensate Reservoir: Field Application," *SPE Production & Facilities*, February 2005, 60-69.

8. Alotaibi, M. B. and Nasr-El-Din, H. A.: "Effect of Brine Salinity on Reservoir Fluids Interfacial Tension," paper SPE 121569, presented at SPE EUROPEC/EAGE Annual Conference and Exhibition held in Amsterdam, the Netherlands, 8-11 June, 2009.

9. Alotaibi, M. B., Nasralla, R. A., and Nasr-EI-Din, H. A.: "Wettability Studies Using Low-Salinity Water in Sandstone Reservoirs," *SPE Reservoir Evaluation & Engineering*, December 2011, 713-725.

10. Allen, F. H. and Roe, R.P.: "Performance Characteristics of a Volumetric Condensate Reservoir," *Petroleum Transactions, AIME, Vol. 189*, 1950, p. 83.

11. Anderson, W. G.: "Wettability Literature Survey—Part 1: Rock/Oil/Brine Interactions and the Effects of Core Handling on Wettability," *Journal of Petroleum Technology*, October, 1986 (a).

12. Anderson, W. G.: "Wettability Literature Survey- Part 2: Wettability Measurement," *Journal of Petroleum Technology*, October, 1986 (b), p.1246-1262.

13. Anderson, W. G.: "Wettability Literature Survey- Part 5: The effects of Wettability on Relative Permeability," *Journal of Petroleum Technology*, November, 1987.

14. Antoci, J. C., Briggiler, N. J. and Chadwich, J. A.: "Crosslink Methanol: Analysis of a Successful Experience in Fracture Gas Wells," paper SPE 69585, presented at SPE Latin American and Caribbean Petroleum Engineering Conference, Buenos Aires, March 25-28, 2001.

15. Araujo, Y. C., Araujo, M., Guzman, H. and Moya, G.: "Effect of the Spreading Coefficient on Two-Phase Relative Permeability," paper SPE 65385, presented at the SPE International Symposium on Oilfield Chemistry held in Houston, Texas, 13-16 February, 2001.

16. Ashraf, A., Hadia, N. J., Torstæer, O. and Tweheyo, M. T.: "Laboratory Investigation of Low Salinity Waterflooding as Secondary Recovery Process: Effect of Wettability," paper SPE 129012, presented at the SPE Oil and Gas India Conference and Exhibition held in Mumbai, India, 20-22 January, 2010.

17. Austad, T. and Standnes, D. C.: "Spontaneous Imbibition of Water into Oil-Wet Carbonates," *Journal of Petroleum Science and Engineering*, 39 (2003) 363-376.

18. Ayirala, S. C.: "Surfactant-induced Relative Permeability Modifications for Oil Recovery Enhancement," M.S. Thesis, Louisiana State University, Baton Rouge, December 2002.

19. Ayirala, S. C. and Rao, D. N.: "Multiphase Flow and Wettability Effects in Porous Media," *Colloids and Surfaces A: Physicochemical and Engineering Aspects*, 241 (2004), p.313.

20. Ayirala, S. C., Vijapurapu, C. S. and Rao, D. N.: "Beneficial Effects of Wettability Altering Surfactants in Oil-Wet Fractured Reservoirs," *Journal of Petroleum Science and Engineering*, 52 (2006), 261 – 274.

21. Ayyalasomayajula, P., Silpngarmlers, N., Berroteran, J., Sheffield, J. and Kamath, J.: "Condensate Relative Permeability Data for Well Deliverability Predictions for A Deep Marine Sandstone Reservoir," paper SCA 2003-33, 2003.

22. Aziz, R.: "Deliverability Projection Model for Overpressured Gas-Condensate Reservoirs," paper SPE 13706, presented at SPE Middle East Technical Conference and Exhibition, Bahrain, March 11-14, 1985.

23. Babadagli, T., "Analysis of Oil Recovery by Spontaneous Imbibition of Surfactant Solution", paper SPE 84866, SPE International Improved Oil Recovery Conference in Asia Pacific, Kuala Lumpur, Malaysia, 20-21October, 2003.

24. Bagci, S., Kok, M. V. and Turksoy, U.: "Effect of Brine Composition on Oil Recovery by Waterflooding," *Petroleum and Technology*, 19(3&4), 359-372, 2001.

25. Baig, T., Droegemueller, U. and Gringarten, A.C.: "Productivity Assessment of Fractured and Non-Fractured Wells in a Lean/Intermediate Low Permeability Gas Condensate Reservoir," paper SPE 93136, presented at SPE Europec/EAGE Annual Conference, Madrid, Spain, 13-16 June 2005.

26. Bang, V., Kumar, V., Ayyalasomayajula, P., Pope, G. A. and Sharma, M. M: "Relative Permeability of Gas-Condensate Fluids: A General Correlation," paper SPE 102741, presented at the SPE Annual Technical Conference and Exhibition, San Antonio, TX, 24-27 September 2006.

27. Bang, V., Pope, G. A. and Sharma, M. M: "Development of a Successful Chemical Treatment for Gas Wells with Water and Condensate Blocking Damage," paper SPE 124977, presented at the SPE Annual Technical Conference and Exhibition, New Orleans, LA, Oct. 4-7, 2009.

28. Bang, V., Pope, G. A., Sharma, M. M, Baran Jr., J. R. and Ahmadi, M.: "A New Solution to Restore Productivity of Gas Wells with Condensate and Water Blocks," *SPE Reservoir Evaluation & Engineering*, April 2010, 323-331.

29. Barnum, R. S., Brinkman, F. P., Richardson, T. W. and Spillette, A. G.: "Gas Condensate Reservoir Behavior: Productivity and Recovery Reduction Due to Condensation," paper SPE 14413 presented at the SPE Annual Technical Conference and Exhibition, Dallas, TX, October 22-25, 1995.

30. Bernard, G. G.: "Effect of Floodwater Salinity on Recovery of Oil from Cores Containing Clays," paper SPE 1725, presented at the 38th Annual California Regional Meeting of the Society of Petroleum Engineers of AIME, Los Angeles, California, 26-27 October, 1967.

31. Boom, W., Wit, K., Zeelenberg, J. P. W., Weeda, H. C. and Maas, J. G.: "On the Use of Model Experiment for Assessing Improved Gas-Condensate Mobility under Near-Wellbore Flow Conditions," paper SPE36714, presented at the SPE Annual Technical Conference and Exhibition held in Denver, Colorado, USA, 6-9 October, 1996.

32. Bozorgzadeh, M. and Gringarten, A. C.: "Condensate-Bank Characterization from Well-Test Data and Fluid PVT Properties," *SPE Reservoir Evaluation & Engineering*, October 2006, 596-611.

33. Buckley, J. S., Takamura, K. and Morrow, N. R.: "Influence of Electrical Surface Charges on the Wetting Properties of Crude Oils," *SPE Reservoir Engineering*, 1989, 4 (3): 332-342.

34. Buckley, J. S., Liu, Y., and Monsterleet, S.: "Mechanisms of Wetting Alteration by Crude Oils," *SPE Journal*, March 1998, 54-61.

35. Cai, B., Yang, J. and Guo, T., "Interfacial Tension of Hydrocarbon + Water/Brine Systems under High Pressure," *Journal of Chemical and Engineering Data* 41 (3):493-496.

36. Cao, H., Tsai, F. T-C. and Rusch, K. A.: "The Impact of Salinity on MS-2 Sorption in Saturated Sand Columns – Fate and Transport Modeling," *Journal of Environmental Engineering, ASCE*, 135 (10), 2009, 1041-1050.

37. Cao, H., Tsai, F. T-C. and Rusch, K. A.: "Salinity and Soluble Organic Matter on Virus Sorption in Sand and Soil Columns," *Ground Water*, 48(1), 2010, 42-52.

38. Catchpole, J. P. and Fulford, G.: "Dimensionless Groups," *Ind. Eng. Chem.*, 58, 1966, p46-60.

39. Clark, T. J.: "The Application of a 2-D Compositional, Radial Model to Predict Single-Well performance in a Rich Gas Condensate Reservoir," paper SPE 14413, presented at the SPE Annual Technical Conference and Exhibition, Las Vegas, NV. Sep. 22-25, 1985.

40. Clementz, D. M.: "Clay Stabilization in Sandstones through Adsorption of Petroleum Heavy Ends," *Journal of Petroleum Technology*, September 1977, 1061-1066.

41. Craig, F. F., "The Reservoir Engineering Aspects of Waterflooding," *Monograph Series, SPE, Richardson*, TX (1971) 3.

42. CYDAR coreflood simulator, http://www.cydarex.fr/, (August, 2010).

43. Derjaguin, B. V., Zorin, Z. M., Churaev, N. V., and Shishin, V. A.: "Examination of Thin Layers of Liquid on Various Solid Substrates," *Wetting, Spreading and Adhesion*, J. F. Padday (ed.), Academic Press, New York (1978).

44. Derjaguin, B. V., Churaev, N. V., and Muller, V. M.: "Surface Forces," Consultants Bureau, New York City, 1987.

45. Derjaguin, B. V., "Theory of Stability of Colloids and Thin Films," Consultants Bureau, New York City, 1989.

46. DSA software data base, Kruss Company.

47. Du, L., Walker, J. G., Pope, G. A., Sharma, M. M, and Wang, P.: "Use of Solvents to Improve the Productivity of Gas Condensate Wells," paper SPE 62935, presented at SPE Annual Technical Conference and Exhibition, Dallas, Texas, 1-4 October, 2000.

48. Duggan, J.O., "The Anderson 'L'- An Abnormally Pressured Gas Reservoir in South Texas," *Journal of Petroleum Technology*, Feb., 1972, 132.

49. Eikeland, K. M. and Hansen, H.: "Dry-Gas Reinjection in a strong Waterdrive Gas-Condensate Field Increases Condensate Recovery-Case study: The Slerpner Ty Field, South Viking Graben, Norwegian North Sea," paper SPE 110309, presented at the SPE Annual Technical Conference and Exhibition, Anaheim, California, Nov. 11-14, 2007.

50. Engineer, R.: "Cal Canal Field California: Case History of a Tight and Abnormally Pressure Gas Condensate Reservoir," paper SPE 13650, SPE California Regional Meeting in Bakersfield, California, March 27-29, 1985.

51. Fahes, M. and Firoozbadi, A.: "Wettability Alteration to Intermediate Gas-Wetting in Gas-Condensate Reservoirs at High Temperatures," *SPE Journal*, December 2007, 397 – 407.

52. Fussell, D. D.: "Single- Well Performance Predictions for Gas Condensate Reservoirs," *Journal of Petroleum Technology*, July 1973, 860-870.

53. Grattoni, C.A., Pingo Almada, M.B. and Dawe, R. A.: "Pore and Core-Scale Displacement Mechanisms with Spreading and Wetting Effects during Three-Phase Flow," paper SPE 39032 presented at the Fifth Latin American and Caribbean Petroleum Engineering Conference and Exhibition held in Rio de Janeiro, Brazil, 30 August-3 September, 1997.

54. Gruesbeck, C. and Collins, R. E.: "Entrainment and Deposition of Fine Particles in Porous Media," *SPE Journal* (Dec. 1982), 847-856.

55. Gupta, A. and Sharma, M. M.: "Stability of Thin Aqueous Films on Solid Surfaces," *Journal of Colloid and Interface Science*, Vol. 149, No. 2, March 1992, 392-406.

56. Gupta, R. and Mohanty, K. K.: "Temperature Effects on Surfactant-aided Imbition into Fractured Carbonates," *SPE Journal*, September 2010, 587-597.

57. Hall, A. C., Collins, S. H. and Melrose, J. C.: "Stability of Aqueous Wetting Films in Athabasca Tar Sands," *Society of Petroleum Engineers Journal*, April 1983, 249-258.

58. Hamouda, A. A. and Karoussi, O.: "Effect of Temperature, Wettability and Relative Permeability on Oil Recovery from Oil-Wet Chalk," *Energies*, 2008, 1:19-34.

59. Henderson, G. D., Danish, A., Tehrani, D. H. and Al-Kharusi, B.: "The Relative Significance of Positive Coupling and Inertial Effects on Gas Condensate Relative Permeabilities at High Velocity," paper SPE 62933 presented at the SPE Annual Technical Conference and Exhibition, Dallas, TX, Oct.1-4, 2000.

60. Hinchman, S. B. and Barree, R. D.: "Productivity Loss in Gas Condensate Reservoirs," paper SPE 14203 presented at the SPE Annual Technical Conference and Exhibition, Las Vegas, NV. Sep. 22-25, 1985

61. Hirasaki, G. J.: "Wettability: Fundamentals and Surface Forces," *SPE Formation Evaluation*, June 1991: 217-226.

62. Hirasaki, G. J. and Zhang, D. L.: "Surface Chemistry of Oil Recovery from Fractured, Oil-Wet, Carbonate Formations," *SPE Journal*, June 2004, 151-162.

63. Hirasaki, G. J., Miller, C. A. and Puerto, M.: "Recent Advances in Surfactant EOR," paper SPE 115386, presented at the SPE Annual Technical Conference and Exhibition held in Denver, Colorado, USA, 21-24 September 2008.

64. HØgnesen, E. J., Strand, S. and Austad, T.: "Waterflooding of Preferential Oil-Wet Carbonates: Oil Recovery Related to Reservoir Temperature and Brine Composition," paper SPE 94166, presented at the SPE Europec/EAGE Annual Conference held in Madrid, Spain, 13-16 June, 2005.

65. Hoier, L., Cheng, N. and Whitson, C.H.: "Miscible Gas Injection in Undersaturated Gas-Oil Systems," paper SPE 90379 presented at the SPE Annual Technical Conference and Exhibition, Houston, TX, Sep. 26-29, 2004.

66. Hough, E. W., Rzasa, M. J. and Wood, B. B.: "Interfacial Tensions at Reservoir Pressures and Temperatures; Apparatus and the Water-Methane System", *Trans., AIME* (1951) Vol. 192, 57-60

67. Iler, R. K.: "*The Chemistry of Silica*" (Wiley, New York, 1979).

68. Israelachvili, J. N.: "Intermolecular and Surface Forces," Academic Press, New York City, 1985.

69. Jamaluddin, A. K. M., Ye, S., D'Cruz, D. and Nighswander, J.: "Experimental and Theoretical Assessment of Using Propane to Remediate Liquid Buildup in Condensate Reservoirs," paper SPE 71526, presented at presented at the SPE Annual Technical Conference and Exhibition, New Orleans, Louisiana, 30 Sep.-3 Oct., 2001.

70. Jennings, H. Y. JR, and Newman, G. H.: "The Effect of Temperature and Pressure on the Interfacial Tension of Water against Methane-Normal Decane Mixtures," *SPE Journal*, June, 1971: 171-175.

71. Johnson, E. P., Bossler, D. P. and Naumann, V. O.: "Calculation of Relative Permeability from Displacement Experiments," *Petroleum Transactions, AIME*, 216(1959).

72. Khilar, K. C. and Folger, H. S.: "Water Sensitivity of Sandstones," *SPEJ* (Feb. 1983), 55-64.

73. Klins, M.A.: "Carbon Dioxide Flooding – Basic Mechanisms and Project Design," International Human Resources Development Corporation, Boston, 1984.

74. Kumar, V., Pope, G. A. and Sharma, M. M: "Improving the Gas and Condensate Relative Permeability Using Chemical Treatments," paper SPE 100529 presented at SPE Gas Technology Symposium, Calgary, Alberta, Canada, May 15-17, 2006a.

75. Kumar, V., Pope, G. A. Sharma, M. M, Ay, Ayyalasomayajula, P. S., and Kamath, J.: "Chemical Stimulation of Gas-Condensate Reservoirs," paper SPE 102669, presented at the SPE Annual Technical Conference and Exhibition, San Antonio, Texas, USA, 24-27 September 2006b.

76. Lager, A., Webb, K. J., Black, J. J., Singleton, M. and Sorbie, K. S.: "Low Salinity Oil Recovery – An Experimental Investigation," paper SCA2006-36, presented at the International Symposium of the Society of Core Analysis held in Trondheim, Norway, 12-16 September, 2006.

77. Lager, A., Webb, K. J., Collins I. R. and Richmond, D. M.: "LoSal^{TM} Enhanced Oil Recovery: Evidence of Enhanced Oil Recovery at the Reservoir Scale," paper SPE 113976, presented at the SPE/DOE Improved Oil Recovery held in Tulsa, Oklahoma, USA, 19-23 April, 2008.

78. Lemon, P., Zeinijahromi, A., Bedrikovetsky, P. and Shahin, I.: "Effects of Injected Water Chemistry on Waterflood Sweep Efficiency via Induced Fines Migration," paper SPE 140141, presented at the SPE International Symposium on Oilfield Chemistry held in The Woodlands, Texas, USA, 11-13 April 2011.

79. Li, J., Wang, W., Gu, Y.: "Dynamic Interfacial Tension Phenomenon and Wettability Alteration of Crude Oil-Rock-Alkaline-Surfactant Solution Systems," paper SPE 90207, presented at the SPE Annual Technical Conference and Exhibition, Houston, TX, 26-29 September 2004.

80. Li, K. and Firoozbadi, A.: "Experiment Study of Wettability Alteration to Preferential Gas-Wetness in Porous Media and its Effect," *SPE Reservoir Evaluation & Engineering*, April 2000, 139 – 149.

81. Luo, K., Li, S., Zheng, X., Chen, G., Dai, Z. and Liu, N.: "Experimental Investigation into Revaporization of Retrograde Condensate by Lean Gas Injection," paper SPE 68683, SPE Asia Pacific Oil Conference and Exhibition, Jakarta, Indonesia, April 17-19, 2001.

82. Maeda, H. and Okatsu, K.: "EOR Using Thin Oil Film Drainage Mechanism in Water Wet Oil Reservoir," SPE 116532, paper presented at the 2008 SPE Asia Pacific Oil & Gas Conference and Exhibition held in Perth, Australia, 20-22 October 2008.

83. Mannhardt, K.: "The Measurement of Interfacial Tension by the Spinning Drop Apparatus", Technical Report Submitted to Petroleum Recovery Institute, Calgary, Canada, March 13 (1987).

84. Martin, J. C.: "The Effects of Clays on the Displacement of Heavy Oil by Water," paper presented at the 3th Annual Venezuelan Regional Meeting of AIME, Caracas, October 1959.

85. McCain, Jr., W.D.: "The Properties of Petroleum Fluids (Second Edition)," PennWell Publishing Co., Tulsa, 1990.

86. McGuire, P. L., Chatham, J. R., Paskvan, F. K., Sommer, D. M. and Carini, F. H.: "Low Salinity Oil Recovery: An Exciting New EOR Opportunity for Alaska's North Slope," paper SPE 93093, presented at the SPE Western Regional Meeting Held in Irvine, CA, USA, 30 March-1 April, 2005.

87. Mohan, J.: "Modeling of Gas Condensate Wells with and without Hydraulic Fractures," MS Thesis, University of Texas at Austin, August, 2005.

88. Mohan, J., Pope, G. A. and Sharma, M. M.: "Effect of Non-Darcy Flow on Well Productivity of a Hydraulically Fractured Gas-Condensate Well," *SPE Reservoir Evaluation & Engineering*, August 2009, 576-585.

89. Morrow, N. and Buckley, J.: "Improved Oil Recovery by Low-Salinity Waterflooding," *Journal of Petroleum Technology*, May 2011, 106~112.

90. Mott, R., Cable, A. and Spearing, M.: "Measurements and Simulation of Inertial and High Capillary Number Flow Phenomena in Gas-Condensate Relative Permeability," paper SPE 62932, presented at the SPE Annual Technical Conference and Exhibition, Dallas, TX, Oct.1-4, 2000.

91. Mungan, N.: "Permeability Reduction through Changes in PH and Salinity," *Journal of Petroleum Technology*, December 1965, 1449-1453.

92. Mungan, N.: "Interfacial Effect in Immiscible Liquid-Liquid Displacement in Porous Media," *Soc. Pet. Eng. J.* Sept. 1966, 247-253.

93. Mwangi, P.: "An Experimental Study of Surfactant Enhanced Waterflooding," M.S. Thesis, Louisiana State University at Baton Rouge, December 2010.

94. Nagarajan, N. R., Honarpour, M. M., Sampath, K. and McMichael, D.: "Comparison of Gas-Condensate Relative Permeability Using Live Fluid vs. Model Fluids," SCA 2004-09, 2004.

95. Nasralla, R. A., Alotaibi, M. B. and Nasr-El-Din, H. A.: "Efficiency of Oil Recovery by Low Salinity Water Flooding in Sandstone Reservoirs," paper SPE 144602, presented at the SPE Western North American Regional Meeting held in Anchorage, Alaska, USA, 7-11 May 2011.

96. National Institute of Standards and Technology (NIST), http://webbook.nist.gov/chemistry/

97. Noh, M. and Firoozabadi, A.: "Effect of Wettability on High-Velocity Coefficient in Two-Phase Gas/Liquid Flow," *SPE Journal*, September 2008, 298-204.

98. Odi, U.: "Analysis and Potential of CO_2 Huff-n-Puff for Near Wellbore Condensate Removal and Enhanced Gas Recovery," paper SPE160917, presented at SPE Annual Technical Conference and Exhibition held in San Antonio, Texas, USA 8-10 October, 2012.

99. Okasha, T. M. and Al-Shiwaish, A. A.: "Effect of Brine Salinity on Interfacial Tension in Arab-D Carbonate Reservoir, Saudi Arabia," paper SPE 119600, presented at the SPE Middle East Oil & Gas Show and Conference in the Bahrian International Exhibition Centre, Kingdom of Bahrain, 15-18 March, 2009.

100. Okazawa, T.: "User's Manual for ANRPM and EXRPM Relative Permeability Simulators," Petroleum Recovery Institute, Calgary, AB, 1983.

101.   Oren, P. E., Billiotte, J. and Pinczewski, W. V.: "Mobilization of Waterflood Residual Oil by Gas Injection for Water-Wet Conditions," *SPE Formation Evaluation*, March 1992, p.70-78.

102.   Oren, P. E., and Pinczewski, W. V.: "Effect of Wettability and Spreading on Recovery of Waterflood Residual Oil by Immiscible Gasflooding," *SPE Formation Evaluation*, June, 1994, p. 149-156.

103.   Othman, M., Yang, J., Chong, M. O., Zakaria, M. S., Ali, B. A. and Cheng, C. B.: "Angsi K-Sand Production Performance: A Case History of Hydraulically Fractured Retrograded Gas Condensate Reservoir," paper SPE 113816, presented at SPE Europec/EAGE Annual Conference and Exhibition, Rome, Italy, June 9-12, 2008.

104.   Pashley, R. M.: "Forces between Mica Surfaces in La^{3+} and Cr^{3+} Electrolyte Solutions," *Journal of Colloid and Interface Science*, 102 (1984) 23-35.

105.   Patil, S., Dandekar, A. Y., Patil, S. L., and Khataniar, S.: "Low Salinity Brine Injection for EOR on Alaska North Slope (ANS)," paper IPTC 12004, presented at the International Petroleum Technology Conference, Kuala Lumpur, Malaysia, 3-5 December, 2008.

106.   Porter, M. R.: "Handbook of Surfactants, second edition," Blackie Academic & Professional, 1994.

107.   Rao, D. N., Girard, M. and Sayegh, S. G.: "Impact of Miscible Flooding on Wettability, Relative Permeability, and Oil Recovery," *SPE Reservoir Engineering*, May 1992, 204-212.

108.   Rao, D. N. and Girard, M. G.: "A New Technique for Reservoir Wettability Characterization," *Journal of Canadian Petroleum Technology*, 1996, Vol. 35, No.1:31- 39.

109.   Rao, D. N.: "Wettability Effects in Thermal Recovery Operations," *SPE Reservoir Evaluation & Engineering*, Vol. 2, No. 5, October 1999, 420-430.

110.   Rao, D. N.: "Correlation of Oil-Water Flow Behavior in Reservoir Rocks with Dynamic Contact Angles," *Journal of Canadian Petroleum Technology*, July, 2002.

111.   Rao, D. N.: "The Concept, Characterization, Concerns and Consequences of Contact Angles in Solid-Liquid-Liquid Systems," *Contact Angle, Wettability and Adhesion*, 2003, Vol. 3, pp.191-210.

112.   Rao, D. N., Ayirala, S. C., Abe, A. A. and Xu, W.: "Impact of Low-Cost Dilute Surfactants on Wettability and Relative Permeability," paper SPE 99609, presented at the SPE/DOE Symposium on Improved Oil Recovery held in Tulsa, Oklahoma, 22-26 April 2006.

113.   Rapoport, L. A. and Leas, W. J.: "Properties of Linear Waterfloods," *Petroleum Transactions, AIME*, 198(1953), 139-148.

114.   Robertson E. P.: "Low-Salinity Waterflooding to Improve Oil Recovery-Historical Field Evidence," paper SPE 109965, presented at the SPE Annual Technical Conference and Exhibition, Anaheim, California, USA, 11-14 November, 2007.

115.   Ryan, J. N. and Elimelech, M.: "Colloid Mobilization and Transport in Groundwater," *Colloids and Surfaces A: Physicochemical and Engineering Aspects*, 107 (1996), 1-56.

116.   Sarkar, A. K. and Sharma, M. M.: "Fines Migration in Two-Phase Flow," *Journal of Petroleum Technology,* May 1990, 646-652.

117.   Schramm, L. L.: "Surfactants: Fundamentals and Applications in the Petroleum Industry," Cambridge University Press, 2000.

118.   Seccombe, J. C., Lager, A., Webb, K., Jerauld, G. and Fueg, E.: "Improving Waterflood Recovery: LoSal ^{TM} EOR Field Evaluation," paper SPE 113480, presented at the SPE/DOE Improved Oil Recovery held in Tulsa, Oklahoma, USA, 19-23 April, 2008.

119.   Seethepalli, A., Adibhatla, B. and Mohanty, K.K.: "Physicochemical Interactions During Surfactant Flooding of Fractured Carbonate Reservoirs", *SPE Journal*, December 2004.

120.   Sequeira, D. S.: "Compositional Effects on Gas-Oil Interfacial Tension and Miscibility at Reservoir," M.S. Thesis, Louisiana State University, Baton Rouge, December 2006.

121.   Settari, A., Bachman, R. C., Hovem, K. and Paulson, S. G.: "Productivity of Fractured Gas Condensate Wells - a Case Study of Smorbukk Field," paper SPE 35604, presented at Gas Technology Conference, Calgary, Canada, 28April-1May, 1996.

122.   Sharma, M. M. and Filoco, P. R.: "Effect of Brine Salinity and Crude-oil Properties on Oil Recovery and Residual Oil Saturations," *SPE Journal* 5(3), September, 2000, p.293-300.

123.   Shi, C. and Horne, R. N.: "Improved Recovery in Gas-Condensate Reservoirs Considering Compositional Variations," paper SPE 115786, presented at the SPE Annual Technical Conference and Exhibition held in Denver, Colorado, USA, 21-24 September 2008.

124.   Skrettingland, K., Holt, T., Tweheyo, M. T. and Skjevrak, I.: "Snorre Low-Salinity-Water Injection—Coreflooding Experiments and Single-Well Field Pilot," *SPE Reservoir Evaluation & Engineering*, April 2011, 182-192.

125.   Smith, K. W.: "Brines as Flooding Liquids," paper presented at 7th Annual Tech. meeting, Min. Ind. Expt. Sta., Penn State College, November 1942.

126.   Somasundaran, P. and Zhang, L.: "Adsorption of Surfactants on Minerals for Wettability Control in Improve Oil Recovery Processes," *Journal of Petroleum Science & Engineering*, 52(2006), 198-212.

127.   Takamura, K. and Chow, R. S.: "The Electric Properties of the Bitumen/Water Interface Part II. Application of the Ionizable Surface-Group Model," *Colloid and Surfaces*, 1989, 15: 35-48.

128.   Tang, G. and Firoozbadi, A.: "Relative Permeability Modification in Gas/Liquid Systems through Wettability Alteration to Intermediate Gas Wetting," *SPE Reservoir Evaluation & Engineering*, December 2002, 427 – 436.

129.   Tang, G. Q. and Morrow, N. R.: "Salinity, Temperature, Oil Composition, and Oil Recovery by Waterflooding," *SPE Reservoir Engineering*, November, 1997:269-276.

130.   Tang, G. Q. and Morrow, N. R.: "Influence of Brine Composition and Fines Migration on Crude Oil/Brine/Rock Interactions and Oil Recovery," *Journal of Petroleum Science and Engineering*, 24(1999) 99-111.

131.   Valdya, R. N. and Fogler, H. S.: "Fines Migration and Formation Damage: Influence of pH and Ion Exchange," *SPE Production Engineer*, November 1992, 325-330.

132.   Vijapurapu, C. S., Rao, D. N. and Lian, K: "The Effect of Rock Surface Characteristics on Reservoir Wettability," paper SPE 75211, presented at the SPE/DOE Improved Oil Recovery Symposium held in Tulsa, Oklahoma, 13-17 April 2002.

133.   Vijapurapu, C. S. and Rao, D. N.: "Compositional Effects of Fluids on Spreading, Adhesion and Wettability in Porous Media," *Colloids and Surfaces A: Physicochemical and Engineering Aspects*, 241(2004) 335-342.

134.   Vizika, O. and Lombard, J. M.: "Wettability and Spreading: Two Key Parameters in Oil Recovery with Three-Phase Gravity Drainage," *SPE Reservoir Engineering*, February 1996, 54-60.

135.   Webb, K. J., Black, J. J and Al-Ajeel, H.: "Low Salinity Oil Recovery-Log-Inject-Log," paper SPE 89379, presented at the SPE/DOE Fourteen Symposium on Improved Oil Recovery held in Tulsa, Oklahoma, USA, 17-21 April, 2004.

136.   Wheaton, R. J. and Zhang, H. R.: "Condensate Banking Dynamics in Gas Condensate Fields: Compositional changes and Condensate Accumulation around Production Wells," paper SPE 62930, presented at the SPE Annual Technical Conference and Exhibition, Dallas, TX, Oct.1-4, 2000.

137.   White, C. D., Bradurn, F. R., Brown, R. L., and Thieme, M. A.: "Reservoir Potential of Thin-Bedded Turbidites: Prospect Tahoe," paper SPE 24875, presented at the 67th Annual Technical Conference and Exhibition of the Society of Petroleum Engineers held in Washington, DC, October 4-7, 1992.

138.   Xu, W.: "Experimental Investigation of Dynamic Interfacial Tensions at Reservoir Conditions," M.S. Thesis, Louisiana State University at Baton Rouge, May 2005.

139.   Zhang, L, Somasundaran, P. and Maltesh, C.: "Adsorption of n-Dodecyl-β-D-Maltoside on Solids," *Journal of Colloid and Interface Science* 191, 202-208 (1997).

140. Zhang, Y., Xie, X and Morrow, N. R.: "Waterflood Performance by Injection of Brine with Different Salinity for Reservoir Cores," paper SPE 109849, presented at the SPE Annual Technical Conference and Exhibition,, Anaheim, California, USA, 11-14 November, 2007.

141. Zhang, Y. P., Sayegh, S. G., Huang, S. and Dong, M.: "Enhanced Light-Oil Recovery by CO_2/Flue Gas Huff-n-Puff Process," *Journal of Canadian Petroleum Technology*, Vol. 45, No. 2, February 2006, 24-32.

142. Zisman, W. A.: "Contact Angle, Wettability and Adhesion," *Adv. Chem.* Ser.43, ACS, Washington, DC, USA (1964).

APPENDIX: HISTROY MATCH OF RECOVERY AND PRESSURE DROP AND RESULTS OF RELATIVE PERMEABILITIES FROM COREFLOOD SIMULATOR
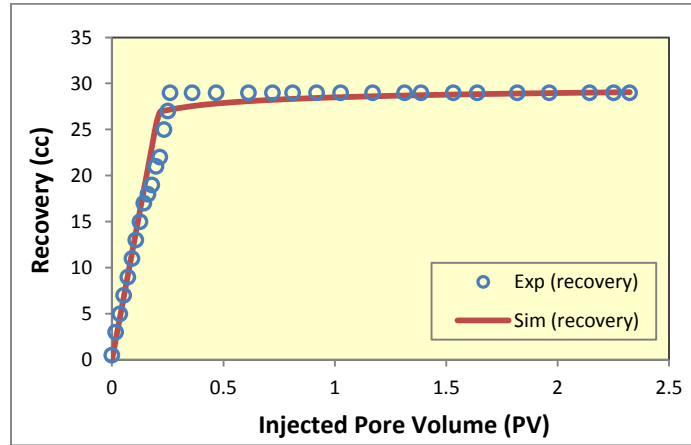
Figure A1: Recovery Results of Experiment and Simulation for 0 ppm at 68 °F
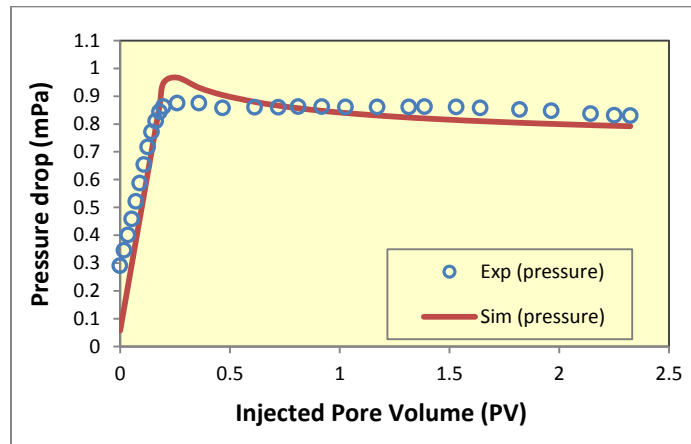
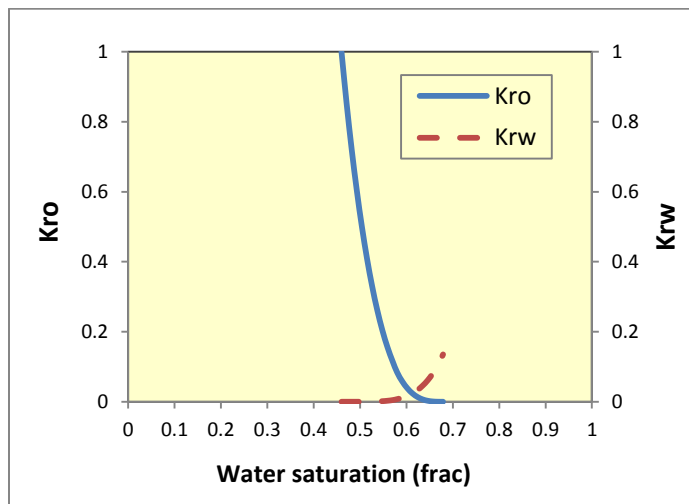Figure A2: Pressure Drop Results of Experiment and Simulation for 0 ppm at 68 °F
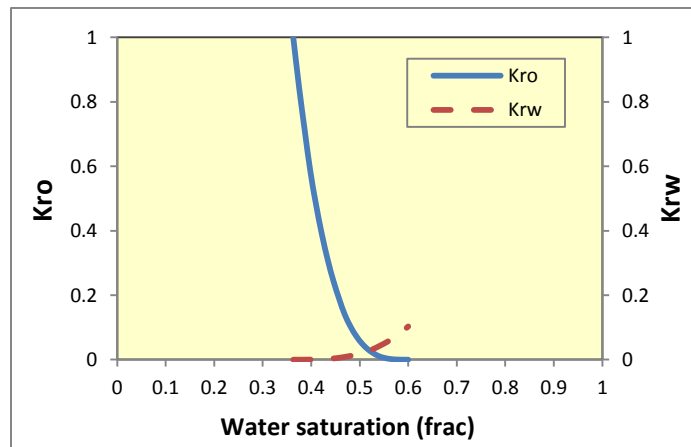
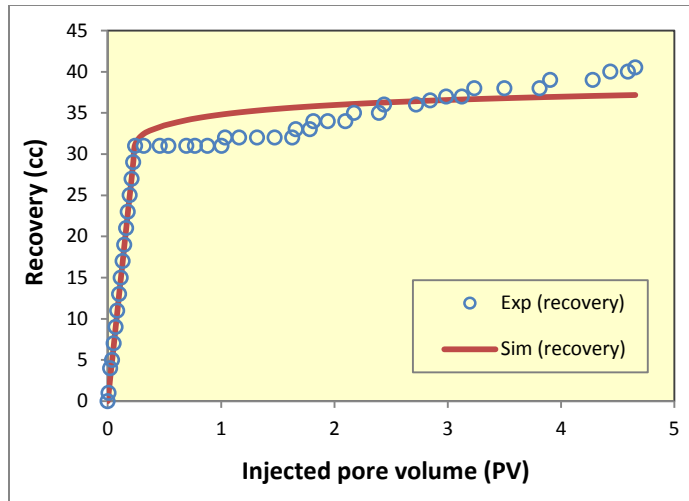Figure A3: Oil-Water Relative Permeability for 0 ppm at 68 °F

171
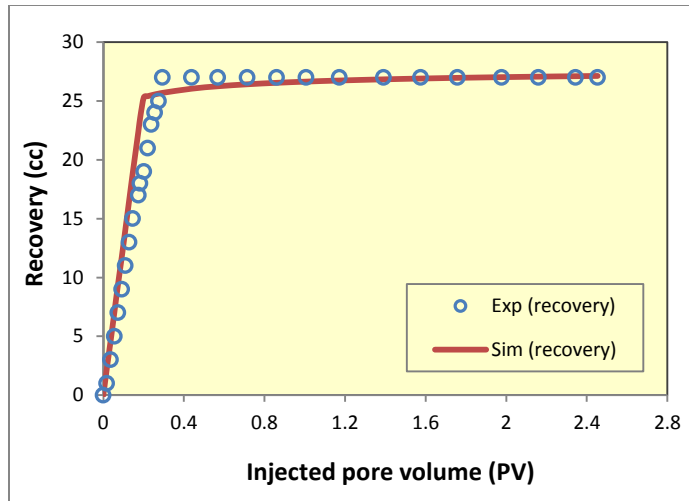
Figure A4: Recovery Results of Experiment and Simulation for 0 ppm at 210 °F
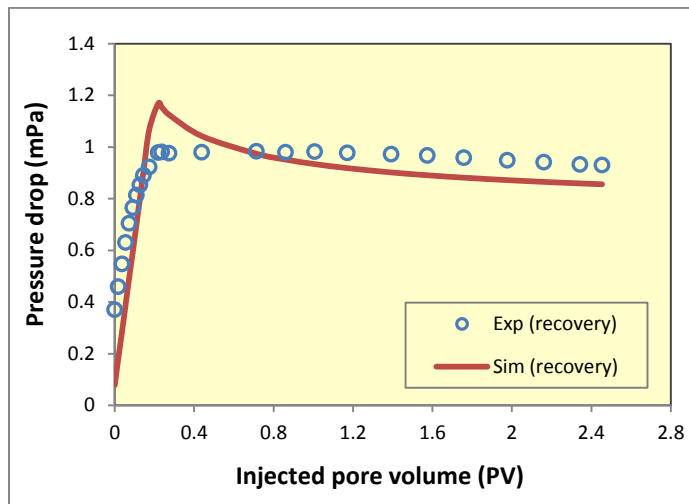
Figure A5: Pressure Drop Results of Experiment and Simulation for 0 ppm at 210 °F

Figure A6: Oil-Water Relative Permeability for 0 ppm at 210 °F

172

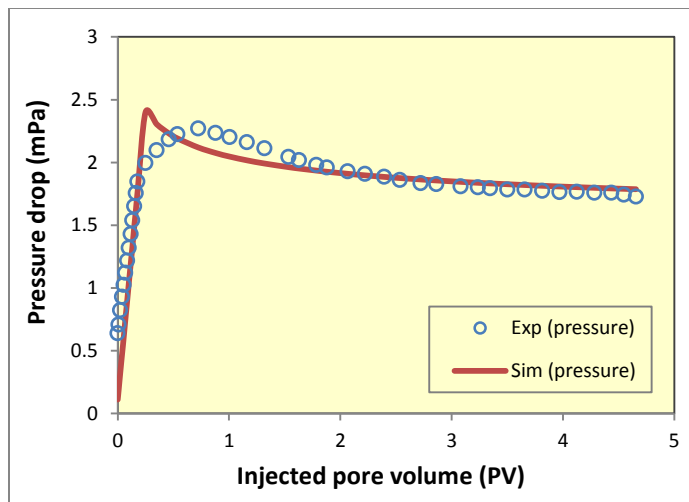Figure A7: Recovery Results of Experiment and Simulation for 1500 ppm

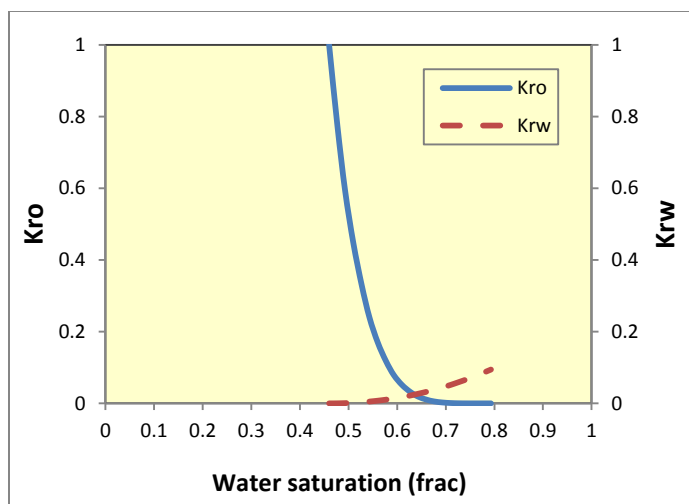Figure A8: Pressure Drop Results of Experiment and Simulation for 1500 ppm
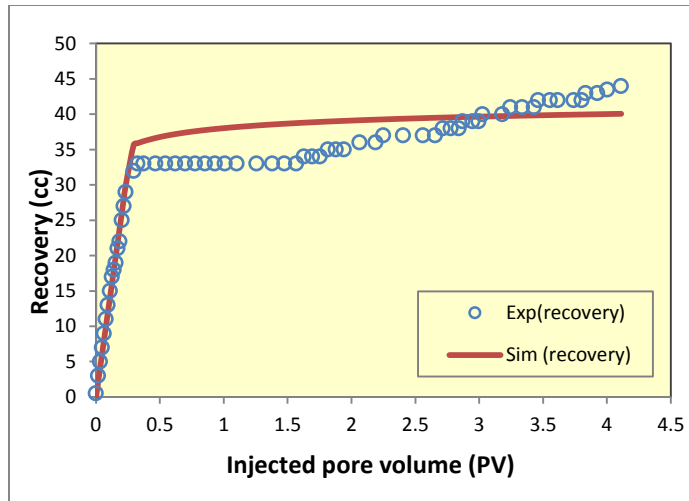

Figure A9: Oil-Water Relative Permeability for 1500 ppm

173

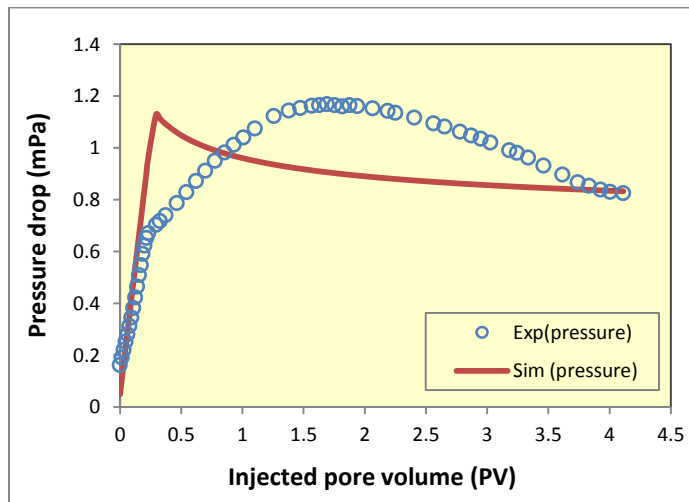**Figure A10: Recovery Results of Experiment and Simulation for 3000 ppm**

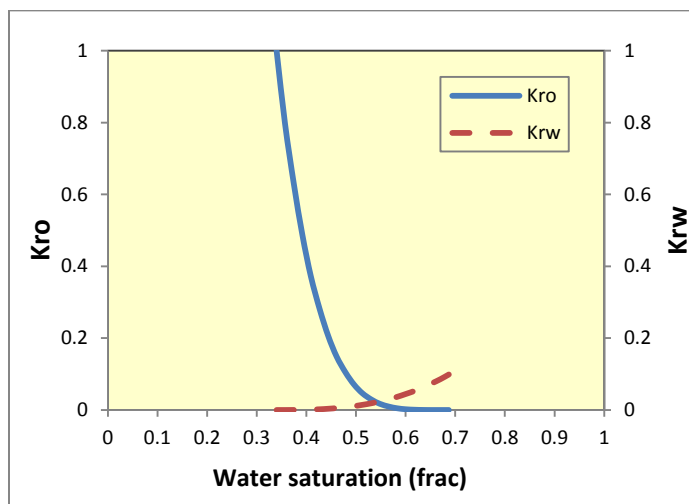**Figure A11: Pressure Drop Results of Experiment and Simulation for 3000 ppm**

Figure A12: Oil-Water Relative Permeability for 3000 ppm

174

VITA

Yu Zheng, the daughter of Yicai Zheng and Jinlan Wang, was born and raised in Lu'an, China. She obtained her Bachelor of Science degree in Chemical Engineering from Shandong Institute of Mining Technology, China, in 1994. After she graduated from the college, she joined Qingdao Gas Group, China and worked as a chemical engineer for seven years. In 2001, she reentered the Qingdao University of Science & Technology, China, to pursue her master degree. And she obtained her Master of Science degree in Chemical Engineering in 2004. In August 2007, she joined the PhD program in the Craft and Hawkins Department of Petroleum Engineering at Louisiana State University, Baton Rouge. The doctoral degree in Petroleum Engineering will be conferred in December 2012.